This is to certify that the

thesis entitled

THE NUMERICAL TREATMENT OF BODY FORCES,
DISLOCATION FIELDS, AND ARRAYS OF CRACKS
IN PLANE ELASTOSTATICS PROBLEMS

presented by

Gary J. Burgess

has been accepted towards fulfillment
of the requirements for

Ph.D. degree in Mechanics

Nicholas J. Altiero

Major professor

Date August 11, 1981

O-7639

THE NUMERICAL TREATMENT OF BODY FORCES, DISLOCATION FIELDS, AND ARRAYS OF CRACKS IN PLANE ELASTOSTATICS PROBLEMS

By

Gary J. Burgess

A DISSERTATION

Submitted to
Michigan State University
in partial fulfillment of the requirements
for the degree of

DOCTOR OF PHILOSOPHY

Department of Metallurgy, Mechanics and Materials Science

1981

ABSTRACT

The numerical solution of plane elasticity problems in which the body is of arbitrary shape and is subjected to various loading conditions is first considered. The method employed is based on embedding the body of interest in the infinite plane and satisfying prescribed boundary conditions using a collection of concentrated loads acting outside the body. The procedure developed is then extended to include internal sources of stress such as body forces, fields of edge dislocations and their dipoles, isolated cracks, and finally dense arrays of cracks. In the treatment of crack problems, the actual crack boundary is replaced by a dislocation dipole which acts as a passive radiator of stress in the presence of an applied external stress field. Since each crack is given this status and since the strength of any given dipole depends on the stresses produced by its neighbors and by boundary tractions, there is a high degree of interaction between dipoles. The approach yields a system of matrix equations to be solved for the dipole strengths which are subsequently used to determine the state of stress anywhere within the body. Comparison of numerical results to known solutions indicates that the dipole model of a crack is an accurate one for most applications and that the numerical methods developed perform satisfactorally. This work should therefore be

useful in the study of damage due to progressive crack growth in engineering materials such as metals and rock.

ACKNOWLEDGEMENTS

I would like to thank the members of my doctoral committee, Professors Nicholas J. Altiero, George E. Mase, Robert Wm. Little, and Albert N. Andry for contributing to the academic background necessary for the preparation of this dissertation and for the accommodating atmosphere they provided during the course of my research.

I would also like to thank Ms. Jan Swift for her haste in preparing this manuscript on such short notice. Welcomed financial assistance was provided for by the Department of Metallurgy, Mechanics, and Materials Science, the Division of Engineering Research, and by the National Science Foundation (NSF Grant # ENG-76-18355).

TABLE OF CONTENTS

LIST OF TABLES

LIST OF FIGURES

LIST OF SYMBOLS

A	Area
b_i	Burger's vector in the i-direction
B_i	Body force in the i-direction
c	Crack half-length
$\underline{C}(mxn)$	Matrix with m rows and n columns
c_{mn}, d_{mn}	Fourier coefficients
d_x, d_y, d_{xy}	Dislocation dipole strengths
E	Modulus of elasticity
f_i, g_i	Resultant forces at point i
G	Shear modulus
h_x, h_y	Dipole spacings
$\hat{i}$, $\hat{j}$, $\hat{k}$	Unit vectors in the x, y, z directions
I_k	Integral with parameter k
J	Auxilliary integral
K_x, K_y, K_{xy}	Constants related to dislocations and dipoles
K_I, K_{II}	Mode I and II stress intensity factors
L_x, L_y	Lengths in the x and y directions
m, n	Indices in Fourier series
P_i	Concentrated load in the i-direction
P, Q, R, S, T	Terms used in the influences due to Fourier distributions of internal stress
r	Relative distance between source and field points

s	Shape factor for grains
t_i	Traction vector in the i-direction
u_x, u_y	Displacements in the x and y directions
u, v	Displacements or integral substitutions
$\underline{w}(n)$	Column vector containing n rows
x, y	Rectangular coordinates
$\bar{x}$, $\bar{y}$	Coordinates in a rotated system

Greek

α, β, γ	Constants
$\beta(\xi)$	Dislocation density along a line
Δ	Dipole density in an area
$\bar{\nabla}$, ∇^2	Gradient and Laplace operators
ε	Crack density in a granular medium
ε_x, ε_y, γ_{xy}	Engineering strains
θ	Angle between x and $\bar{x}$ axes
ν	Poisson's ratio
σ_{ij}	The ij stress component
σ_{ij}^*	Dislocation dipole stresses
Σ	Summation symbol
τ	Shear stress
ϕ	Airy stress function or special integral
ω	Rigid body rotation or angular velocity
$\int_A$	Integral over area A

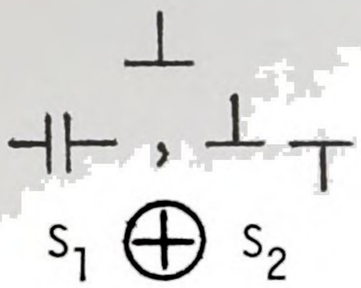

Edge dislocation

Dislocation dipoles

$S_1 \oplus S_2$ Superposition of states 1 and 2

CHAPTER 1

INTRODUCTION

The linear and nonlinear theories of elasticity, plasticity and fracture mechanics are composed of two parts: the development of constitutive equations describing the material response to applied loads and the determination of the stress fields resulting from an application of these equations to boundary value problems of interest. This dissertation deals with the latter.

Beginning with Chapter 2 the numerical solution to linear elasticity problems with emphasis on efficiency is addressed and the method developed is then extended to include body forces, fields of dislocations, dislocation dipoles, isolated cracks and finally a dense array of microcracks. Common to all solution methods in problems of plasticity, nonlinear elasticity and fracture mechanics is the need for an accurate assessment of the stress fields arising from distributed internal sources of stress, such as a body force field. Also common to these methods is the incremental nature of the approach. Consequently, the basic process of solving a linear elasticity problem must be performed repeatedly, requiring the numerical procedure to be both accurate and efficient.

In classical plasticity theory, a rearrangement of the elastic-plastic Navier equation shows that the plasticity problem can

be regarded as an elasticity problem with a suitably modified body force [1,2]. The body force carries the effects of plasticity for a given set of constitutive relations and is typically not known apriori since it is expressed in terms of the displacement field. The same is true of nonlinear elasticity problems [3]. The nonlinear terms occupy the same position in the Navier equation as does the body force term. In both plasticity and non-linear elasticity, the determination of the body force distributions for a given loading system is typically done iteratively. The load is then given an increment and the procedure is repeated until some predetermined loading program is completed. It is therefore necessary to solve a series of elasticity problems with body forces for each increment of the load.

Attempts to obtain the stress field due to body forces by replacing the distribution with a collection of point loads [1], gives poor results near the points of application of these loads due to the singular nature of the point load solution [4]. The same is true of quadrature rules used in numerical integration techniques [2] which are aimed at smearing the point load solution over polygon-shaped areas. The finite element approach [5] of dividing the body into elements and assigning some simple distribution to the body force over each element is cumbersome and numerically inefficient. In Chapter 2 it is shown that the problem can be treated very effectively by characterizing the body force field by a set of Fourier coefficients which are then used to determine the stress field at any point from simple expressions.

Equally important is that the integrals associated with the smearing of point loads over an area to obtain a body force distribution are exactly the same as those required to smear dislocations and dislocation dipoles over an area. In problems where the dislocation distribution is known, the methods of Chapter 2 allow for the calculation of the associated stress field with a minimum of effort. A known distribution however is likely to be the exception rather than the rule. As with plasticity and nonlinear elasticity, the distribution is usually determined iteratively by satisfying some kind of constitutive criterion [6]. Nye [7] and Eshelby [8] have independently developed continuum theories of dislocations but both are described by a set of partial differential equations which are unlikely to be solved in even the most elementary problems.

In fracture mechanics [9], the prediction of stress levels at which crack growth takes place is of primary importance. The determination of stress intensity factors [5, 9, 10, 11, 12] is aimed at accomplishing this. The subsequent problem of following the progression of crack growth is an area of current research [13, 14, 15, 16, 17, 18, 19]. Fundamental to the success of this research is the ability to characterize the stress field of a collection of cracks with a minimum of effort. It has been customary to focus attention on one or two cracks in simple geometries under conditions of uniform stress [9, 10, 11, 12]. The solution to the problem of a single crack in uniaxial tension in the infinite plane is no simple matter and therefore points to the need to develop unconventional methods of solution. In Chapter 3 a dislocation dipole model for a crack

[6] is proposed which simplifies matters considerably while preserving the general features of a crack and eventually allows for the solution of general boundary value problems in which the body contains an arbitrary array of cracks with varying sizes, orientations and locations within the body. The application of this model to problems with known solutions indicates that it compares favorably with more refined models and requires very little effort to apply numerically. Ultimately, this model is used in conjunction with the results of Chapter 2 to treat the limiting case of a dense array of microcracks characterized by a 'microcrack density'. It is hoped that, when used with constitutive models of crack growth (yet to be developed), these results will prove to be an integral part of the problem solution process.

No attempt has been made to develop or incorporate already existing crack growth models into the material presented here. Efforts to classify materials according to their behavior in the realm of progressive crack growth [13, 14, 15, 16, 17, 18, 19, 20] indicate that this stage of the problem needs further development. Dragon and Mroz [14] come closest to defining the state of the art approach to crack problems. In their approach, they use an abstract quantity introduced by Vakulenko and Kachanov [21] called the crack tensor and pursue a potential theory development similar to that used in plasticity. Their development, however, is largely phenomenological and lacks justification in many places. The crack tensor idea is nevertheless an advantageous contribution and is very similar to the'dipole state' used here to represent a crack field. In view of the successes met with in the example problems presented in Chapter 4, this type of approach looks promising for future use in the incremental treatment

of crack growth problems. For the sake of clarity, the methods presented in the following chapters deal with the treatment of body forces, dislocations and cracks individually. The versatility of the numerical approach must however be emphasized; there is no restriction preventing these methods from being used in concert to treat the general problem of elastic-plastic-dislocation-fracture mechanics.

CHAPTER 2

THE NUMERICAL SOLUTION OF ELASTICITY PROBLEMS BY THE SUPERPOSITION METHOD

2.1 Background

The governing equations of linear elastostatics applied to a homogeneous isotropic body in a state of plane stress are [4] the equilibrium equations,

$$\frac{\partial \sigma_x}{\partial x} + \frac{\partial \tau_{xy}}{\partial y} + B_x = 0,$$

$$\frac{\partial \tau_{xy}}{\partial x} + \frac{\partial \sigma_y}{\partial y} + B_y = 0, \tag{2.1}$$

the compatibility conditions,

$$\nabla^2(\sigma_x + \sigma_y) = -(1 + \nu)\, \overline{\nabla} \cdot \overline{B}, \tag{2.2}$$

the stress-strain law,

$$\varepsilon_x = \frac{1}{E}(\sigma_x - \nu\sigma_y),$$

$$\varepsilon_y = \frac{1}{E}(\sigma_y - \nu\sigma_x), \tag{2.3}$$

$$\gamma_{xy} = \frac{1}{G}\tau_{xy},$$

and the strain-displacement relations,

$$\varepsilon_x = \frac{\partial u}{\partial x},$$

$$\varepsilon_y = \frac{\partial v}{\partial y}, \tag{2.4}$$

$$\gamma_{xy} = \frac{\partial u}{\partial y} + \frac{\partial v}{\partial x},$$

where σ_x, σ_y, τ_{xy} are the stresses; B_x, B_y are the body forces; ε_x, ε_y, γ_{xy} are the strains; u, v are the displacements; E, G, ν are the usual material properties.

In what follows, the body will always be assumed to be in a state of plane stress. The interested reader can easily convert any results to satisfy plane strain conditions. Any stress field, $(\sigma_x, \sigma_y, \tau_{xy})$, which satisfies both the equilibrium equations and compatibility is a solution to some boundary value problem in elastostatics. Satisfaction of compatibility insures the integrability of Equations (2.4) to obtain a displacement field, (u, v).

Of particular importance in the theory of elasticity are the principle of superposition, which follows from the linearity of the governing equations, and the uniqueness theorem due to Kirchhoff. The principle of superposition allows one to construct new solutions from linear combinations of old solutions. The solution to a typical problem in elasticity involves the satisfaction of the governing equations at every point inside the body and the matching of boundary conditions at every point on the

boundary of the body. The theorem of Kirchhoff guarantees uniqueness of the solution provided that the boundary conditions are of the form usually encountered,

$$\sigma_{ij} n_j = t_i^* \qquad \text{on } B_t,$$
$$u_i = u_i^* \qquad \text{on } B_u, \tag{2.5}$$

where B_t and B_u are those parts of the boundary on which tractions, t_i^*, and displacements, u_i^*, are prescribed, respectively. Consequently, a solution obtained by any means is the only solution.

Two basic solutions, the concentrated load and the edge dislocation solutions, will be used in what follows. Figures 2.1a and 2.1b show concentrated loads of magnitudes P_x and P_y acting at the origin in the infinite plane in the absence of body forces. The resultant stress and displacement fields shown in matrix form are

$$\begin{bmatrix} u_x \\ u_y \\ \sigma_x \\ \sigma_y \\ \tau_{xy} \end{bmatrix} = -\frac{P_x(1+\nu)}{2\pi} \cdot \begin{bmatrix} \frac{1}{4G}\left[\left(\frac{3-\nu}{1+\nu}\right) \ln r + \frac{y^2}{r^2}\right] \\ -\frac{1}{4G} \cdot \frac{xy}{r^2} \\ \frac{x}{r^2}\left(\beta + \frac{x^2}{r^2}\right) \\ \frac{x}{r^2}\left(-\beta + \frac{y^2}{r^2}\right) \\ \frac{y}{r^2}\left(\beta + \frac{x^2}{r^2}\right) \end{bmatrix} \tag{2.6a}$$

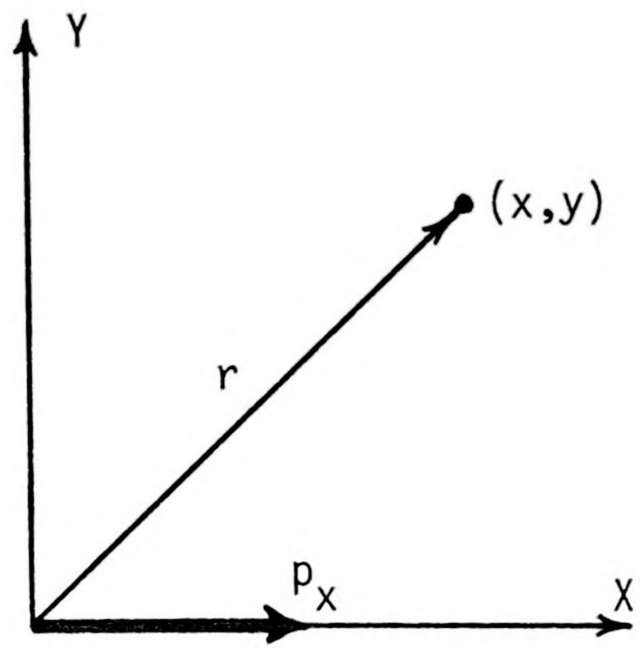

a. A concentrated force acting in the x direction.

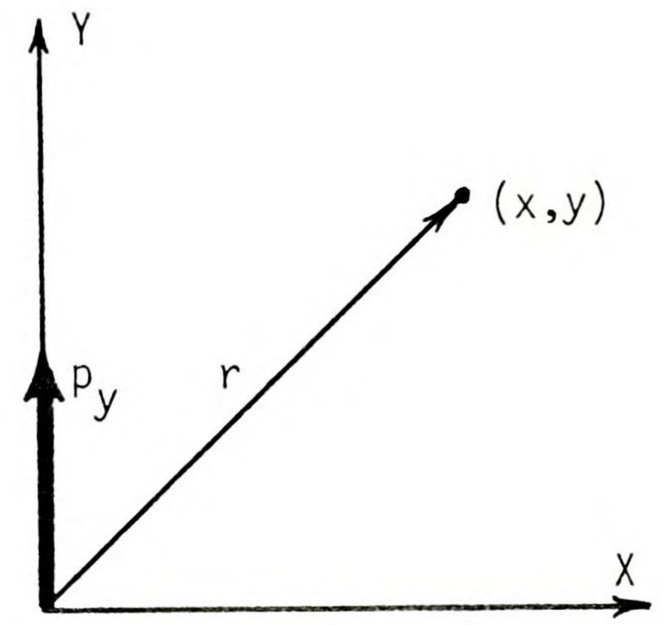

b. A concentrated force acting in the y direction.

Figure 2.1. Concentrated loads in the infinite plane.

and

$$\begin{bmatrix} u_x \\ u_y \\ \sigma_x \\ \sigma_y \\ \tau_{xy} \end{bmatrix} = -\frac{P_y(1+\nu)}{2\pi} \cdot \begin{bmatrix} -\frac{1}{4G}\frac{xy}{r^2} \\ \frac{1}{4G}\left[\left(\frac{3-\nu}{1+\nu}\right) \ln r + \frac{x^2}{r^2}\right] \\ \frac{y}{r^2}\left(-\beta + \frac{x^2}{r^2}\right) \\ \frac{y}{r^2}\left(\beta + \frac{y^2}{r^2}\right) \\ \frac{x}{r^2}\left(\beta + \frac{y^2}{r^2}\right) \end{bmatrix}, \qquad (2.6b)$$

respectively, where

$$r^2 = x^2 + y^2,$$

$$\beta = \frac{1}{2}\left(\frac{1-\nu}{1+\nu}\right). \qquad (2.7)$$

An edge dislocation is given the symbol, $\perp$. Operationally, the dislocation is formed by slicing the infinite plane along a line and inserting a slab of material of width b into the cut. The stem of the $\perp$ refers to this slab of material. Figure 2.2 shows dislocations of various orientations situated at the origin in the infinite plane. The accompanying 'Burger's vectors', $\underline{b}$, represents the net discontinuity in the elastic displacement taken counterclockwise around a closed circuit enclosing the leading edge of the inserted slab [6]: in Figure 2.2, the leading

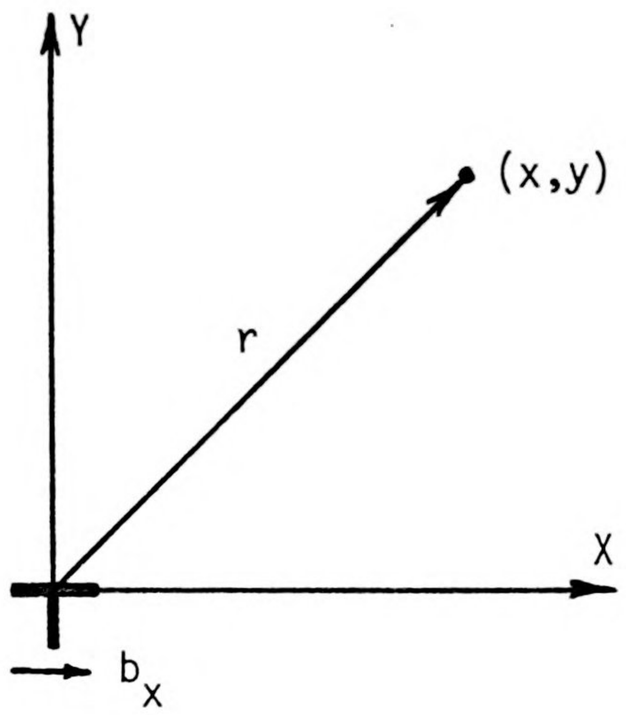

a. An edge dislocation with Burger's vector, b_x.

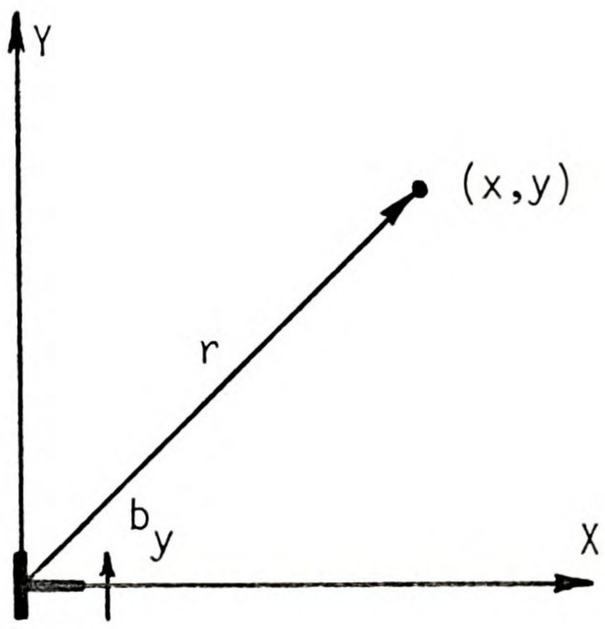

b. An edge dislocation with Burger's vector, b_y.

Figure 2.2. Edge dislocations in the infinite plane.

edge lies along the z axis. An excellent discussion of edge dislocations and their stress and displacement fields is given in [6]. The stress fields corresponding to Figures 2.2a and 2.2b are

$$\sigma_x = K_x \cdot \frac{y(3x^2+y^2)}{r^4} ,$$

$$\sigma_y = -K_x \cdot \frac{y(x^2-y^2)}{r^4} , \qquad (2.8a)$$

$$\tau_{xy} = -K_x \cdot \frac{x(x^2-y^2)}{r^4} ,$$

and

$$\sigma_x = K_y \cdot \frac{x(y^2-x^2)}{r^4} ,$$

$$\sigma_y = -K_y \cdot \frac{x(3y^2+x^2)}{r^4} , \qquad (2.8b)$$

$$\tau_{xy} = K_y \cdot \frac{y(y^2-x^2)}{r^4} ,$$

where

$$K_x = \frac{Eb_x}{4\pi} ,$$

$$K_y = \frac{Eb_y}{4\pi} . \qquad (2.8c)$$

It can easily be shown that the so-called Burger's vector is in fact a vector. Referring to Figure 2.3a, the proof is effected by writing out the stress field for this rotated dislocation

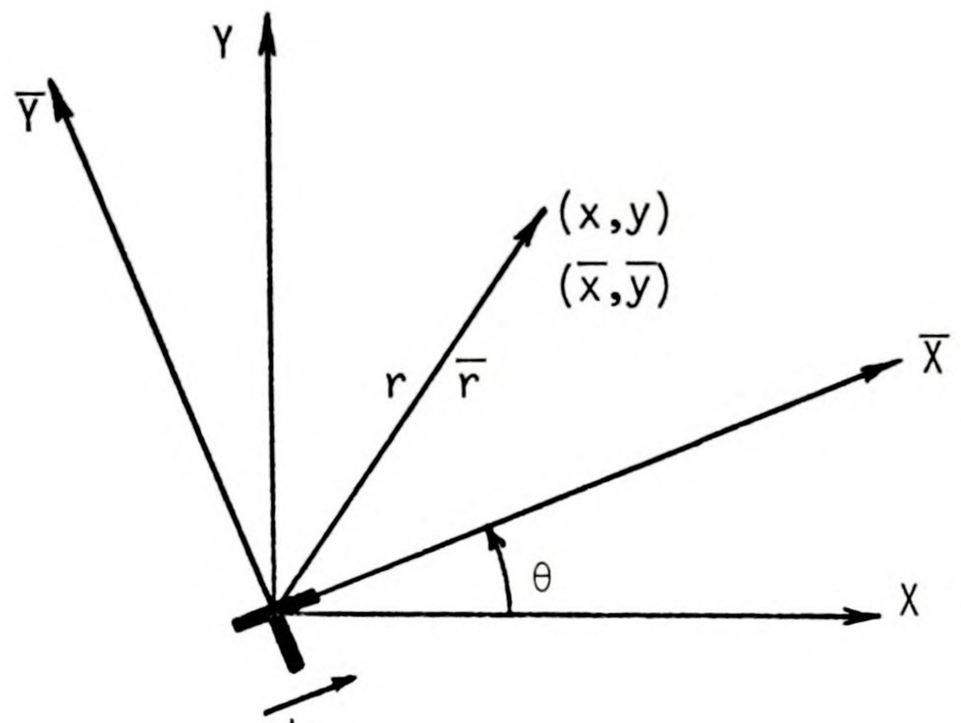

a. A rotated edge dislocation with Burger's vector, b.

b. The vector nature of the 'Burger's vector'.

Figure 2.3. Transformation properties of edge dislocations.

referred to the $\bar{x}$-$\bar{y}$ system,

$$\sigma_{\bar{x}} = K \cdot \frac{y(3\bar{x}^2 + \bar{y}^2)}{\bar{r}^4},$$

$$\sigma_{\bar{y}} = K \cdot \frac{\bar{y}(\bar{y}^2 - \bar{x}^2)}{\bar{r}^4}, \qquad (2.9a)$$

$$\tau_{\bar{x}\bar{y}} = K \cdot \frac{\bar{x}(\bar{y}^2 - \bar{x}^2)}{\bar{r}^4},$$

where $K = \frac{Eb}{4\pi}$.

This state of stress may now be transformed back to the x-y system. For example, with $\sin\theta = s$ and $\cos\theta = c$,

$$\sigma_x = \sigma_{\bar{x}} c^2 + \sigma_{\bar{y}} s^2 - 2\tau_{\bar{x}\bar{y}}\, sc. \qquad (2.9b)$$

Substituting Equations (2.9a) into (2.9b) and rearranging gives

$$\sigma_x = \frac{K}{\bar{r}^4}\left[\bar{y}^3 + \bar{x}^2\bar{y}\,(3c^2 - s^2) + 2\bar{x}(\bar{x}^2 - \bar{y}^2)\, sc\right]. \qquad (2.9c)$$

Finally, using the coordinate transformations,

$$\bar{x} = xc + ys,$$

$$\bar{y} = -xs + yc,$$

Equation (2.9c) becomes after simplification

$$\sigma_x = \frac{K}{r^4}\,[y(3x^2+y^2)c + x(y^2-x^2)s]. \qquad (2.9d)$$

The stresses, σ_y and τ_{xy}, can be treated in a similar manner. Now if one defines $b_x = b \cdot c$ and $b_y = b \cdot s$, Equation (2.9d) can be written as

$$\sigma_x = K_x \cdot \frac{y(3x^2+y^2)}{r^4} + K_y \cdot \frac{x(y^2-x^2)}{r^4}\,, \qquad (2.9e)$$

which is recognized as the superposition of the states of stress given in Equations (2.8a) and (2.8b) with K_x and K_y defined as in Equation (2.8c).

This result is shown symbolically in Figure 2.3b where the expressions in parenthesis below each symbol correspond to their Burger's vectors.

2.2 The Superposition Method in the Absence of Body Forces

An efficient compact numerical technique for the solution of plane elasticity problems in which the body is of arbitrary shape and is subjected to any boundary conditions of the form mentioned in the uniqueness theorem can be developed using only the concentrated load solution. The procedure is as follows (see Figure 2.4):

1) Embed the body of interest in the infinite plane of the same material.
2) Place 2n concentrated loads at arbitrary locations outside the body. The orientations of the loads are as shown in Figure 2.4 and the magnitudes are as yet unknown.

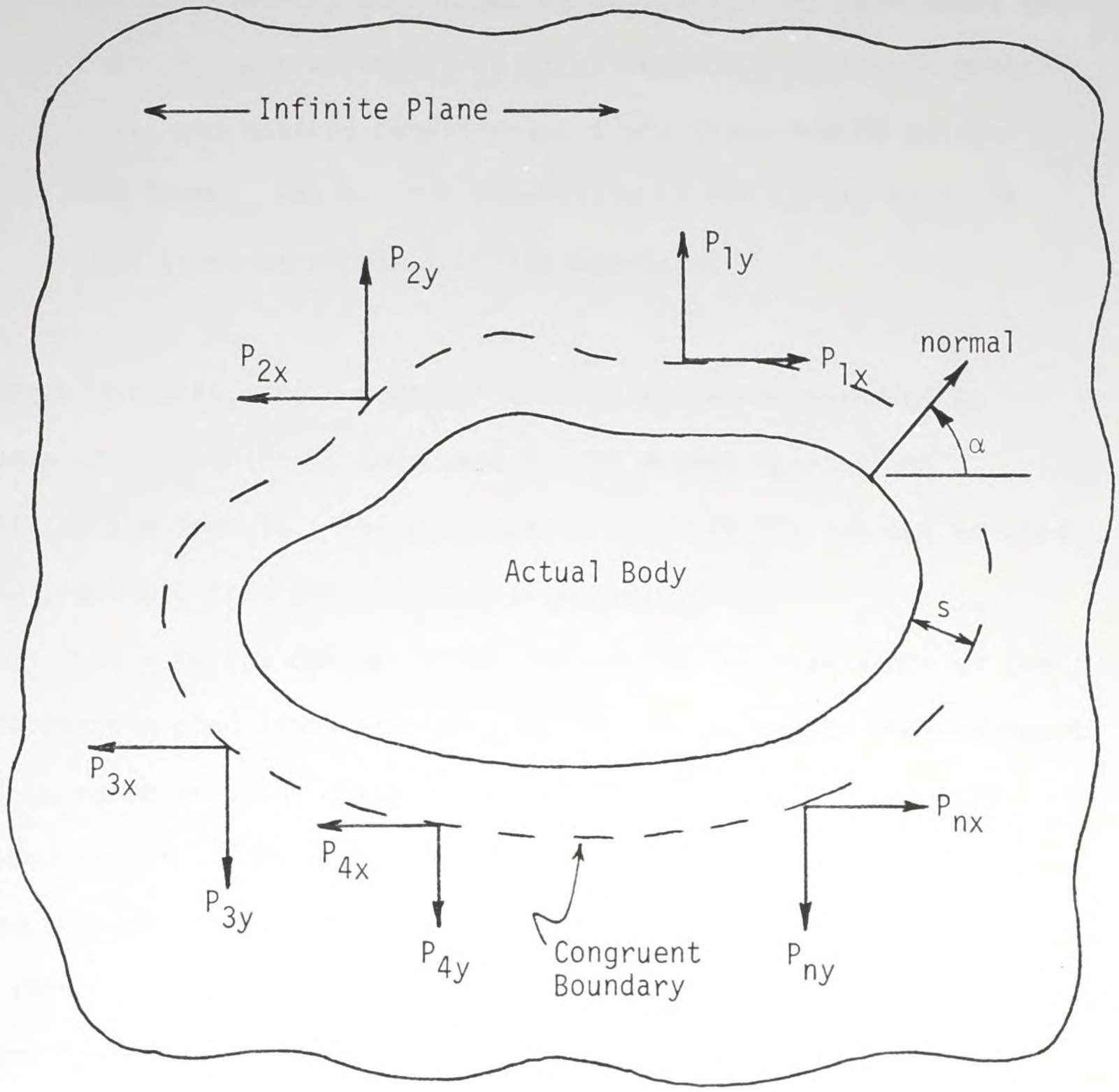

Figure 2.4. Embedding the body in the infinite plane.

3) Satisfy boundary conditions by adjusting load magnitudes so that the superposed effect of all 2n loads acting in concert gives the desired conditions. Since there are 2n unknown magnitudes, one has the capability of satisfying boundary conditions at n points on the boundary.

For simplicity, the concentrated loads are arranged so as to act on a contour which is congruent to the actual boundary at a distance s from it. The parameter s is arbitrary and can be used to prevent $\underline{C}$ from becoming too ill-conditioned.

Let $\underline{w}$ be the column vector containing the magnitudes of the 2n concentrated loads and let $\underline{C}$ be the square matrix whose element, C_{ij}, represents the contribution of the j^{th} unit concentrated load to the i^{th} boundary condition. Finally, let $\underline{b}$ be the column vector containing the prescribed values of the 2n boundary conditions. The superposition of the 2n concentrated loads to satisfy the boundary conditions is represented by

$$\underline{b} = \underline{C}\ \underline{w}, \tag{2.10a}$$

and if $\underline{C}$ is nonsingular,

$$\underline{w} = \underline{C}^{-1}\ \underline{b}. \tag{2.10b}$$

The stresses and displacements at any point in the body can be calculated by summing the contributions due to each of concentrated loads, the magnitudes of which are now known.

The numerical procedure just described solves an elastostatics problem in the sense that equilibrium and compatibility are satisfied at every point inside the body and boundary conditions are satisfied at a finite number of points on the boundary. The approximation therefore lies in the neglect of boundary conditions not directly accounted for in the matching technique. Refinements in the solution may therefore be made by considering more points at which conditions are to be satisfied. This of course necessitates more concentrated loads so that the size of the matrix, $\underline{C}$, and hence the amount of computation increase considerably.

An alternative procedure allows for the satisfaction of an arbitrary number of boundary conditions in a least squares sense while maintaining a constant matrix size. The problem is still defined as

$$\underline{b} = \underline{C}\ \underline{w},$$

where C now has 2N rows and 2n columns with N > n. Since C is nonsquare, the inverse of $\underline{C}$ does not exist and there is no way in general to choose the 2n unknowns in $\underline{w}$ so as to satisfy the 2N conditions in $\underline{b}$. Therefore, for a given $\underline{w}$, one may define the nonzero error vector,

$$\underline{e} = \underline{b} - \underline{C}\ w, \tag{2.11}$$

and the accumulated square error,

$$E^2 = \underline{e}^T \underline{e}, \tag{2.12}$$

and choose $\underline{w}$ so that the square error is a minimum. This requires that

$$\delta(E^2) = \underline{e}^T \delta\underline{e} + \delta\underline{e}^T \underline{e} = 2\underline{e}^T \delta\underline{e} = 0.$$

However,

$$\delta\underline{e} = - \underline{C}\ \delta\underline{w}, \tag{2.13}$$

so that

$$\underline{e}^T \delta\underline{e} = (\underline{b}^T - \underline{w}^T \underline{C}^T)(-\underline{C}\delta\underline{w}) = 0,$$

which must hold for arbitrary $\delta\underline{w}$. Therefore,

$$(\underline{b}^T - \underline{w}^T \underline{C}^T)\underline{C} = 0,$$

or, transposing,

$$\underline{C}^T \underline{C}\ \underline{w} = \underline{C}^T \underline{b}\ . \tag{2.14}$$

In retrospect, this merely amounts to premultiplying the original equation,

$$\underline{b} = \underline{C}\ \underline{w},$$

by $\underline{C}^T$.

Equation (2.14) has the property that $\underline{C}^T\underline{C}$ is square so that $\underline{w}$ is uniquely determined by

$$\underline{w} = (\underline{C}^T\underline{C})^{-1}\underline{C}^T\underline{b}. \tag{2.15}$$

It should be remarked that the least squares approach may not be desirable in certain cases. If, for example, the boundary conditions vary rapidly over small distances, this approach will tend to smooth out these fluctuations giving conservative values in cases where accurate values are desired. As a final note, one may generalize the type of boundary condition prescribed to the form

$$au_x + bu_y + c\sigma_x + d\sigma_y + e\tau_{xy} = f, \tag{2.16}$$

where the constants a, b, c, d, e, and f are specified. The matrix element, C_{ij}, is then the influence given by the left hand side of Equation (2.16) at the boundary point i due to a unit concentrated load applied at point j outside the body. The right hand side, f, appears in the ith row of the column vector, $\underline{b}$. Of course this type of boundary condition forces one to forfeit certainty about the uniqueness of the solution, but is nevertheless useful for contact problems and problems in which the boundary is subject to friction and spring loading.

2.3 The Superposition Method in the Presence of Body Forces and Other Sources of Internal Stress

The presence of body forces does not seriously complicate the numerical solution to an elastostatics problem. The procedure is as follows.

1) Embed the body in the infinite plane of the same material and let the body forces act.
2) Determine the stresses and displacements on the boundary of the embedded body caused by these body forces.
3) The difference between these boundary values and the prescribed boundary conditions is then eliminated by adjusting the magnitudes of the concentrated loads outside the body.

This procedure gives a unique solution in the sense that the equations of elasticity with body forces are satisfied at every point inside the body while boundary conditions of the type mentioned in the uniqueness theorem are partially satisfied on the boundary. The stresses and displacements at any point inside the body can be calculated by superposing the effects of the body force field and the concentrated loads, the magnitudes of which are known at the conclusion of step 3.

It is important to note that the solution inside the embedded body is unique. The difference referred to in step 3 is certainly dependent upon the body forces acting outside the body but this difference is compensated for by the selection of the concentrated load magnitudes.

The only difficult part of this procedure is the calculation of the stress field produced by an arbitrary distribution of body forces (step 2). One may approximate the continuous body force field by a set of concentrated loads acting at various locations throughout the body, but due to the singular nature of the concentrated force solution, the stresses and displacements near the points of application of these loads are highly exaggerated and even diverge at the points themselves. For the sake of accuracy, the only alternative is to continuously distribute infinitesimal point forces over the body. For example, using Equations (2.6), the stress, σ_x, at the point (a,b), caused by the body force, $B_x(x,y)$, acting inside of an area, A, embedded in the infinite plane is, by superposition,

$$\sigma_x(a,b) = \int_A - \frac{dPx}{2\pi}(1+\nu)\left(\frac{a-x}{r^2}\right)\left(\frac{1-\nu}{1+\nu}\cdot\frac{1}{2} + \frac{(a-x)^2}{r^2}\right),$$

where

$$r^2 = (a-x)^2 + (b-y)^2$$

and

$$dP_x = B_x(x,y)\, dA.$$

With B_x known,

$$\sigma_x(a,b) = -\frac{1+\nu}{2\pi}\int_A \frac{(a-x)}{r^2}\left(\frac{1-\nu}{1+\nu}\cdot\frac{1}{2}+\frac{(a-x)^2}{r^2}\right) B_x(x,y)dA. \tag{2.17}$$

As mentioned earlier, the field, $B_x(x,y)$, may be allowed to act over the entire infinite plane without affecting the solution to the elastostatics problem, provided that the stress and displacement fields caused by this do not diverge as a result. To insure convergence, one may assign to B_x the desired value inside the body and any value whatsoever outside which does not accumulate influences to the point of divergence. Such a distribution may, for example, be the Fourier series representation for B_x,

$$B_x(x,y) = \sum_i \sum_j c_{ij} \cos\frac{i\pi x}{L_x}\cos\frac{j\pi y}{L_y}\,. \tag{2.18}$$

Here, the body is embedded in a rectangle as shown in Figure 2.5 and the Fourier coefficients, c_{ij}, are evaluated by point matching or by

$$c_{ij} = \frac{4}{L_x L_y}\int_o^{Ly}\int_o^{Lx} B_x(x,y)\cos\frac{i\pi x}{L_x}\cos\frac{j\pi y}{L_y}\,. \tag{2.19}$$

It is not necessary to place the rectangle in the first quadrant but it is imperative that it be placed in one of the four quadrants to the exclusion of all others since this distribution is an even function in both x and y and consequently forces $B_x(x,y)$ to be even

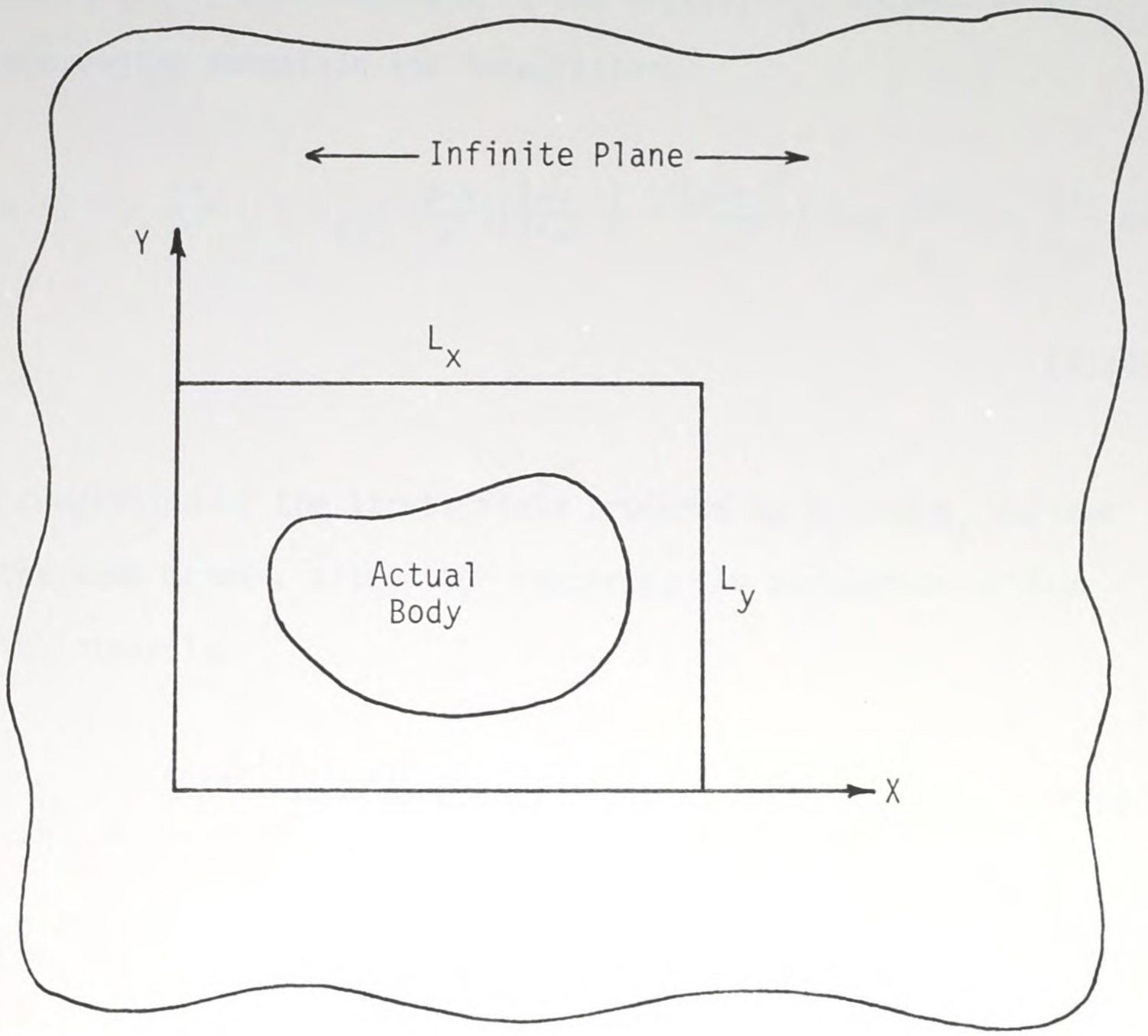

Figure 2.5. Embedding the body in a rectangle in preparation for its Fourier series representation.

as well. Substituting the Fourier representation for B_x into Equation (2.17) and letting $A \to \infty$, the stress, σ_x, becomes after interchanging summation and integration,

$$\sigma_x(a,b) = -\frac{1+\nu}{2\pi} \sum_i \sum_j c_{ij} \int_\infty \left(\frac{a-x}{r^2}\right)\left(\frac{1-\nu}{1+\nu} \cdot \frac{1}{2} + \frac{(a-x)^2}{r^2}\right) \cos \frac{i\pi x}{L_x} \cos \frac{j\pi y}{L_y} \, dA. \tag{2.20}$$

The completion of the stress field produced by B_x and B_y follows in the same manner, altogether requiring the evaluation of four basic integrals,

$$I_k = \int_\infty \frac{(a-x)^{3-k}(b-y)^k}{r^4} \cos mx \cdot \cos ny \, dA, \tag{2.21}$$

where

$$k = 0, 1, 2, 3$$

and

$$r^2 = (a-x)^2 + (b-y)^2.$$

Note that m and n need not be integers. These integrals are difficult to evaluate and appear in Appendix A. From Appendix A,

$$I_o = (\frac{\pi}{2} + 1)a,$$
$$I_1 = (\frac{\pi}{2} - 1)b,$$
$$I_2 = (\frac{\pi}{2} - 1)a, \qquad (2.22a)$$
$$I_3 = (\frac{\pi}{2} + 1)b,$$

for m=n=0. Otherwise,

$$I_o = \frac{\pi m(m^2+3n^2)}{(m^2+n^2)^2} \sin ma \cdot \cos nb,$$

$$I_1 = \frac{\pi n(n^2-m^2)}{(m^2+n^2)^2} \cos ma \cdot \sin nb, \qquad (2.22b)$$

$$I_2 = \frac{\pi m(m^2-n^2)}{(m^2+n^2)^2} \sin ma \cdot \cos nb,$$

$$I_3 = \frac{\pi n(n^2+3m^2)}{(m^2+n^2)^2} \cos ma \cdot \sin nb.$$

The stress, $\sigma_x(a,b)$, due to constant body forces, $B_x = c_{oo}$ and $B_y = d_{oo}$, acting over the entire infinite plane is, from Equation (2.20),

$$\sigma_x(a,b) = -\frac{1+\nu}{2\pi} c_{oo} [\frac{1-\nu}{1+\nu} \cdot \frac{1}{2} (I_o+I_2) + I_o]$$
$$- \frac{1+\nu}{2\pi} d_{oo} [- \frac{1-\nu}{1+\nu} \frac{1}{2} (I_1+I_3) + I_1], \qquad (2.23)$$

where the values for the four integrals are taken from the m=n=0 case of Equation (2.22a). After simplification, this becomes

$$\sigma_x\ (a,b) = -\frac{1}{2}\, c_{oo}\ (1 + \frac{1+\nu}{\pi})a - \frac{1}{2}\, d_{oo}\ (\nu - \frac{1+\nu}{\pi})b.$$

Performing similar operations for the remaining stresses and making the interchanges, a→x and b→y, the stress field at the point (x,y) due to constant body forces is

$$\sigma_x = -\frac{1}{2}\,[c_{oo}\ (1 + \frac{1+\nu}{\pi})x + d_{oo}\ (\nu - \frac{1+\nu}{\pi})y],$$

$$\sigma_y = -\frac{1}{2}\,[c_{oo}\ (\nu - \frac{1+\nu}{\pi})x + d_{oo}\ (1 + \frac{1+\nu}{\pi})y], \qquad (2.24)$$

$$\tau_{xy} = -\frac{1}{2}\ (1 - \frac{1+\nu}{\pi})\ (c_{oo}y + d_{oo}x).$$

It is a simple matter to verify that both equilibrium and compatibility are satisfied.

The extension of these results to body forces of the form

$$B_x = c_{mn} \cos mx \cdot \cos ny$$

$$B_y = d_{mn} \cos mx \cdot \cos ny \qquad (2.25)$$

acting over the entire infinite plane follows in exactly the same manner. The complete stress field at the point (x,y) generated by these body forces for m and n not both zero is

$$\sigma_x = R[m(m^2 + (2 + \nu)n^2)c_{mn} \cdot P + n(\nu n^2 - m^2)d_{mn} \cdot Q]$$

$$\sigma_y = R[m(\nu m^2 - n^2)c_{mn} \cdot P + n(n^2 + (2 + \nu)m^2)d_{mn} \cdot Q], \quad (2.26)$$

$$\tau_{xy} = R[n(n^2 - \nu m^2)c_{mn} \cdot Q + m(m^2 - \nu n^2)d_{mn} \cdot P],$$

where $P = \sin mx \cdot \cos ny$,

$Q = \cos mx \cdot \sin ny$,

$$R = -\frac{1}{(m^2+n^2)^2}.$$

Again, it is easy to show that both equilibrium and compatibility are satisfied. The body forces are now completely characterized by their Fourier coefficients, c_{mn} and d_{mn}, and the state of stress associated with these is given by Equations (2.24) and (2.26). The displacement field can be obtained by inserting the stresses into Equation (2.3) to obtain the strains and then integrating the strain-displacement relations of Equation (2.4) for the displacements,

$$u = -\frac{R(1+\nu)}{E}[(m^2(1-\nu) + 2n^2)c_{mn}T + nm(1+\nu)d_{mn}S]$$

$$- \omega y + \alpha,$$

$$(2.27)$$

$$v = -\frac{R(1+\nu)}{E}[mn(1+\nu)c_{mn}S + (n^2(1-\nu) + 2m^2)d_{mn}T]$$

$$+ \omega x + \beta,$$

where R is defined as in Equation (2.26), and

$$S = \sin mx \cdot \sin ny,$$

$$T = \cos mx \cdot \cos ny,$$

ω, α, β are arbitrary constants.

One may choose ω so that the rigid body rotation is zero and α and β so that the displacements at the origin are zero,

$$\omega = 0,$$

$$\alpha = \frac{R(1+\nu)}{E}\,[m^2(1-\nu) + 2n^2]c_{mn}, \tag{2.28}$$

$$\beta = \frac{R(1+\nu)}{E}\,[n^2(1-\nu) + 2m^2]d_{mn}.$$

2.4 Fields of Edge Dislocations and Their Dipoles

Fields of dislocations can be handled in a manner similar to that used for body forces. Ascribe to the field a Burger's vector density given by

$$\frac{db_x}{dA} = c_{mn} \cos mx \cdot \cos ny, \tag{2.29}$$

$$\frac{db_y}{dA} = d_{mn} \cos mx \cdot \cos ny.$$

Recalling the edge dislocation solution given by Equations (2.8), the stress, σ_x, at the point (a,b) due to this field acting over the infinite plane is

$$\sigma_x(a,b) = \frac{E}{4\pi} \int_{\infty} \frac{(b-y)(3(a-x)^2 + (b-y)^2)}{r^4} c_{mn} \cos mx \cdot \cos ny \, dA$$

$$+ \frac{E}{4\pi} \int_{\infty} \frac{(a-x)(b-y)^2 - (a-x)^2)}{r^4} d_{mn} \cos mx \cdot \cos ny \, dA,$$

$$\text{or} \quad \sigma_x(a,b) = \frac{E}{4\pi} [c_{mn}(3I_1+I_3) + d_{mn} (I_2-I_o)]. \tag{2.30}$$

For a constant density, m=n=0, and this reduces to

$$\sigma_x(a,b) = \frac{E}{2\pi} [(\pi-1)c_{oo}b - d_{oo}a]. \tag{2.31}$$

Otherwise,

$$\sigma_x(a,b) = \frac{En^2}{(m^2+n^2)^2} [nc_{mn} \cos ma \cdot \sin nb - md_{mn} \sin ma \cdot \cos nb]. \tag{2.32}$$

The remaining stresses, σ_y and τ_{xy}, are obtained in a similar manner. The complete state of stress at the location (x,y) generated by the dislocation field described by Equation (2.29) acting over the entire infinite plane is

$$\sigma_x = \frac{E}{2\pi}[(\pi-1)\, c_{oo}y - d_{oo}x],$$

$$\sigma_y = \frac{E}{2\pi}[c_{oo}y - (\pi-1)d_{oo}x], \qquad (2.33a)$$

$$\tau_{xy} = \frac{E}{2\pi}[-c_{oo}x + d_{oo}y],$$

for m=n=0, and

$$\sigma_x = Rn^2[nc_{mn}P - md_{mn}Q],$$

$$\sigma_y = Rm^2[nc_{mn}P - md_{mn}Q], \qquad (2.33b)$$

$$\tau_{xy} = Rmn[-nc_{mn}Q + md_{mn}P],$$

for m and n not both zero, where

$$R = \frac{E}{(m^2+n^2)^2},$$

$$P = \cos mx \cdot \sin ny, \qquad (2.33c)$$

$$Q = \sin mx \cdot \cos ny.$$

Equilibrium in the absence of body forces is satisfied at every point whereas compatibility is satisfied nowhere since

$$(\sigma_x+\sigma_y) = \frac{E}{m^2+n^2}\,[nc_{mn}P - md_{mn}Q],$$

$$\nabla^2(\sigma_x+\sigma_y) = -E(nc_{mn}P - md_{mn}Q) \qquad (2.34)$$

$$= -E\,\hat{k} \cdot \overline{\nabla} \times \overline{D},$$

where $\overline{D} = \frac{db_x}{dA}\,\hat{i} + \frac{db_y}{dA}\,\hat{j}.$

It is not surprising that compatibility is violated in view of the fact that the hallmark of a dislocation is its discontinuous elastic displacement field. Nonetheless, the significance of Equation (2.34) is not understood. Of course, violation of compatibility destroys the integrability of the strain-displacement relations so that the stresses are the only influences obtainable, except in the case where $\vec{D}$ is irrotational,

$$\overline{\nabla} \times \overline{D} = 0, \qquad (2.35)$$

for which

$$\nabla^2(\sigma_x+\sigma_y) = 0.$$

For this case, a displacement field exists.

Closely related to the edge dislocation is the dislocation dipole, which is useful in the modelling of cracks. There are two basic dipoles, the normal and the shear dipoles. Both are the limiting cases of two edge dislocations of equal and opposite Burger's

vectors approaching each other in such a way that the product of their separation and Burger's vector remains constant. Figure 2.6 shows normal and shear dipoles at various orientations. In Figure 2.6a, let $\sigma(x,y)$ be the state of stress at the point (x,y) generated by the edge dislocation with the positive Burger's vector, b_x, situated at the origin. Let $\sigma^*(x,y)$ be the combined effect of this dislocation and its opposite, located at a distance, h_y, above it. Then

$$\sigma^*(x,y) = \sigma(x,y) - \sigma(x,y-h_y) \doteq h_y \frac{\partial}{\partial y} \sigma(x,y), \qquad (2.36)$$

as $h_y \to 0$. The stress field, $\sigma^*(x,y)$, is defined to be that generated by the normal dipole of Figure 2.6a in the limiting case, $h_y \to 0$ and $b_x \to \infty$, in such a way that the product, $d_x = b_x h_y$, remains constant. This product is termed the strength of the dipole. The important result here is that the stress field, σ^*, of the dipole can be obtained from that of the edge dislocation by replacing the Burger's vector, b_x, occuring in the stress field, σ, by an operator, $d_x \frac{\partial}{\partial y}$, and performing the indicated operation. Symbolically,

$$(b_x \to d_x \frac{\partial}{\partial y}) \to (\sigma \to \sigma^*), \qquad (2.37)$$

which is read: the replacement of b_x by $d_x \frac{\partial}{\partial y}$ generates the stress field σ^* from σ. Similar operations, listed symbolically in Figure 2.6, hold for shear dipoles.

Upon performing the operations indicated in Figure 2.6, the following stress fields are obtained:

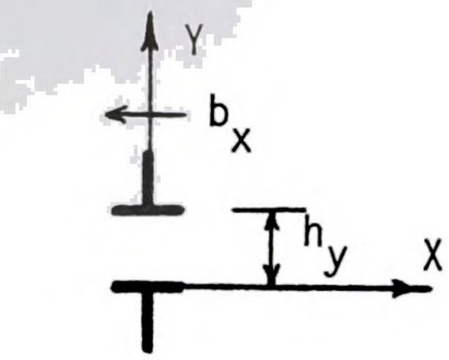

$$(b_x \rightarrow d_x \frac{\partial}{\partial y}) \rightarrow (\sigma \rightarrow \sigma^*)$$

a. A normal dipole with $d_x = b_x h_y$.

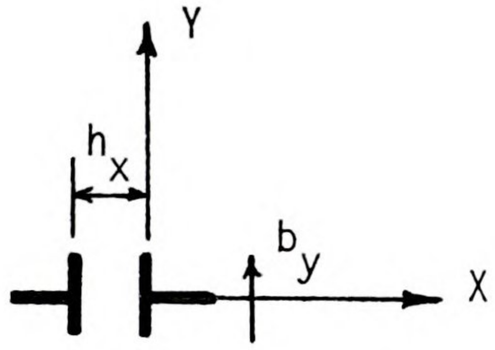

$$(b_y \rightarrow -d_y \frac{\partial}{\partial x}) \rightarrow (\sigma \rightarrow \sigma^*)$$

b. A normal dipole with $d_y = b_y h_x$.

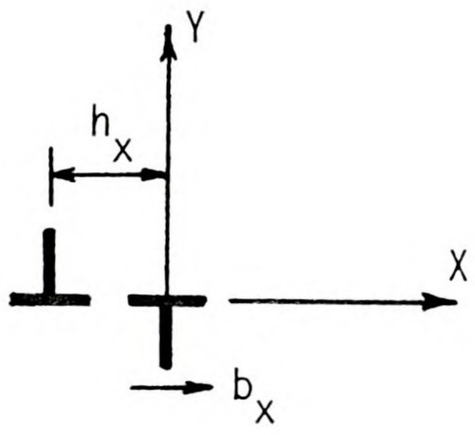

$$(b_x \rightarrow -d_{xy} \frac{\partial}{\partial x}) \rightarrow (\sigma \rightarrow \sigma^*)$$

c. A shear dipole with $d_{xy} = b_x h_x$.

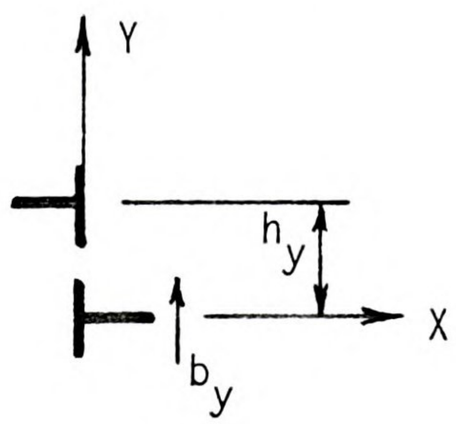

$$(b_y \rightarrow d_{yx} \frac{\partial}{\partial y}) \rightarrow (\sigma \rightarrow \sigma^*)$$

d. A shear dipole with $d_{yx} = b_y h_y$.

Figure 2.6. Normal and shear dipoles in the infinite plane.

$$\sigma_x^* = K_x \cdot (y^4 + 6x^2y^2 - 3x^4),$$

$$\sigma_y^* = K_x \cdot (x^4 - 6x^2y^2 + y^4), \qquad (2.38a)$$

$$\tau_{xy}^* = K_x \cdot 2xy\,(y^2-3x^2),$$

where $$K_x = -\frac{Ed_x}{4\pi r^6}$$

for the dipole shown in Figure 2.6a:

$$\sigma_x^* = K_y(x^4 - 6x^2y^2 + y^4),$$

$$\sigma_y^* = K_y(x^4 + 6x^2y^2 - 3y^4), \qquad (2.38b)$$

$$\tau_{xy}^* = K_y \cdot 2xy\,(x^2 - 3y^2),$$

where $$K_y = -\frac{Ed_y}{4\pi r^6}$$

for the dipole shown in Figure 2.6b:

$$\sigma_x^* = K_{xy} \cdot 2xy\,(y^2 - 3x^2),$$

$$\sigma_y^* = K_{xy} \cdot 2xy\,(x^2-3y^2), \qquad (2.38c)$$

$$\tau_{xy}^* = K_{xy} \cdot (x^4 - 6x^2y^2 + y^4),$$

where $K_{xy} = -\frac{Ed_{xy}}{4\pi r^6}$ or $-\frac{Ed_{yx}}{4\pi r^6}$

for the dipoles shown in Figures 2.6c or 2.6d.

If a dipole is not located at the origin of coordinates, then the x and y coordinates appearing in these equations are relative coordinates,

$$x = x_P - x_D,$$
$$y = y_P - y_D,$$

where (x_P, y_P) and (x_D, y_D) are the coordinates of the point P, at which the stress field is desired, and of the point D, at which the dipole is located, both referred to some global coordinate system. Evidently,

$$\frac{\partial}{\partial x} \equiv \frac{\partial}{\partial x_P},$$

and

$$\frac{\partial}{\partial y} \equiv \frac{\partial}{\partial y_P},$$

so that there is no ambiguity in the operation, $d_x \frac{\partial}{\partial y}$, if the relative y coordinate is replaced by the global y coordinate of the point P, irrespective of the location of the dipole. It is for this reason that the stress field due to the dipole density,

$$\frac{d(d_x)}{dA} = c_{mn} \cos mx \cdot \cos ny, \qquad (2.39a)$$

acting over the infinite plane can be calculated easily from Equations (2.33) by replacing the scalar, c_{mn}, by the operator, $c_{mn} \frac{\partial}{\partial y}$, with $d_{mn} = 0$. Having done this, c_{mn} is associated with the dipole density of Equation (2.39a). The smearing of dipoles over the infinite plane is equivalent to the smearing of edge dislocations with their Burger's vectors replaced by the operators described in Figure 2.6. Therefore, this trick merely takes advantage of the interchangeability of the order of integration involved in the smearing process and partial differentiation involved in the process of generating dipole stress fields from dislocation stress fields. For the distribution of normal dipoles whose density is given by Equation (2.39a), the corresponding state of stress is

$$\sigma_x = \frac{\pi-1}{2\pi} E c_{oo},$$

$$\sigma_y = \frac{E}{2\pi} c_{oo}, \qquad (2.39b)$$

$$\tau_{xy} = 0,$$

for m=n=0, whereas for m and n not both zero,

$$\sigma_x = Rn^2 c_{mn} \cos mx \cdot \cos ny,$$

$$\sigma_y = Rm^2 c_{mn} \cos mx \cdot \cos ny, \qquad (2.39c)$$

$$\tau_{xy} = Rmn c_{mn} \sin mx \cdot \sin ny,$$

where $R = \frac{En^2}{(m^2+n^2)^2}$.

The normal and shear dipoles of Figures 2.6b and 2.6c can also be continuously distribued over the infinite plane with densities similar to that of Equation (2.39a), with d_x replaced by d_y and d_{xy} respectively. The corresponding stress fields are obtained by replacing c_{mn} and d_{mn} in Equations (2.33) by the operators

$$d_{mn} \rightarrow -d_{mn} \frac{\partial}{\partial x} \text{ and } c_{mn} = 0, \tag{2.40}$$

and

$$c_{mn} \rightarrow -c_{mn} \frac{\partial}{\partial x} \text{ and } d_{mn} = 0,$$

thereby obtaining for the distribution,

$$\frac{d(d_y)}{dA} = d_{mn} \cos mx \cdot \cos ny, \tag{2.41a}$$

$$\sigma_x = \frac{E}{2\pi} d_{oo},$$

$$\sigma_y = \frac{\pi-1}{2\pi} E d_{oo}, \tag{2.41b}$$

$$\tau_{xy} = 0,$$

for m=n=0. For m and n not both zero,

$$\sigma_x = Rn^2 d_{mn} \cos mx \cdot \cos ny,$$

$$\sigma_y = Rm^2 d_{mn} \cos mx \cdot \cos ny, \qquad (2.41c)$$

$$\tau_{xy} = Rmn d_{mn} \sin mx \cdot \sin ny,$$

with $$R = \frac{Em^2}{(m^2+n^2)^2}.$$

For the shear dipole distribution with density

$$\frac{d(d_{xy})}{dA} = c_{mn} \cos mx \cdot \cos ny, \qquad (2.42a)$$

$$\sigma_x = \sigma_y = 0, \qquad (2.42b)$$

$$\tau_{xy} = \frac{E}{2\pi} c_{oo},$$

for m=n=0, and for m and n not both zero,

$$\sigma_x = Rn^2 c_{mn} \sin mx \cdot \sin ny,$$

$$\sigma_y = Rm^2 c_{mn} \sin mx \cdot \sin ny, \qquad (2.42c)$$

$$\tau_{xy} = Rmn C_{mn} \cos mx \cdot \cos ny,$$

with $$R = \frac{Emn}{(m^2+n^2)^2}.$$

Of course, for the stress fields of Equations (2.39c), (2.41c), and (2.42c), equilibrium is satisfied at every point in the infinite plane while compatibility is satisfied nowhere. Both the normal and shear dipole may be rotated through an arbitrary angle and the resulting stress fields calculated. The topic of dipole transformations is taken up in Appendix B and is later referred to in the discussion of crack fields.

The numerical procedure for the solution of elasticity problems described earlier can now be extended to include sources of internal stress other than body forces, such as edge dislocation fields and their dipoles. As with body forces, the field is first characterized by a set of Fourier coefficients chosen to represent the field inside the body without regard to what it represents outside. These coefficients are then used to ascertain boundary conditions already present as a result of the field, and the concentrated loads acting outside the body are used to adjust these boundary conditions to those desired. The resulting interior stress field is obtained by superposing the separate effects of the concentrated loads and of all sources of internal stress. The only restriction placed on this method when used with dislocations and dipoles is that displacement boundary conditions may not be prescribed. Violation of compatibility prohibits the integration of the strain-displacement relations so that displacement fields for distributions of dislocations and dipoles are unobtainable. This inadequacy can be attributed to the fact that a continuum of dislocations is physically unattainable. The initial continuum into which the body is embedded is altered by

the introduction of dislocations which add and subtract material at every point, thereby creating a new continuum. The preceding results are nevertheless useful, for if a large but finite number of dislocations are known to exist in a given area, the stress field caused by these is much more easily and accurately approximated by proceeding to the limit and assigning a density to this collection than by treating each dislocation individually. Furthermore, since the displacement field will oscillate rapidly inside this area and since uncertainties in the displacement field due to the approximations used in the linear theory of elasticity are on the order of magnitude of the displacements themselves [6], the value of such results is questionable.

CHAPTER 3

THE NUMERICAL SOLUTION OF CRACK PROBLEMS

3.1 The Modelling of Cracks by Dipoles

Edge dislocations can be used advantageously to model cracks in both tension and shear. Figure 3.1a shows a slit crack of length 2c situated in an infinite plate in uniform tension, σ, applied at infinity. Figure 3.1b shows the same plate with the crack removed and a line distribution of infinitesimal edge dislocations in its place. The distribution can be made to model the crack by requiring that the total stress field satisfy traction free boundary conditions along the portion of the x axis, $|x| < c$, representing the crack. That is,

$$\sigma_y(x,0) = \tau_{xy}(x,0) = 0, \qquad (3.1)$$

for $|x| < c$. These tractions result from the combined effect of the external stress field, σ, hereafter referred to as the resolved stress field, and the stress field due to the dislocations themselves, hereafter referred to as the self stress field. The shear condition is satisfied automatically by the type of dislocation chosen to represent the crack. That is, for the single edge dislocation of Figure 2.2b, the shear stress on the x-axis is zero by Equation (2.8b), whereas the normal stress is

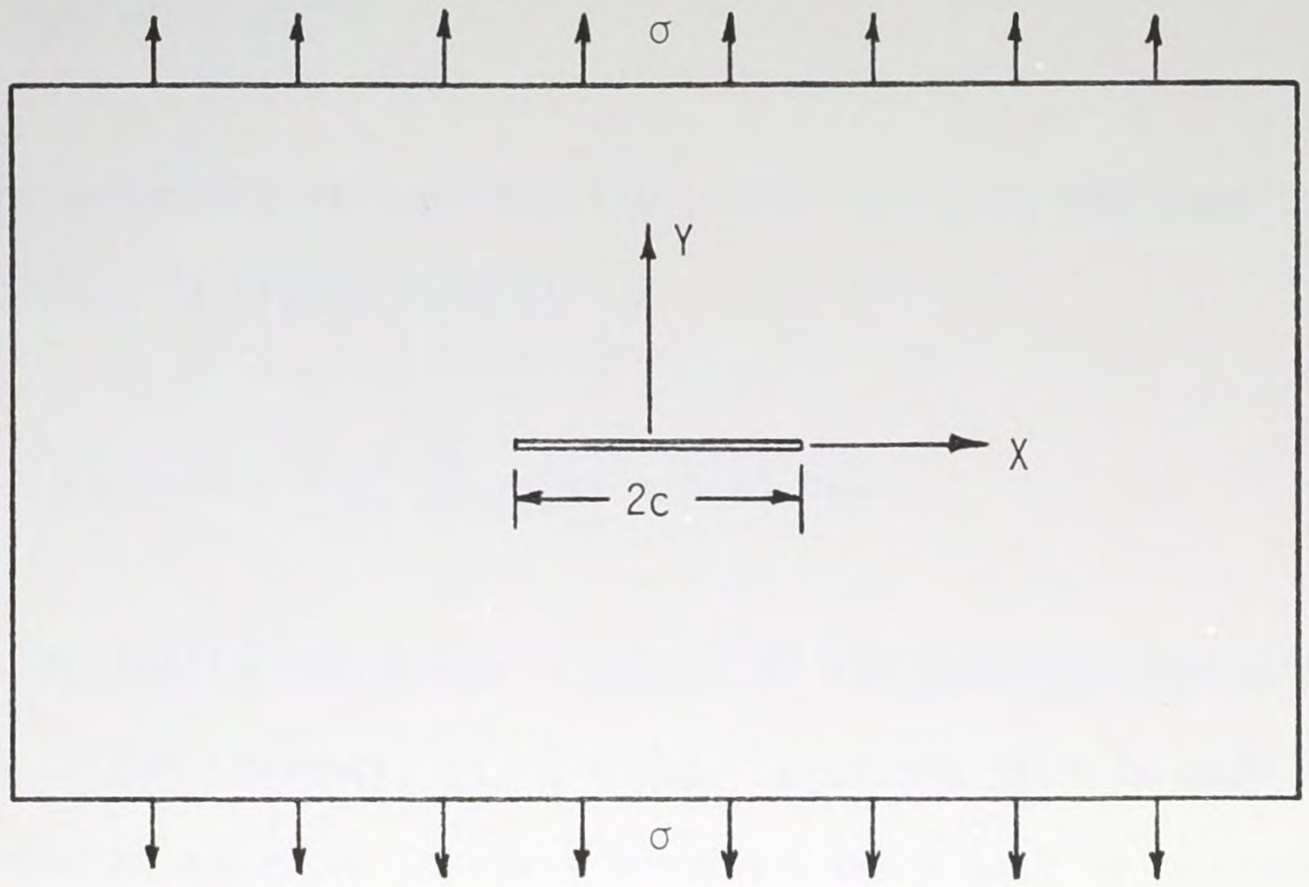

a. A slit crack in an infinite plate under uniform tension.

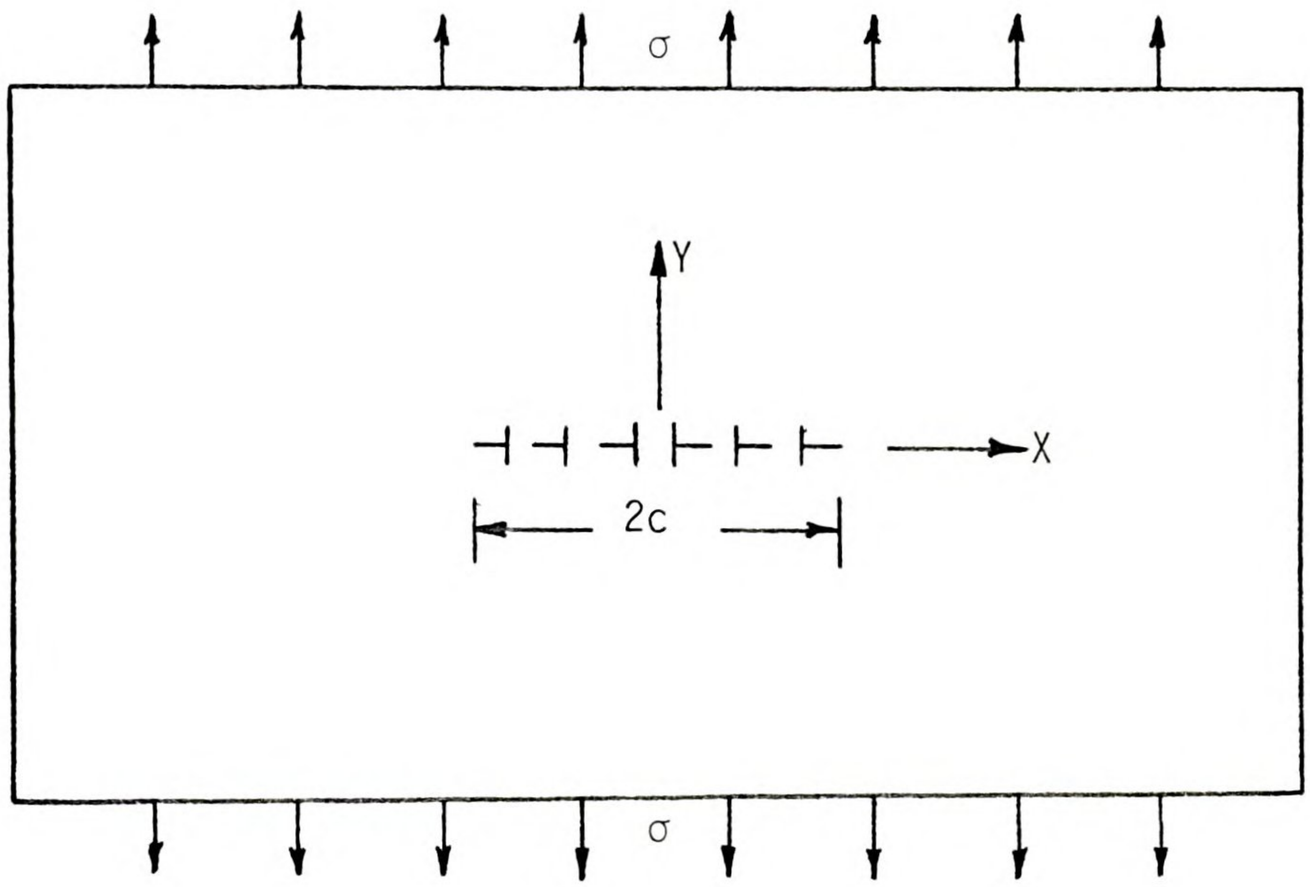

b. A slit crack modelled by a dislocation line.

Figure 3.1. A slit crack and its dislocation equivalent.

$$\sigma_y(x,0) = \frac{-Eb_y}{4\pi x}.$$

By the principle of superposition, the stress on the x-axis corresponding to Figure 3.1b is

$$\sigma_y(x,0) = \sigma + \int_{-c}^{c} \frac{-E}{4\pi} \frac{1}{(x-\xi)} \cdot \beta(\xi)\, d\xi, \qquad (3.2)$$

where $\beta(\xi)d\xi$ is the Burger's vector of the infinitesimal dislocation lying in the interval, $(\xi, \xi + d\xi)$. Equating this to zero and rearranging gives an integral equation which must be satisfied identically in x for $|x| < c$. The solution makes use of the Hilbert transform discussed in [6]:

$$\frac{-4\pi\sigma}{E} = \int_{-c}^{c} \frac{\beta(\xi)d\xi}{x-\xi}, \qquad (3.3a)$$

requiring that

$$\beta(\xi) = -\frac{4\sigma}{E} \frac{\xi}{(c^2-\xi^2)^{1/2}}. \qquad (3.3b)$$

Physically, this corresponds to inserting a slab of material of length 2c and of variable width into the slit crack of Figure 3.1a. This results in a compressive self stress field at the crack faces which is subsequently removed by the tension, σ, at infinity. The distribution, $\beta(\xi)$, is valid only for the loading shown in Figure 3.

However, a stress, σ_x, may be imposed without affecting the results. The stress, σ, may be assigned negative values, provided that the crack is regarded as an 'open crack'. That is, it is

assumed that a compressive stress is never large enough to close the crack, thereby effectively eliminating the presence of the crack.

When the loading in Figure 3.1 is changed to a constant shear stress, τ, the dislocations in Figure 3.1b are rotated clockwise through a right angle and distributed according to

$$db_x = \beta(\xi)d\xi. \tag{3.4}$$

The only nontrivial boundary condition to be satisfied in this case is

$$\tau_{xy}(x,0) = \tau + \int_{-c}^{c} \frac{-E}{4\pi} \cdot \frac{1}{x-\xi} \cdot \beta(\xi)d\xi. \tag{3.5}$$

The solution to this equation is identical to that in Equation (3.3b) with σ replaced by τ.

The self stress field of Figure 3.1b at any point in the infinite plane can now be obtained by superposition, using the known distribution of Equation (3.3b). Figure 3.2 shows such a point, P, with rectangular coordinates (ac, bc), and crack tip coordinates, (rc, θ), where c is the crack half-length. The determination of the stress field requires the evaluation of four integrals,

$$I_n = \int_{-c}^{c} \frac{(ac-x)^n \cdot (bc)^{3-n}}{[(ac-x)^2 + (bc)^2]^2} \cdot \frac{xdx}{(c^2-x^2)^{1/2}} \tag{3.6}$$

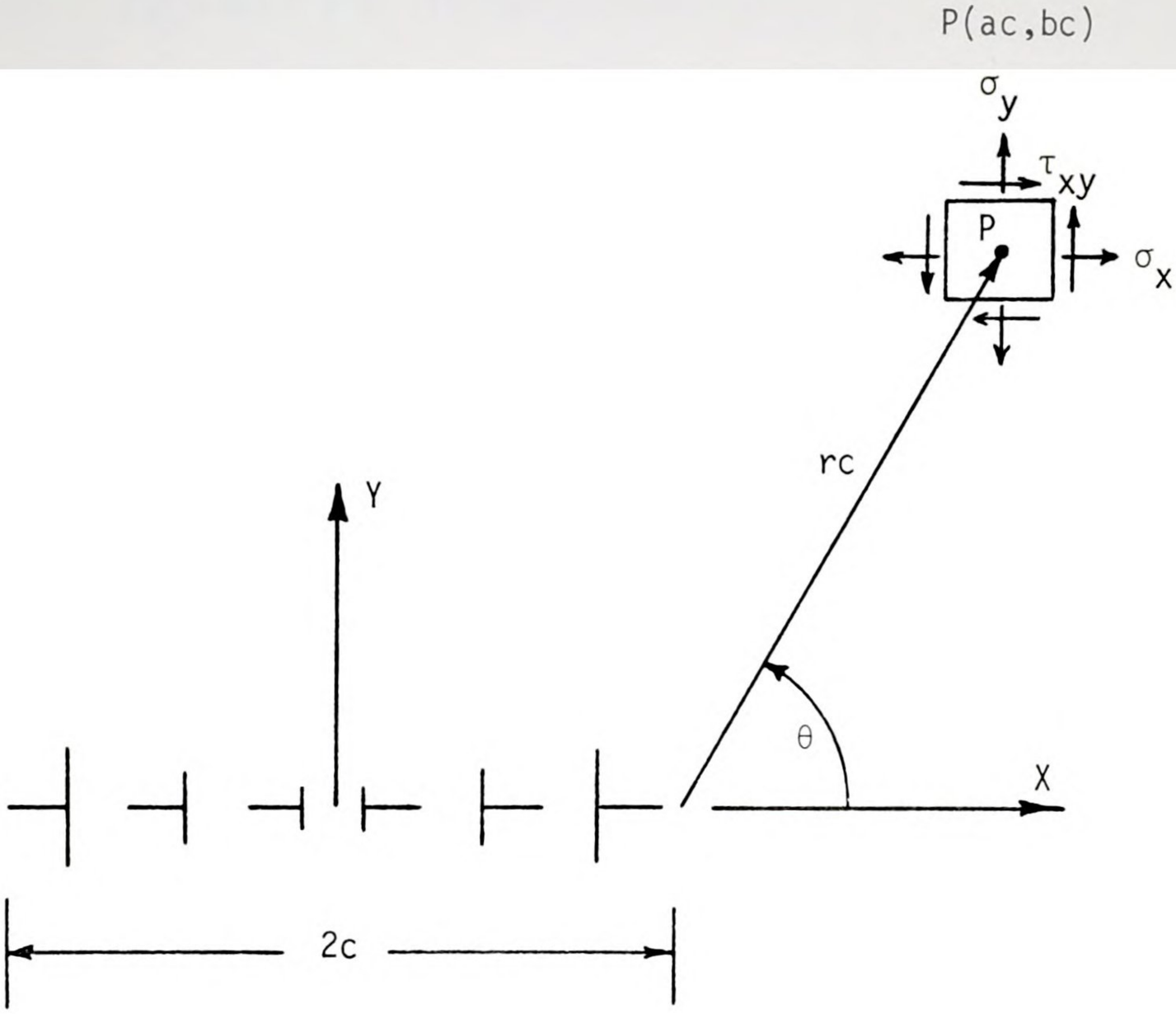

Figure 3.2. The self-stress field at point P.

where n = 0, 1, 2, 3. These integrals are treated in Appendix C.

Using Equations (2.8), (3.3b), and (3.6), the self stress field for a crack in tension becomes

$$\sigma_x = \frac{E}{4\pi}\left(\frac{-4\sigma}{E}\right)(I_1-I_3),$$

$$\sigma_y = -\frac{E}{4\pi}\left(\frac{-4\sigma}{E}\right)(3I_1+I_3), \qquad (3.7)$$

$$\tau_{xy} = \frac{E}{4\pi}\left(\frac{-4\sigma}{E}\right)(I_0-I_2).$$

Using Equations (2.8), (3.3b), and (3.6), the self stress field generated by the dislocation model of a crack in a state of shear becomes

$$\sigma_x = \frac{E}{4\pi}\left(\frac{-4\tau}{E}\right)(3I_2+I_0),$$

$$\sigma_y = -\frac{E}{4\pi}\left(\frac{-4\tau}{E}\right)(I_2-I_0), \qquad (3.8)$$

$$\tau_{xy} = -\frac{E}{4\pi}\left(\frac{-4\tau}{E}\right)(I_3-I_1).$$

Substituting the asymptotic expressions for the integrals, I_n, as $r \to 0$ from Appendix C into Equations (3.7) and (3.8) yields the stresses in the immediate vicinity of the crack tip. For a crack in tension, the self stress of the dislocation distribution is, after simplification,

$$\sigma_x = \frac{K_I}{(2\pi rc)^{1/2}} \cos\frac{\theta}{2}\left[1 - \sin\frac{\theta}{2}\sin\frac{3\theta}{2}\right],$$

$$\sigma_y = \frac{K_I}{(2\pi rc)^{1/2}} \cos\frac{\theta}{2}\left[1 + \sin\frac{\theta}{2}\sin\frac{3\theta}{2}\right], \qquad (3.9a)$$

and $$\tau_{xy} = \frac{K_I}{(2\pi rc)^{1/2}} \sin\frac{\theta}{2}\cos\frac{\theta}{2}\cos\frac{3\theta}{2},$$

where $K_I = \sigma(\pi c)^{1/2}$.

Similarly, for a crack in shear, the self stress is

$$\sigma_x = -\frac{K_{II}}{(2\pi rc)^{1/2}} \sin\frac{\theta}{2}\left[2 + \cos\frac{\theta}{2}\cos\frac{3\theta}{2}\right],$$

$$\sigma_y = \frac{K_{II}}{(2\pi rc)^{1/2}} \cos\frac{\theta}{2}\sin\frac{\theta}{2}\cos\frac{3\theta}{2}, \qquad (3.9b)$$

$$\tau_{xy} = \frac{K_{II}}{(2\pi rc)^{1/2}} \cos\frac{\theta}{2}\left[1 - \sin\frac{\theta}{2}\sin\frac{3\theta}{2}\right],$$

where $K_{II} = \tau(\pi c)^{1/2}$.

The load and geometry dependent terms, K_I and K_{II}, are the classical mode I (tension) and mode II (shear) stress intensity factors of fracture mechanics, derived here in a different way than that used by Irwin [22], who found a series expansion of a stress function obtained by complex variable methods for a highly eccentric elliptical hole in an infinite plate. It is important to note that the values for σ and τ in the stress intensity factors are the resolved stress values; that is, the stresses due to all

influences excluding the crack itself. More specifically, in the event that the resolved stress field varies appreciably over the length of the crack, σ and τ are the resolved stresses at the crack tip.

Now to an observer situated at a point several crack lengths away from the crack itself, the dislocation equivalent of Figure 3.1b appears as a superdipole, or simply a normal dipole at the origin of strength d_y, consistent with the notation used in Figure 2.6b. Moreover, the stress fields of the original dislocation distribution and the dipole at points far from the crack do not differ significantly provided that d_y is chosen properly. The strength of the infinitesimal dipole formed by the dislocations of Burger's vector, $\beta(x)dx$, at the points $(-x, 0)$ and $(x, 0)$ is

$$d(d_y) = (\beta(x)dx) \cdot (2x) = -\frac{8\sigma}{E} \frac{x^2 dx}{(c^2-x^2)^{1/2}}, \tag{3.10}$$

which implies that

$$d_y = -\frac{8\sigma}{E} \int_0^c \frac{x^2 dx}{(c^2-x^2)^{1/2}} = -\frac{2\pi c^2}{E} \sigma. \tag{3.11}$$

The same reasoning is used for the shear dipole which models a crack in shear:

$$d_{xy} = -\frac{2\pi c^2}{E} \tau. \tag{3.12}$$

Figure 3.3a shows a slit crack of length 2c in an infinite plate in a general state of stress while Figure 3.3b shows the dipole model of this where the dipole strengths are given by

$$d_x = 0,$$

$$d_y = -\frac{2\pi c^2}{E}\sigma_y, \tag{3.13}$$

$$d_{xy} = -\frac{2\pi c^2}{E}\tau_{xy}.$$

If the crack is now rotated through an angle, θ, as shown in Figure 3.4a, the dipole state referred to the $\bar{x}$-$\bar{y}$ system is given by

$$d_{\bar{x}} = 0,$$

$$d_{\bar{y}} = -\frac{2\pi c^2}{E}\sigma_{\bar{y}}, \tag{3.14}$$

$$d_{\bar{x}\bar{y}} = -\frac{2\pi c^2}{E}\tau_{\bar{x}\bar{y}}.$$

Using the transformation properties of dipoles described in Appendix B, this dipole state referred to the x-y system is

$$d_x = d_{\bar{y}} \sin^2\theta - d_{\bar{x}\bar{y}} \sin\theta\cos\theta,$$

$$d_y = d_{\bar{y}} \cos^2\theta + d_{\bar{x}\bar{y}} \sin\theta\cos\theta, \tag{3.15}$$

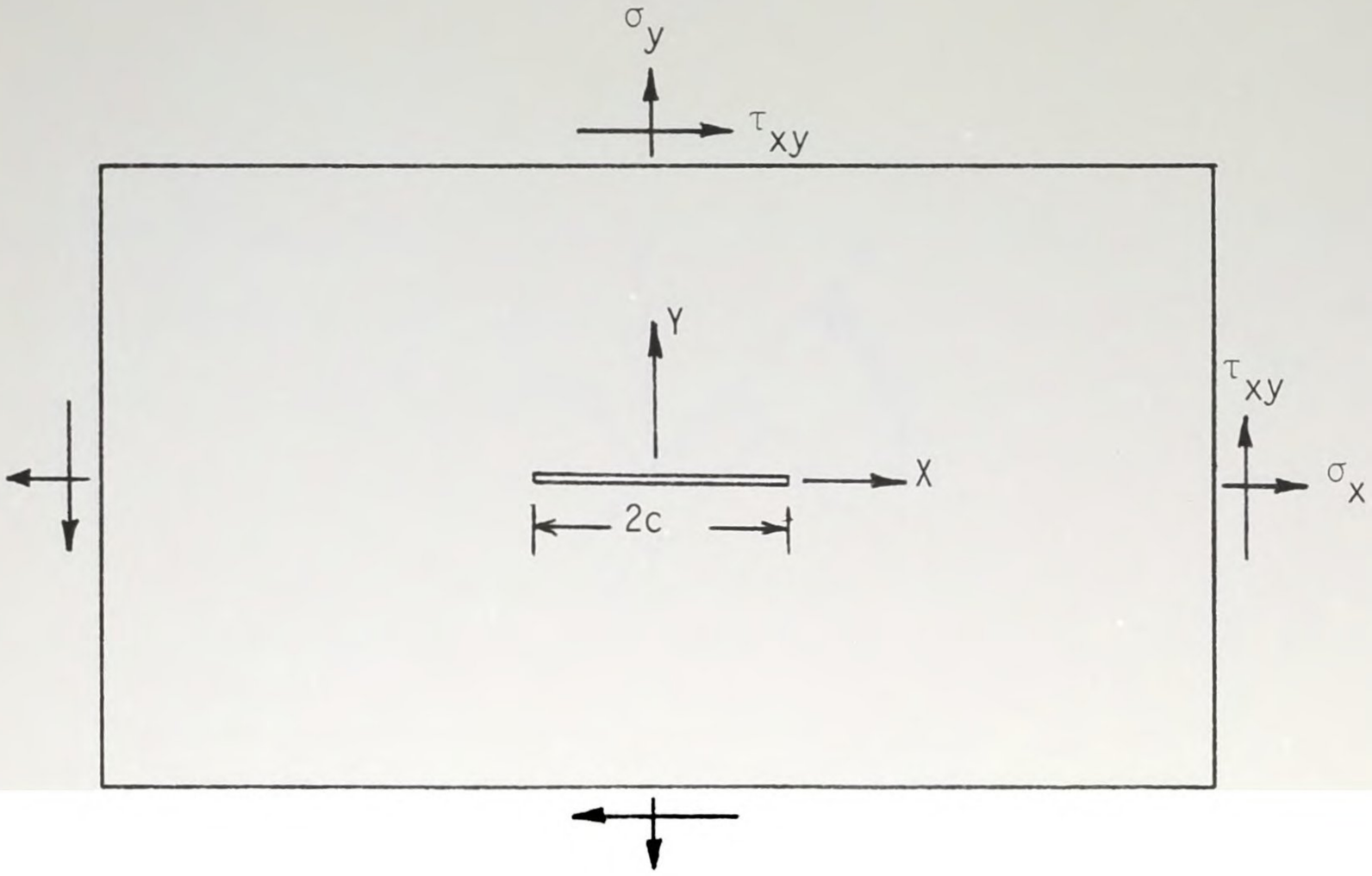

a. A crack in a general state of stress.

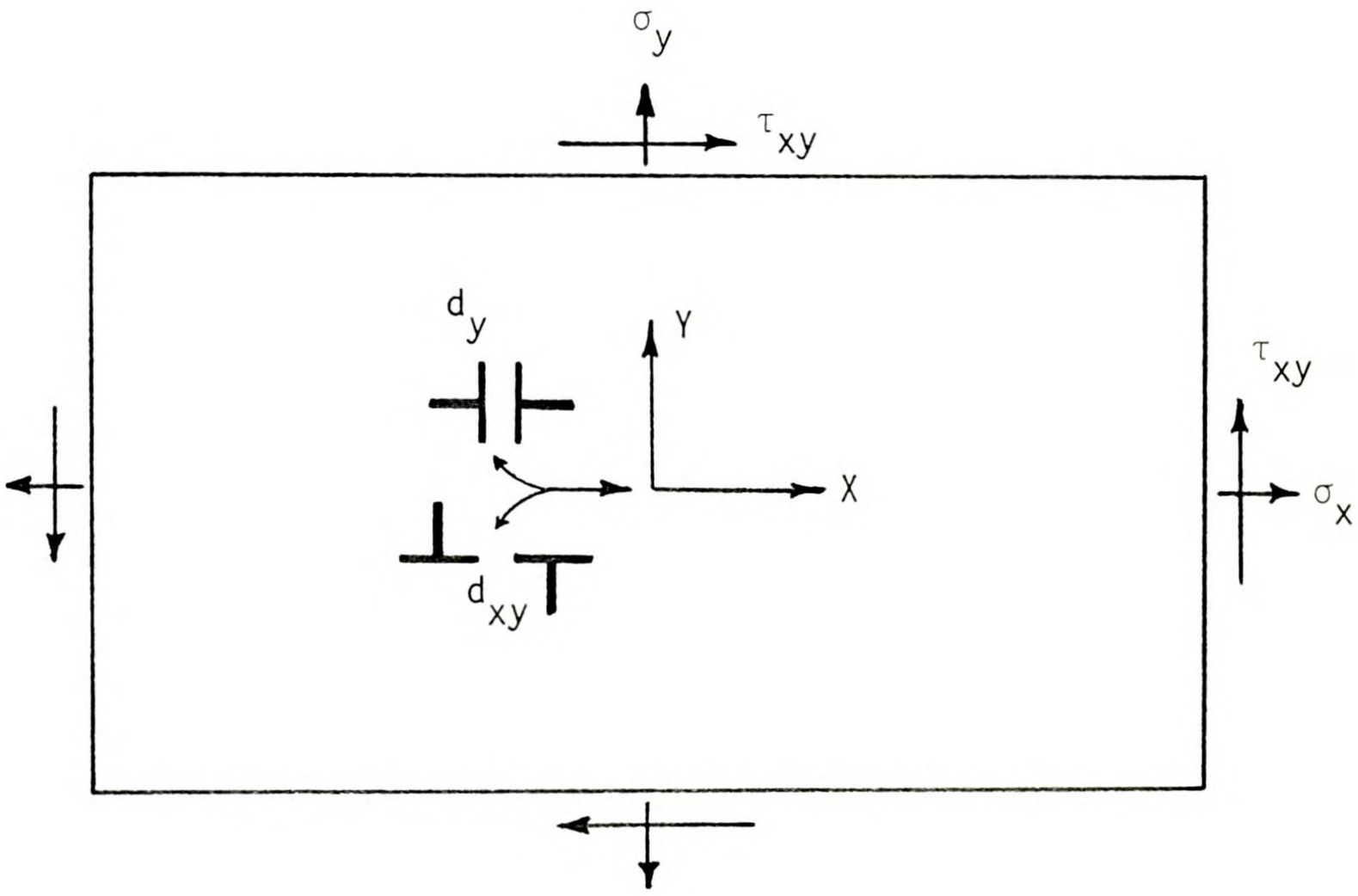

b. The dipole model.

Figure 3.3. A crack and its dipole model.

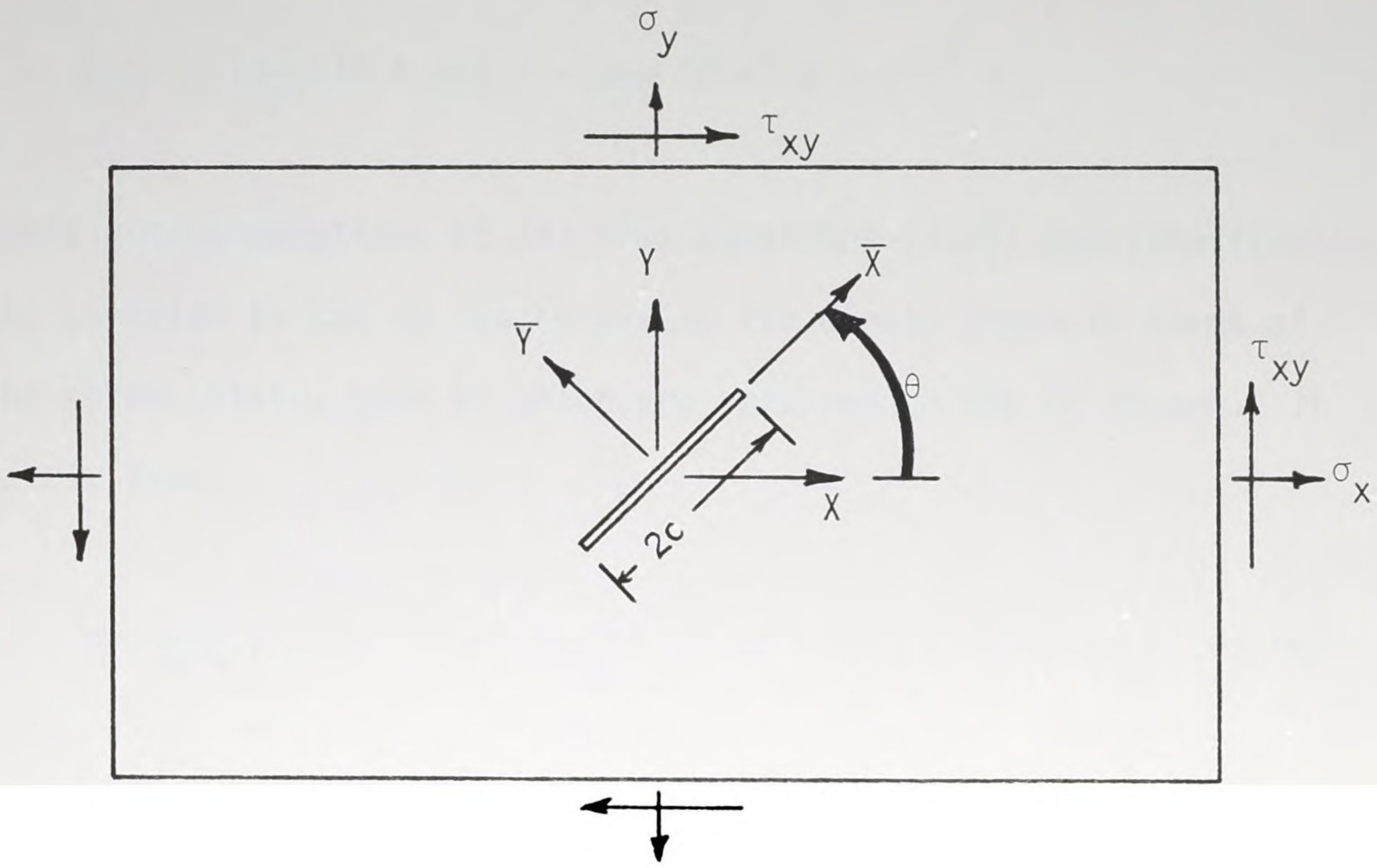

a. A rotated crack in a general state of stress.

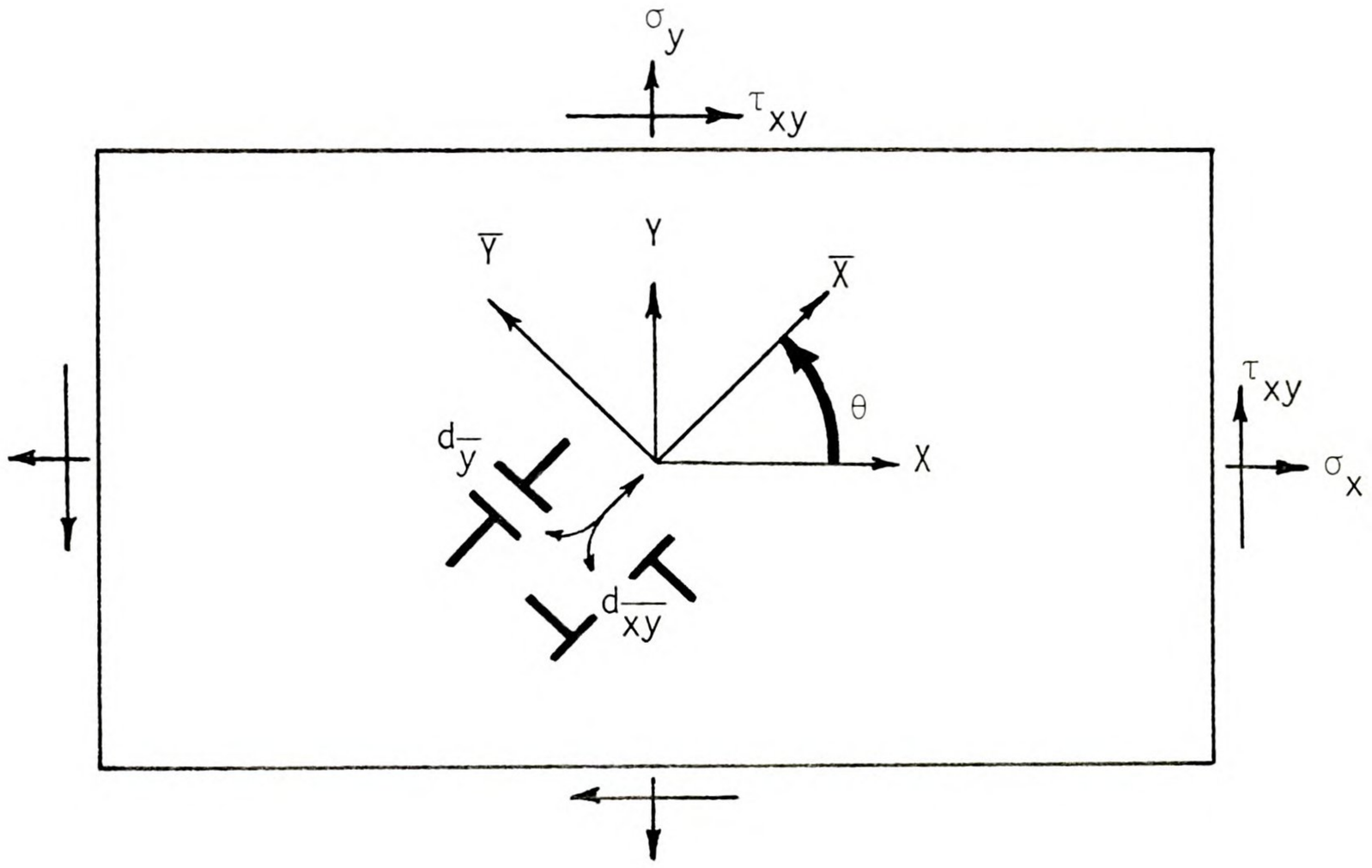

b. The dipole model referred to the $\overline{xy}$ system.

Figure 3.4. A rotated crack and its dipole model.

$$d_{xy} = -2d_{\overline{y}} \sin\theta \cos\theta + d_{\overline{xy}} (\cos^2\theta - \sin^2\theta).$$

Substituting Equations (3.14) into Equations (3.15) and transforming the stresses to the xy system yields the dipole state in terms of the stress state, both of which are referred to the xy system. In matrix form,

$$\underline{d} = \underline{P}\,\underline{\sigma}\ , \tag{3.16a}$$

where

$$\underline{d}^T = (d_x,\ d_y,\ d_{xy}), \tag{3.16b}$$

$$\underline{\sigma}^T = (\sigma_x,\ \sigma_y,\ \tau_{xy}),$$

and

$$\underline{P} = -\frac{2\pi c^2}{E}\begin{bmatrix} \alpha & 0 & \beta \\ 0 & 1-\alpha & \beta \\ \beta & \beta & 1 \end{bmatrix} \tag{3.16c}$$

with $\alpha = \sin^2\theta$ and $\beta = -\sin\theta\cos\theta$.

It can be shown that P is singular. This means that the inverse problem of specifying the dipole state and determining the corresponding stress state for a given crack geometry is not possible. Restated, a given dipole state is not necessarily the model of some crack in a state of stress. Rather, a very limited class of dipole states are admissable as crack models.

3.2 Solutions to Crack Problems

Numerical techniques, as presented here, for obtaining the stress and displacement fields in bodies containing cracks can be divided into two categories, iterative and direct. Both techniques use the dipole model for cracks and are capable of handling any finite number of cracks of arbitrary size, orientation, and location within the body. Of the two techniques, the iterative one is simpler in content and will be presented first. The input information required to solve the problem consists of the locations, lengths, and orientations of all cracks as well as prescribed boundary conditions. The iterative method proceeds as follows:

1) Solve the elasticity problem in the manner described in Chapter 2 (see Equations (2.10)) initially as if there were no cracks present.
2) Having determined the state of stress, $\underline{\sigma}$, at each of the crack sites, infer what the dipole state should now be from Equations (3.16), using the actual crack lengths and orientations.
3) The nonzero dipole field of step (2) perturbs the boundary conditions previously satisfied at the conclusion of step (1), thus requiring an adjustment in the external concentrated loads of Figure 2.4 to remove these perturbations.
4) This having been done, repeat steps (2) and (3) until convergence is obtained. That is, until successive iterates of the dipole state cease to change.

Recall that Equations (3.16) apply only to open cracks. If a crack is allowed to close (to touch faces) under a compressive stress normal to the crack face, then the dipole strength, $d_{\overline{y}}$, of Equation (3.14) should be set equal to zero. This necessitates changing the $\underline{P}$ matrix of Equation (3.9) to

$$\underline{P} = -\frac{2\pi c^2}{E}\begin{bmatrix} \alpha & -\alpha & -\beta \\ -\alpha & \alpha & \beta \\ -\beta & \beta & \gamma \end{bmatrix} \tag{3.17a}$$

where
$$\alpha = \sin^2\theta \cdot \cos^2\theta,$$
$$\beta = \sin\theta\cos\theta(\cos^2\theta - \sin^2\theta), \tag{3.17b}$$
$$\gamma = (\cos^2\theta - \sin^2\theta)^2.$$

The appropriate $\underline{P}$ matrix is chosen according to the situation encountered in step (2).

As with any iterative technique, convergence depends upon the initial choice of the iterate. In this case, the iterate is the dipole state and its initial value is zero. If convergence is not obtained by this choice, step (1) may be performed on an initial dipole state which is based on an intelligent guess as to what the end result should be, or, the entire iterative method may be used to refine the results obtained from the direct method.

In the direct method, several vectors and matrices are used with the convention that a lower case letter, such as $\underline{b}(n \times 1)$, represents a column vector with n rows while an upper case

letter, $\underline{C}(n \times m)$, represents a matrix with n rows and m columns Let there be n prescribed boundary conditions and m crack sites assigned to the interior of the body.

Introduce the following quantities:

1) $\underline{b}(n \times 1)$, containing the prescribed boundary values.
2) $\underline{w}(n \times 1)$, containing the magnitudes of the concentrated loads outside the body.
3) $\underline{d}(3m \times 1)$, containing the dipole states for each of the m crack sites; partitioned as m triplets, (d_x, d_y, d_{xy}).
4) $\underline{\sigma}(3m \times 1)$, containing the resolved stress state at each of the m crack sties; also partitioned as m triplets, $(\sigma_x, \sigma_y, \tau_{xy})$.
5) $\underline{P}(3m \times 3m)$, relating the dipole state to the stress state via Equation (3.9); tridiagonal.
6) $\underline{C}(n \times n)$, relating the influence of the concentrated loads on the boundary conditions.
7) $H(n \times 3m)$, containing the influence of the dipole field on the boundary.
8) $G(3m \times n)$, containing the influence of the concentrated loads on the resolved stress field.
9) $Q(3m \times 3m)$, containing the influence of the dipole field on itself.

The context in which these vectors and matrices are used should serve to clarify their meaning. Satisfaction of prescribed boundary conditions requires that

$$\underline{b} = \underline{C}\,\underline{w} + \underline{H}\,\underline{d}. \tag{3.18}$$

The resolved stress field at the crack sites is due to both the concentrated loads and the dipole field acting in concert,

$$\underline{\sigma} = \underline{G}\,\underline{w} + \underline{Q}\,\underline{d}. \tag{3.19}$$

The modelling of cracks by dipoles is represented by the expanded version of Equations (3.16),

$$\underline{d} = \underline{P}\,\underline{\sigma}. \tag{3.20}$$

The principle of superposition provides the justification for the form of the above equations. Substituting Equation (3.20) into Equation (3.19) and solving for the resolved stresses yields

$$\underline{\sigma} = \underline{B}\,\underline{w}, \tag{3.21}$$

where

$$\underline{B} = (\underline{I} - \underline{Q}\,\underline{P})^{-1}\,\underline{G}. \tag{3.22}$$

Equation (3.20) now becomes

$$\underline{d} = \underline{P}\,\underline{B}\,\underline{w}, \tag{3.23}$$

which is substituted into Equation (3.18) to yield

$$\underline{w} = (\underline{C} + \underline{H}\,\underline{P}\,\underline{B})^{-1}\,\underline{b}. \tag{3.24}$$

Now that $\underline{w}$ is known, the resolved stress field can be calculated by Equation (3.21). Hence, the stress intensity factors, K_I and K_{II}, are known at each crack site. One may now refine the stress field in the vicinity of a crack by removing the representative dipole there and returning to the original linear distribution of infinitesimal edge dislocations from which the dipole state was created (see Figure 3.1). That is, return to each crack the spatial extent which it had before being reduced to a set of dipoles acting at a point.

The well known Griffith criterion,

$$K_I = \sigma_o(\pi c)^{1/2} = 2\gamma E, \tag{3.25}$$

may also be used at this point to determine which cracks, if any, will propagate. This criterion is founded on an energy argument applied to the crack in Figure 3.1a. Basically, it states that a crack will propagate when the release of elastic strain energy stored in the plate accompanying an incremental increase in crack length is at least as great as the energy absorbed by the crack in the creation of new crack surfaces. See [6] for a more detailed discussion. The terms appearing in Equation (3.25) are c, the crack half-length, γ, the surface energy density for the

material considered, E, the modulus of elasticity, and σ_o, the nominal stress normal to the crack face at which propagation takes place, and which should be compared to the resolved stresses, $\underline{\sigma}$, of Equation (3.21).

Experimental evidence [6] indicates that for granular media,

$$\sigma_o \propto d^{-1/2}, \tag{3.26a}$$

where d is the grain diameter, whereas Griffith's criterion implies that

$$\sigma_o \propto c^{-1/2}. \tag{3.26b}$$

The two can be made compatible by assuming that cracks are the result of unbonded surfaces occurring on grain boundaries and that statistically,

$$c \propto d.$$

Now since

$$d \propto L,$$

where L is the circumference of a typical grain, the ratio of the crack length or unbonded length to the grain circumference is expected to be a material property,

$$\frac{c}{L} = \varepsilon < 1, \tag{3.27}$$

specifying the extent to which the body is cracked. Strictly speaking, ε is not a material property in that it cannot be ascribed to every point in the body. Rather, it is a property assigned to a very small but nevertheless finite area, A_g, the grain area.

The transition from a discrete distribution of finite sized cracks to a continuous distribution of microcracks can be accomplished by replacing the dipole representing the single crack associated with a particular grain site by a constant distribution of infinitesimal dipoles acting over the grain area. From Equation (3.20) the dipole model of a single crack is characterized by

$$d = -\frac{2\pi c^2}{E}\sigma.$$

Dividing this expression by the grain area and using Equation (3.27) gives

$$\frac{d}{A_g} = -\frac{2\pi\varepsilon^2}{E}\left(\frac{L^2}{A_g}\right)\sigma. \tag{3.28}$$

The continuous distribution of microdipoles replacing this single dipole is now assigned the density

$$\Delta = \frac{d(d)}{dA} = \frac{d}{A_g} = -\frac{2\pi}{E}\varepsilon^2 s\sigma, \tag{3.29}$$

where $s = \frac{L^2}{A_g}$.

Density is a property at a point in a continuum. The point at which Δ is assigned can legitimately be taken as anywhere within the grain area since the context in which it will be used, namely elasticity theory, suffers from ambiguities of a similar nature. The right hand side of Equation (3.29) also qualifies as a property defined at a point since both ε and s are grain <u>shape</u> dependent not grain <u>size</u> dependent. Of course, σ and E are already properties defined at a point. The modelling of a continuum filled with microcracks by a density of dipoles is therefore characterized by a relationship similar to Equations (3.16),

$$\underline{\Delta} = \underline{P}\,\underline{\sigma}, \tag{3.30a}$$

where

$$\underline{\Delta}^T = (\Delta_x, \Delta_y, \Delta_{xy}), \tag{3.30b}$$

and

$$\underline{P} = -\frac{2\pi}{E}\varepsilon^2 s \begin{bmatrix} \alpha & 0 & \beta \\ 0 & 1-\alpha & \beta \\ \beta & \beta & 1 \end{bmatrix} \tag{3.30c}$$

The densities may now be expanded into Fourier series representing the dipole distributions inside the body and with the aid of Equations (2.39c), (2.41c), and (2.42c), the Fourier coefficients determine the stress field anywhere in the body. As with the discrete distribution of cracks, either an iterative or a direct technique may be used to solve problems with a known distribution of microcracks inside the body. The iterative method is almost identical to that described earlier with only minor alterations and consequently will not be recalled here. The direct approach involves the introduction of some new terms:

1) $\underline{\Delta}(3m \times 1)$, containing the dipole densities at m arbitrarily chosen sites. Crack sites are now everywhere and Equation (3.30**a**) must be satisfied at every point in the body. This of course poses an enormous problem so that one must settle for satisfaction at m points only.
2) $\underline{f}(3m \times 1)$, containing the Fourier coefficients associated with $\underline{\Delta}$.
3) $\underline{F}(3m \times 3m)$, relating $\underline{f}$ to $\underline{\Delta}$.

The satisfaction of prescribed boundary conditions requires that

$$\underline{b} = \underline{C}\,\underline{w} + \underline{H}\,\underline{f}. \tag{3.31}$$

The resolved (now total) stress field at the chosen crack sites is

$$\underline{\sigma} = \underline{G}\,\underline{w} + \underline{Q}\,\underline{f}. \tag{3.32}$$

The model of a cracked continuum by a dipole continuum is defined by

$$\underline{\Delta} = \underline{P}\,\underline{\sigma}, \tag{3.33}$$

and the Fourier expansions satisfy

$$\underline{f} = \underline{F}\,\underline{\Delta}. \tag{3.34}$$

When used in the context above, $\underline{F}$ is highly redundant; that is, it is nine times the necessary size. Substituting Equation (3.33) into Equation (3.34) and the result into Equation (3.32) yields a relation which can be solved for $\underline{\sigma}$,

$$\underline{\sigma} = \underline{B}\,\underline{w}, \tag{3.35}$$

where

$$\underline{B} = (\underline{I} - \underline{Q}\,\underline{F}\,\underline{P})^{-1}\underline{G}. \tag{3.36}$$

Now

$$\underline{f} = \underline{F}\,\underline{P}\,\underline{\sigma} = \underline{F}\,\underline{P}\,\underline{B}\,\underline{w}, \tag{3.37}$$

which is substituted into Equation (3.31) to yield

$$\underline{w} = (\underline{C} + \underline{H}\ \underline{F}\ \underline{P}\ \underline{B})^{-1}\underline{b}. \tag{3.38}$$

Now that $\underline{w}$ is known, $\underline{f}$ can be calculated, and the state of stress at any point in the body can be obtained by the application of Equations (2.6), (2.39c), (2.41c), and (2.42c). Therefore, procedurally, the problem is straightforward.

CHAPTER 4

APPLICATIONS AND NUMERICAL RESULTS

4.1 The Basic Computer Program

The basic program which is responsible for the satisfaction of prescribed boundary conditions appears in its skeleton form in Appendix D. The superposition method of Section 2.2 is used in connection with Equations (2.10). The program accomplishes the following: it solves any plane stress/plane strain elasticity problem without body forces or other sources of internal stress where the body is of any shape and is subjected to pure traction boundary conditions. It is also self-contained in the sense that it uses no computer library subroutines. The variables appearing in the program are:

NB The number of boundary points at which boundary conditions are prescribed. Note that there are two conditions to be satisfied at every point so that there are 2 • NB unknown load magnitudes to be adjusted.

NF The number of field points inside the body at which the stresses are desired.

XB(NB x 2) The matrix containing the x and y coordinates of the boundary points.

XS(NB x 2) The matrix containing the source coordinates. The source points are those points at which the concentrated loads are located outside the body.

XF(NF x 2) The matrix containing the field coordinates.

PHI(NB) The vector containing the normal angles, α, shown in Figure 2.4 (in degrees).

C(2NB x 2NB + 1) The influence matrix of Equation (2.10).

S The distance between the actual and the congruent boundary. See Figure 2.4.

$ Line separator - equivalent to another card.

The traction boundary conditions to be satisfied are read into the last column of $\underline{C}$; the first half of this column contains the prescribed tractions in the x-direction and the second half in the y-direction. The calculation of the $\underline{C}$ matrix uses an important characteristic of plane traction boundary value problems, namely that the internal stress field is independent of the material properties, E and ν. As a result of this independence, ν may be treated as an optimization parameter which can be assigned any value whatsoever, in spite of the fact that a value of ν outside of the range, $0 \leq \nu \leq .5$, is physically meaningless. For simplicity, ν is chosen to be equal to 1 here since this simplifies Equations (2.6) by making $\beta = 0$. Furthermore, instead of treating P_x and P_y as unit loads, they are assigned magnitudes of $-\pi$. In this way, at the conclusion of the problem, the load magnitudes at the source points are multiples of $-\pi$ instead of the actual values of the

loads themselves. At each source point there are two loads, one in the x-direction and one in the y-direction. The first half of the vector, $\underline{w}$, of Equations (2.10), which incidentally is stored in the last column of $\underline{C}$ at the conclusion of the solution to the system of equations, contains the magnitudes of the x-loads and the second half, the y-loads. The influence of the j^{th} x-load on the i^{th} boundary point is then, from Equations (2.6a),

$$\sigma_x = x^3/r^4,$$

$$\sigma_y = xy^2/r^4, \tag{4.1a}$$

$$\tau_{xy} = x^2y/r^4,$$

and for the y-load, from Equations (2.6b),

$$\sigma_x = x^2y/r^4,$$

$$\sigma_y = y^3/r^4, \tag{4.1b}$$

$$\tau_{xy} = xy^2/r^4,$$

where x and y are the relative coordinates between the boundary point i and the source point j. These stresses must of course be converted to tractions before they can be assigned to C,

$$t_x = \sigma_x \cos \alpha + \tau_{xy} \sin \alpha,$$

(4.1c)

$$t_y = \tau_{xy} \cos \alpha + \sigma_y \sin \alpha.$$

Finally, the solution to the system of linear equations in Equation (2.10a) is accomplished using SUBROUTINE MATRIX. This subroutine solves an N x N system of equations using the CROUT algorithm [23]. The values to be satisfied by the equations are stored in the augmented column, $C_{\cdot,N+1}$, and are subsequently replaced by the solution vector.

The values printed out by the program are

DET The determinant of the influence matrix, C.

XF, P, Q, S The field coordinates and the stresses, where

$P = \sigma_x$, $Q = \sigma_y$, $S = \tau_{xy}$.

As an example of the accuracy and efficiency of the superposition method, this program was applied to the problem shown in Figure 4.1. The Airy stress function [4],

$$\phi = y^4/24 - x^2y^2/8 + x^2y/2 + 2y^2,$$

corresponding to the stresses,

$$\sigma_x = 4 - x^2/4 + y^2/2,$$

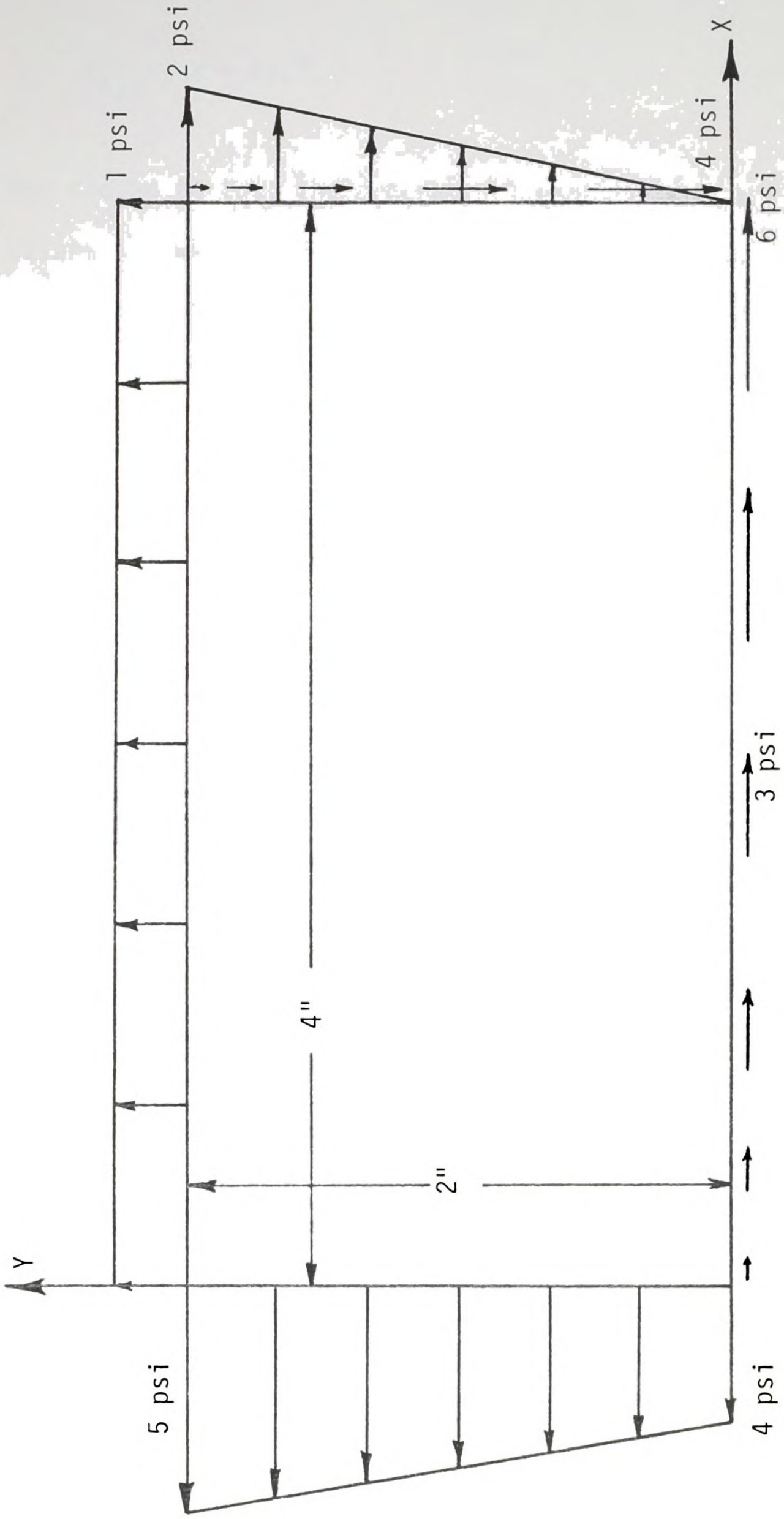

Figure 4.1. A beam loaded on all faces.

$$\sigma_y = y - y^2/4,$$

$$\tau_{xy} = -x + xy/2,$$

was chosen to test the program. These stresses are the exact values and were used to generate the traction boundary conditions at twenty points on the boundary. The data for this problem appears in Appendix D along with the program. The program was run on the CDC 6500 computer, the results of which appear in Table 4.1. The program execution time is labeled CP; here, CP = .065 seconds. As the distance, S, between the congruent boundary and the actual boundary increases, the results get progressively better until a point is reached where the procedure breaks down. This breakdown is due to the fact that the $\underline{C}$ matrix is ill-conditioned to begin with and becomes progressively more so as S increases since the matrix elements of $\underline{C}$ are inversely related to S. The initial ill-conditioning of $\underline{C}$ is due to the following observation: the sum of the rows in the first half of $\underline{C}$ is extremely small. That is,

$$f_j = \sum_{i=1}^{NB} C_{ij} << 1, \text{ for } j = 1, ..2 \cdot NB. \qquad (4.2a)$$

The same is true of the sum of the rows in the last half of $\underline{C}$,

	FIELD POINT		STRESSES: NUMERICAL/EXACT		
	x	y	σ_x	σ_y	τ_{xy}
1	0	0	4.0014/4	.0442/0	0/0
2	1	0	3.7311/3.75	-.0042/0	-1.0046/-1
3	2	0	3.0105/3	0/0	-2/-2
4	3	0	1.7315/1.75	-.0044/0	-2.9956/-3
5	4	0	.0012/0	.0431/0	-3.9994/-4
6	0	1	4.5/4.5	.7686/.75	0/0
7	1	1	4.2533/4.25	.7467/.75	-.5/-.5
8	2	1	3.4991/3.5	.7504/.75	-1/-1
9	3	1	2.2532/2.25	.7468/.75	-1.5/-1.5
10	4	1	.5/.5	.7681/.75	-2/-2
11	0	2	6.0004/6	1.0430/1	0/0
12	1	2	5.7335/5.75	.9962/1	.0040/0
13	2	2	5.0095/5	1/1	0/0
14	3	2	3.7338/3.75	.9963/1	-.0040/0
15	4	2	2.0004/2	1.0414/1	.0004/0

$DET \sim 10^{-121}$

$CP = .065$

Table 4.1. Numerical results for the beam problem.

$$g_j = \sum_{i=NB+1}^{2\cdot NB} C_{ij} << 1, \text{ for } j = 1, ..2 \cdot NB. \qquad (4.2b)$$

The vectors, f_j and g_j, are the net x and y tractions, respectively, due to the j^{th} point load, obtained by summing the tractions generated by this load at each of the NB boundary points. Now since the body is in equilibrium, the integral of the tractions over the surface is exactly zero, and therefore the sum of the tractions at a discrete number of points must be very small. Furthermore, since the determinant of a matrix is unchanged by the addition of rows to each other, the $\underline{C}$ matrix may be regarded as being composed of two nearly zero rows, f_j and g_j. An expansion of the determinant about either of these rows must then yield a very small result; that is, $\underline{C}$ is ill-conditioned. As a result, computer roundoff error accumulates to the point of producing divergent results.

The greatest errors incurred in problems solved by the superposition method typically occur at corners or cusps on the boundary. This is due to the fact that discontinuous tractions are usually specified there. For example, in the problem considered here, at points on the boundary just above the corner located at the origin, $t_x = -4$, whereas for points just to the right of it, $t_x = 0$.

4.2 The Inclusion of Body Forces

The numerical solution to body force problems requires that the body be placed in the first quadrant for reasons given earlier and that the Fourier expansions representing $B_x(x,y)$ and $B_y(x,y)$

be known beforehand. Irregularly shaped bodies may be embedded in a rectangle with sides AA and BB in the first quadrant and the values of B_x and B_y outside the body and inside the rectangle may be assigned as desired. It is best, however, to maintain continuity of value and slope across the boundary since the assignment of discontinuous values usually leads to a Fourier series which converges slowly. The Fourier coefficients may then be evaluated in the usual way,

$$B_x = \sum_m \sum_n C_{mn} \cos \frac{m\pi x}{AA} \cdot \cos \frac{n\pi y}{BB}, \qquad (4.3a)$$

and

$$C_{mn} = \frac{4}{AA \cdot BB} \int_o^{BB} \int_o^{AA} F_x \cos \frac{m\pi x}{AA} \cdot \cos \frac{n\pi y}{BB} \cdot dx\, dy. \qquad (4.3b)$$

Of course, the above equation is valid only for m and n not both zero. Minor alterations are needed for the remaining cases. It is not necessary to evaluate the coefficients in this manner; point matching is also a viable method, as long as it represents the function B_x accurately inside the body.

The computer program for body force problems appears in Appendix E. It uses the basic program of Appendix D with the following additions;

NX The number of Fourier coefficients in the truncated series representing B_x. The m=n=0 coefficient must always be counted even if it is zero.

MX(NX x 2) The matrix containing the values of m and n in the series of Equation (4.3a). The first row of MX is always (0,0), corresponding to m=n=0.

FX(NX) The vector containing the Fourier coefficients, C_{mn}, corresponding to the values of m and n in MX.

NY, MY, FY Similar quantities for B_y.

AA, BB The lengths of the sides of the rectangle into which the body is embedded. Or, if the coefficients are not evaluated in this manner, the values required to bring the series of Equation (4.3a) into agreement with whatever technique is used.

V Poisson's ratio.

TXX, TYY, TXY The stresses, σ_x, σ_y, τ_{xy}.

The only additional calculations that are performed are those which alter the original boundary conditions prescribed to take into account those conditions already satisfied by the body force distribution (see LOOP 1111) and the addition of the body force effects to the stresses at the field points (see LOOP 4). The subroutine, BFORCE, accepts points x and y and returns the stresses at these points using Equations (2.24) and (2.26). The subroutine, MATRIX, in the program in Appendix E has been replaced by a more general subroutine, INVMTX(N,OPT,R), (not shown). This subroutine used hereafter but now shown, either computes the inverse of an N x N matrix (OPT=Ø), or solves an N x N system of equations (OPT=1). It reduces roundoff error by using full pivotal condensation (Gauss-Jordan elimination). It transfers back R, a measure of the

degree of ill-conditioning of C, and the solution; C^{-1} in place of C (OPT=Ø), or the solution vector corresponding to OPT=1, stored in the first column of C.

The body force problem treated here is the rotating disk problem, shown in Figure 4.2a, where the body force is centripetal,

$$B_r = \rho\omega^2 r, \qquad (4.4)$$

$$B_\theta = 0,$$

with ρ, the mass density of the disk, ω, the angular velocity, and r and θ are polar coordinates. This problem has been solved, [4]

$$\sigma_r = \frac{3+\nu}{8}\rho\omega^2(b^2-r^2), \qquad (4.5)$$

$$\sigma_\theta = \frac{1}{8}\rho\omega^2((3+\nu)b^2 - (1+3\nu)r^2),$$

$$\tau_{r\theta} = 0.$$

Choosing $\rho\omega^2 = 12$, $b = 2$, and $\nu = \frac{1}{3}$, this solution becomes

$$\sigma_r = 20 - 5r^2, \qquad (4.6)$$

$$\sigma_\theta = 20 - 3r^2,$$

$$\tau_{r\theta} = 0.$$

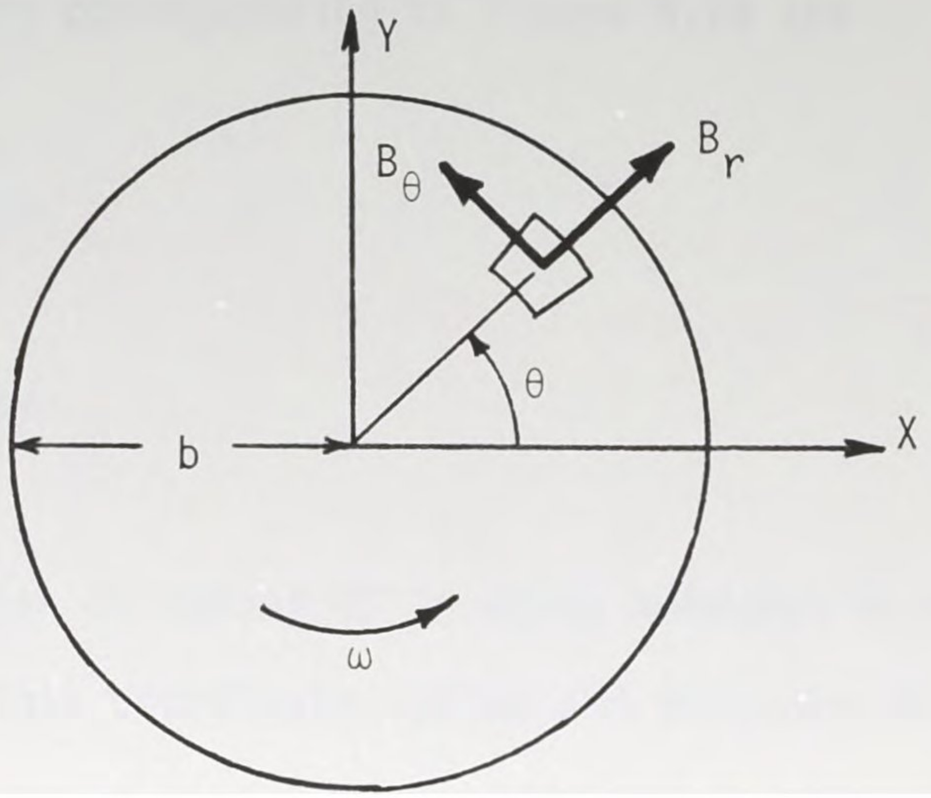

a. A disk rotating about the z-axis with angular velocity, ω.

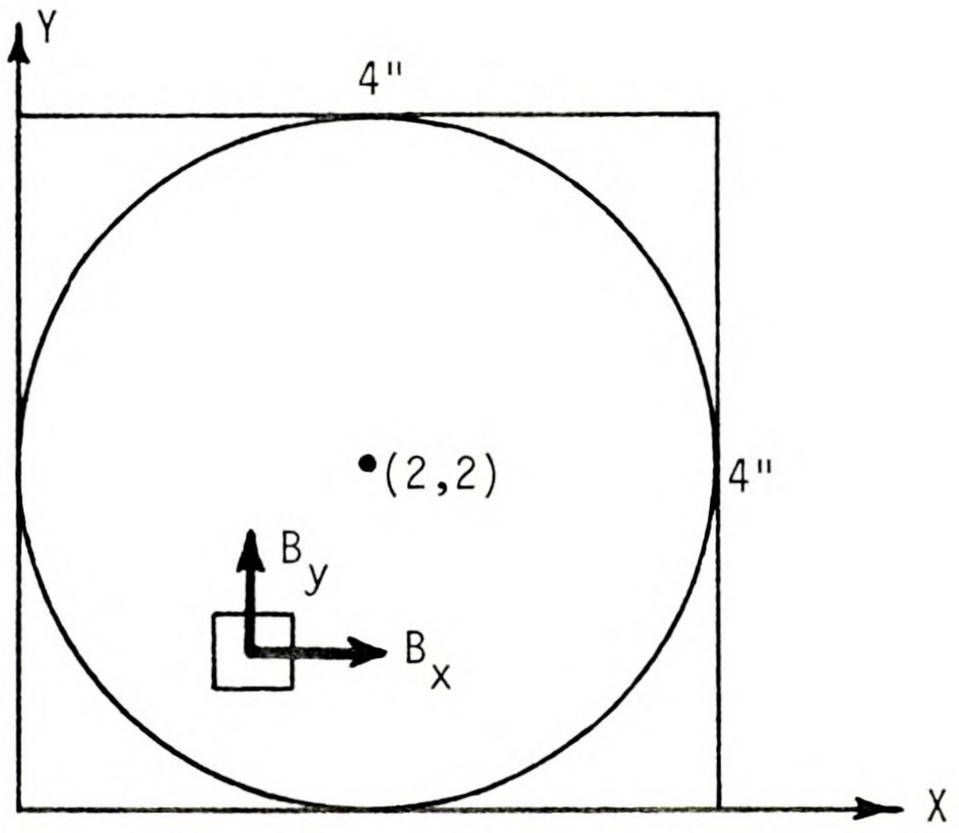

b. The same disk embedded in a 4" square.

Figure 4.2. The rotating disk body force problem.

The x and y body forces corresponding to Figure 4.2a are

$$B_x = B_r \cos\theta = 12x,$$

$$B_y = B_r \sin\theta = 12y. \tag{4.7}$$

In Figure 4.2b, the disk of radius 2" is shown embedded in a 4" square. Referred to this coordinate system and expanded in a Fourier series,

$$B_x = 12(x-2) = -12\left(\frac{4}{\pi}\right)^2 \sum_{i=1}^{\infty} \frac{\cos(2i-1)\frac{\pi x}{4}}{(2i-1)^2},$$

$$B_y = 12(y-2). \tag{4.8}$$

The data necessary to solve this problem is easily generated by the computer in a DATA subroutine and consequently does not appear in the INPUT list in the program in Appendix E. For the sake of clarity, some of the data is listed below. There are twenty boundary points at which zero traction boundary conditions are satisfied, along with twenty Fourier coefficients for B_x and twenty for B_y. Also, the entire second column of MX and first column of MY are zero and

$$MX(i,1) = MY(i,2) = 2i-3,$$

where i = 2, 3, 4...NX = NY = 2Ø.

Finally,

$$FX(i) = FY(i) = -\left(\frac{4}{\pi}\right)^2 \cdot \frac{12}{(2i-3)^2},$$

for $i = 2, 3 \ldots 20,$

$$FX(1) = FY(1) = 0,$$

and $AA = BB = 2.$

The numerical results shown in Table 4.2 are in excellent agreement with the exact values of Equation (4.6). It should be noted that the $\underline{C}$ matrix for this problem would be unchanged if there were no body forces present since $\underline{C}$ depends only on the relative geometry of the source and boundary coordinates. In the case where there are no body forces, the choice of boundary points at which conditions are to be satisfied is made based on the magnitudes and variations of these conditions over the boundary. However, in the presence of body forces, a choice based on the prescribed boundary conditions may not be the best choice since these conditios are altered early in the program. Therefore it is advisable to compute the boundary conditions already present as a result of body forces at many points along the boundary and then select the points at which conditions are to be satisfied based on the difference between the prescribed conditions and those generated by the body forces.

	FIELD POINT		STRESSES: NUMERICAL/EXACT		
	x	y	σ_x	σ_y	τ_{xy}
1	2	2	19.9999/20	19.9999/20	
2	2.4	2	19.1998/19.2	19.5199/19.52	
3	2.6	2	18.1997/18.2	18.9199/18.92	
4	2.8	2	16.7996/16.8	18.0799/18.08	All on the order of 10^{-12}.
5	3	2	14.9995/15	17/17	
6	3.2	2	12.7993/12.8	15.6799/15.68	
7	3.4	2	10.1991/7.2	14.1199/14.12	
8	3.6	2	7.1988/7.2	12.3196/12.32	
9	3.8	2	3.7985/3.8	10.2790/10.28	
10	4.0	2	10^{-13}	7.9982/8	

CP = .1 seconds.

DET = 10^{-131}.

Table 4.2. Numerical results for the rotating disk problem.

4.3 The Inclusion of Edge Dislocations and Their Dipoles

Edge dislocations, dipoles, and body forces may all be included in the same problem simultaneously. However, for the sake of simplicity, only a distribution of edge dislocations will be treated here. The scheme for handling these is identical in form to that for body forces. One need only replace the subroutine, BFORCE, of Appendix E, by EDGE, of Appendix F. Of course, the 'COMMON' and 'CALL' statements must also be changed. It is somewhat pointless to pursue specific problems here since, to the author's knowledge, there are no known solutions to problems of this type with which comparisons can be made. Instead, consider the following observation:

> In the confines of linear elasticity, a body free from dislocations and the same body filled with a constant density of dislocations are indistinguishable.

That this is true follows from the results for a constant density of edge dislocations distributed over the entire infinite plane Inspection of Equations (2.33a) indicates that the stresses satisfy both equilibrium and compatibility. Consequently there is an Airy stress function which will remove these stresses at all points in space, namely,

$$\phi = \frac{E}{12\pi}\left[(\pi-1)d_{oo}x^3 - 3c_{oo}x^2y + 3d_{oo}xy^2 - (\pi-1)\,c_{oo}y^3\right]. \tag{4.9}$$

The stress field inside of a body which is free from tractions on its surface is the superposed effect of the stresses in Equation (2.33a) and those derived from the Airy stress function. Therefore a traction free body filled with a constant density of dislocations is internally stress free. This result is not surprising since a constant density of dislocations introduces an equal amount of material at every point inside the body. The same observation can be applied to a constant density of dipoles. The Airy stress functions which remove the stresses of Equations (2.39b), (2.41b), and (2.42b), for the case m=n=0 are

$$\phi = \frac{Ec_{oo}}{4\pi}\,[x^2 + (\pi-1)y^2),$$

$$\phi = \frac{Ed_{oo}}{4\pi}\,(y^2 + (\pi-1)x^2), \qquad (4.10)$$

$$\phi = -\frac{Ec_{oo}}{2\pi}\,xy,$$

respectively.

4.4 Analytic Solutions to Crack Problems

The types of problems considered here and their method of solution are discussed in Section 3.2. The 'direct' approach will be used at all times. Consider the problem shown in Figure 4.3a in which an array of cracks of the length and spacing shown are situated in the infinite plane under tension. The exact expression for the mode I stress intensity factor is [12],

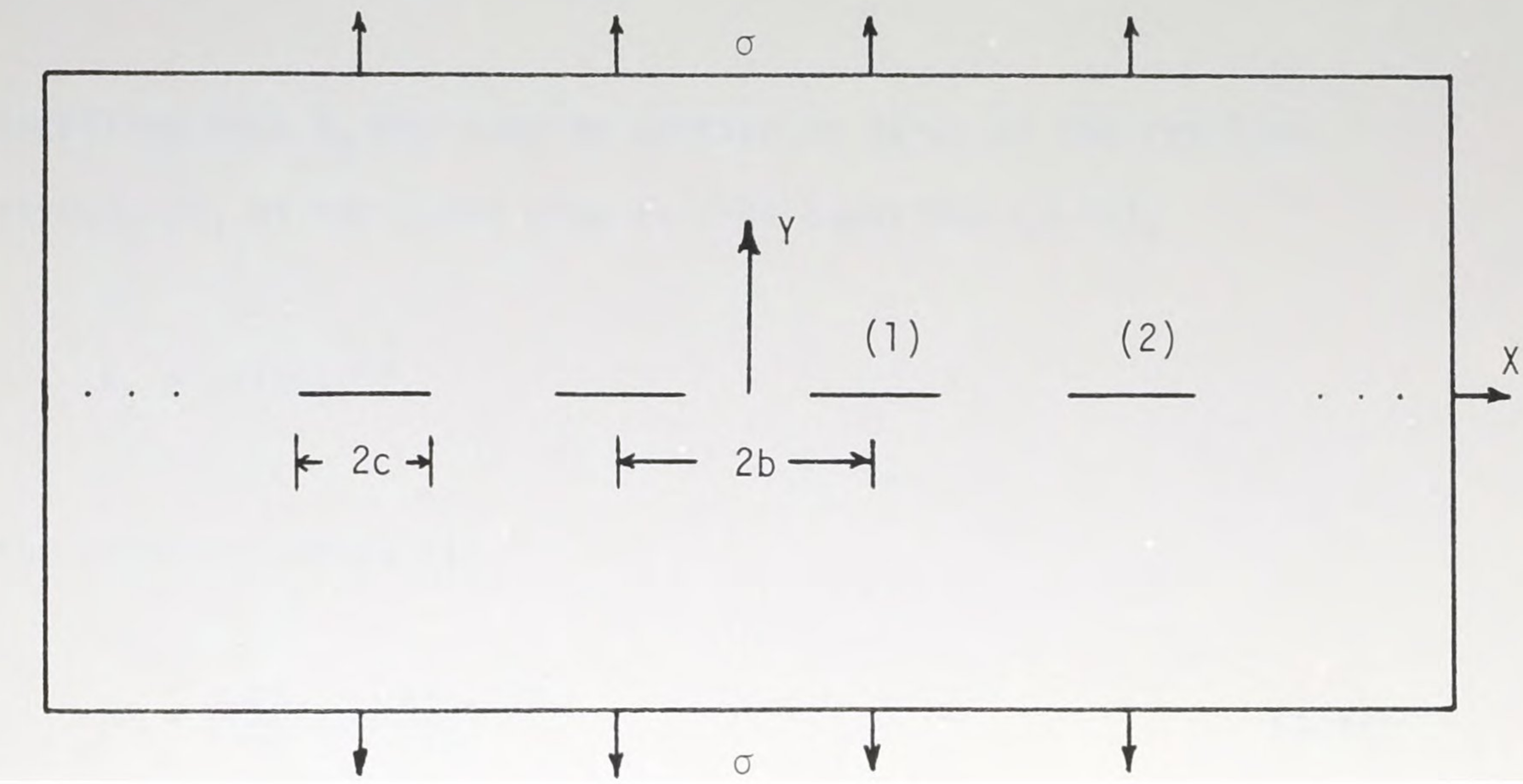

a. An infinite array of cracks in tension.

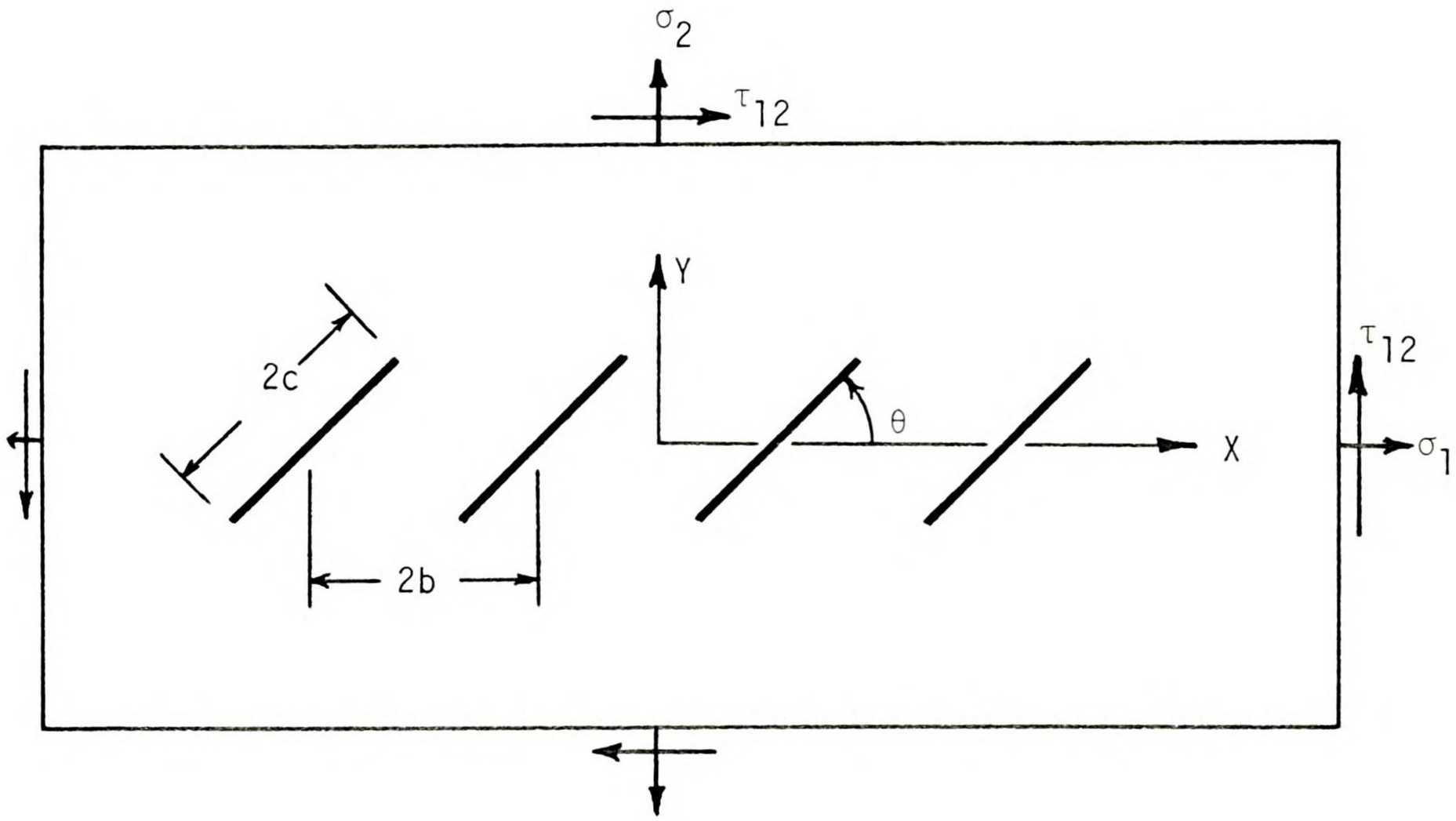

b. An infinite array of cracks under a general state of stress.

Figure 4.3. An infinite array of cracks.

$$K_I = \sigma(\pi c)^{1/2}\left[\frac{2b}{\pi c}\tan\frac{\pi c}{2b}\right]^{1/2}. \qquad (4.11)$$

Recalling that K_I may also be written in terms of the resolved stress, σ^*, at the crack site as (see Equations (3.9)),

$$K_I = \sigma^*(\pi c)^{1/2},$$

the resolved stress is

$$\sigma^* = \sigma\left[\frac{2b}{\pi c}\tan\frac{\pi c}{2b}\right]^{1/2}, \qquad (4.12)$$

which reduces to the result for a single crack in tension,

$$\lim_{b\to\infty} \sigma^* = \sigma,$$

and gives $\sigma^*\to\infty$ for the case where the spacing between cracks is made to vanish. In terms of the dipole model, Equations (3.18), (3.19), and (3.20) define the problem. These must be altered in this case since there is no boundary. In fact, Equation (3.18) becomes nonexistent and Equations (3.19) and (3.20) become

$$\underline{\sigma}^* = \underline{\sigma} + \underline{Q}\,\underline{d},$$

$$\underline{d} = \underline{P}\,\sigma^*, \qquad (4.13)$$

where $\underline{\sigma}^*$ is the vector containing the resolved stresses at the crack sites and σ is the influence of the tension at infinity,

$$\underline{\sigma}^T = (0,\sigma,\ 0,\ 0,\sigma,\ 0,\ 0,\sigma,\ 0...) \tag{4.14}$$

Rearranging Equations (4.13) gives

$$(\underline{I} - \underline{Q}\ \underline{P})\underline{\sigma}^* = \underline{\sigma}. \tag{4.15}$$

The expected form of the resolved stresses is

$$\underline{\sigma}^{*T} = (0,\sigma^*,\ 0,\ 0,\ \sigma^*,\ 0,\ 0,\ \sigma^*,0...), \tag{4.16}$$

which indicates that only the normal dipoles of the type shown in Figure 2.6b are needed to model these cracks. Now from Equations (2.38b) the stress produced by such a dipole located at the origin at the point (x,0) is

$$\sigma_y = -\frac{Ed_y}{4\pi} \cdot \frac{1}{x^2},$$

The same dipole located at the point $(x_2,0)$ produces a stress at the point $(x_1,0)$,

$$\sigma_y = -\frac{Ed_y}{4\pi} \cdot \frac{1}{x_{12}^2}, \tag{4.17}$$

where $x_{12} = x_2 - x_1$. Taking advantage of symmetry and using the labelling of Figure 4.3a, the $\underline{Q}$ matrix used in Equation (4.13) has the form,

$$\underline{Q} = -\frac{E}{4\pi}\begin{bmatrix} 0,0,0 & 0,2x_{12}^{-2},0 & 0,2x_{13}^{-2},0 \ldots \\ 0,0,0 & 0,0,0 & 0,2x_{23}^{-2},0 \ldots \\ 0,0,0 & 0,0,0 & 0,0,0 \ldots \\ \vdots & \vdots & \vdots \end{bmatrix}$$

and $\underline{P} = -\frac{2\pi c^2}{E}\underline{J}$, (4.18)

where J is the m x m diagonal matrix whose diagonal elements are

$$J_{ii} = \begin{bmatrix} 0 & 0 & 0 \\ 0 & 1 & 0 \\ 0 & 0 & 1 \end{bmatrix},$$

and whose off diagonal elements are the 3 x 3 zero matrix. This form for $\underline{P}$ was obtained from Equations (3.16). In a tedious but straightforward manner it can be shown that

$$\underline{Q}\,\underline{P} = \frac{c^2}{2} \cdot \left(-\frac{4\pi}{E}\underline{Q}\right).$$

Substitution of this result into Equation (4.15) and inspection of the result shows that this system of linear equations can be reduced to a single equation,

$$\left[1 - \frac{c^2}{2}\left(\sum_{i=2}^{\infty} 2x_{1i}^{-2}\right)\right]\sigma^* = \sigma. \qquad (4.19)$$

But

$$x_{1i} = (2b)(i-1),$$

so that

$$\sum_{i=2}^{\infty} 2x_{1i}^{-2} = 2 \cdot \frac{1}{4b^2} \cdot \frac{\pi^2}{6} = \frac{\pi^2}{12b^2}. \qquad (4.20)$$

Substituting this result into Equation (4.19) gives

$$\sigma^* = \sigma/[1 - \frac{\pi^2 c^2}{24b^2}] \qquad (4.21)$$

which should be compared to the exact result of Equation (4.12). Before doing so it should be pointed out that this result could have been obtained easily (in this case) by applying Equation (4.17) repeatedly to the crack at the origin. That is, for $x_1=0$,

$$\sigma^*(0,0) = \sigma + (-\frac{Ed_y}{4\pi}) \cdot 2 \sum_{i=2}^{\infty} \frac{1}{x_{1i}^2} = \sigma - \frac{\pi E d_y}{48b^2}, \qquad (4.22)$$

and using the dipole model,

$$d_y = -\frac{2\pi c^2}{E} \sigma^*, \qquad (4.23)$$

the result of Equation (4.21) is obtained.

Now, defining

$$z = \frac{\pi a}{2b}, \tag{4.24}$$

and expanding Equation (4.12) in a Taylor series in z,

$$\sigma^* \doteq \sigma\left(1 + \frac{z^2}{6} + \frac{19}{360} z^4 \ldots\right), \tag{4.25}$$

whereas the expansion of Equation (4.21) is

$$\sigma^* \doteq \sigma\left(1 + \frac{z^2}{6} + \frac{z^4}{36} \ldots\right). \tag{4.26}$$

Evidently, the dipole model produces acceptable results for this problem. In fact, the error in Equation (4.21) does not exceed 10 percent for ratios of (c/b) up to .76 and any error is due of course to treating the crack as a point source, ignoring its spatial extent.

These results can easily by extended to cover the more general case shown in Figure 4.3b. At the origin, the resolved stresses are, from Equations (2.38),

$$\begin{aligned}
\sigma_x^* &= \sigma_1 + \frac{Ed_x}{4\pi} \cdot 3R - \frac{Ed_y}{4\pi} R, \\
\sigma_y^* &= \sigma_2 - \frac{Ed_x}{4\pi} R - \frac{Ed_y}{4\pi} R, \\
\tau_{xy}^* &= \tau_{12} - \frac{Ed_{xy}}{4\pi} R,
\end{aligned} \tag{4.27}$$

where $R = 2 \sum_{i=2}^{\infty} x_{1i}^{-2} = \frac{\pi^2}{12b^2}$.

Modelling the dipoles by cracks uses Equations (3.16),

$$d_x = - \frac{2\pi c^2}{E} (\alpha\sigma_x^* + \beta\tau_{xy}^*),$$

$$d_y = - \frac{2\pi c^2}{E} ((1-\alpha)\sigma_y^* + \beta\tau_{xy}^*), \qquad (4.28)$$

$$d_{xy} = - \frac{2\pi c^2}{E} (\beta\sigma_x^* + \beta\sigma_y^* + \tau_{xy}^*).$$

Substituting Equations (4.28) into (4.27) and rearranging gives a system of linear equations to be solved for the resolved stresses,

$$\sigma_x^*(1+3p\alpha) - \sigma_y^* p(1-\alpha) + \tau_{xy}^*(2p\beta) = \sigma_1,$$

$$-\sigma_x^*(p\alpha) + \sigma_y^*(1+p(1-\alpha)) - \tau_{xy}^*(2p\beta) = \sigma_2, \qquad (4.29)$$

$$-\sigma_x^*(p\beta) - \sigma_y^*(p\beta) + \tau_{xy}^*(1-p) = \tau_{12},$$

where $p = \frac{\pi^2 c^2}{24b^2}$,

$\alpha = \sin^2\theta$,

$\beta = -\sin\theta \cos\theta$.

For $\theta=0$, Equation (4.21) is recovered and

$$\sigma_x^* = \sigma_1 + \frac{\sigma_2 p}{1-p},$$

$$\sigma_y^* = \frac{\sigma_2}{1-p}\ , \qquad (4.30)$$

$$\tau_{xy}^* = \frac{\tau_{12}}{1-p}\ ,$$

For $\theta=90°$, Equations (4.29) produce

$$\sigma_x^* = \frac{\sigma_1}{1+3p}\ ,$$

$$\sigma_y^* = \sigma_2 + \sigma_1 p, \qquad (4.31)$$

$$\tau_{xy}^* = \frac{\tau_{12}}{1-p}\ .$$

The reduced resolved stress, σ_x^*, of Equation (4.31) is attributed to the shielding effect of the cracks in front of and behind the crack at the origin. Evidently, the straining mechanisms find it difficult to 'reach behind' the two cracks on either side of the origin to produce the resolved stress, σ_1, which would appear if these cracks were not present. A similar situation arises in quantum mechanics when first order perturbation theory is applied to orbital energies in atomic arrangements. The electrons in outer orbitals are shielded from the electrostatic field of the

nucleus by electrons in inner orbitals resulting in a reduced field as seen by the outer electrons.

4.5 Numerical Solutions to Crack Problems

A computer program which handles bodies of arbitrary shape in a state of plane stress/plane strain, subjected to pure traction boundary conditions and containing an arbitrary number of cracks of any (reasonable) size, orientation and location within the body is shown in Appendix G. The program uses the direct method described in Section 3.2. The labelling used in the COMMENT statements is the same as that used in Equations (3.18) through (3.24) with the additional abbreviations, "...stored in RH of C, NBB + ...", which indicates that a particular matrix is being stored in the right half of the general purpose matrix, C, beyond column NBB, for reasons of economy. The additional variables not already accounted for are described below.

NC The number of cracks.

XC(NC x 2) The coordinates of the crack sites.

D(NC x 2) The lengths and inclinations (in degrees) of the cracks.

P(3NC x 3) The P matrix of Equations (3.16) for each crack.

C(a x b) General purpose matrix where a = max (2NB, 3NC),

b = a + 3NC + 2.

B(3NC x 2NB) The B matrix in Equation (3.22).

The program prints out the determinant of (I-QP), the determinant of (C + HPB), the crack coordinates and the corresponding resolved stresses. The particular problem chosen for solution appears in Figure 4.4 and the results are shown in Table 4.3. The results for the resolved stresses in the x-direction for the two cracks located at the section, x=.5, are consistent with the crude observation that since the amount of material left to carry the load at this section after the introduction of the cracks is reduced by an amount equal to the sum of the crack lengths, the average stress (an approximation to the resolved stress) is

$$\sigma = \frac{1x2}{2-2(.1)} = 1.111...$$

Moreover, it is easily demonstrated that the imposition of a uniform stress, σ_y, on the top and bottom faces of the block in Figure 4.4 alters only the resolved stresses in the y-direction.

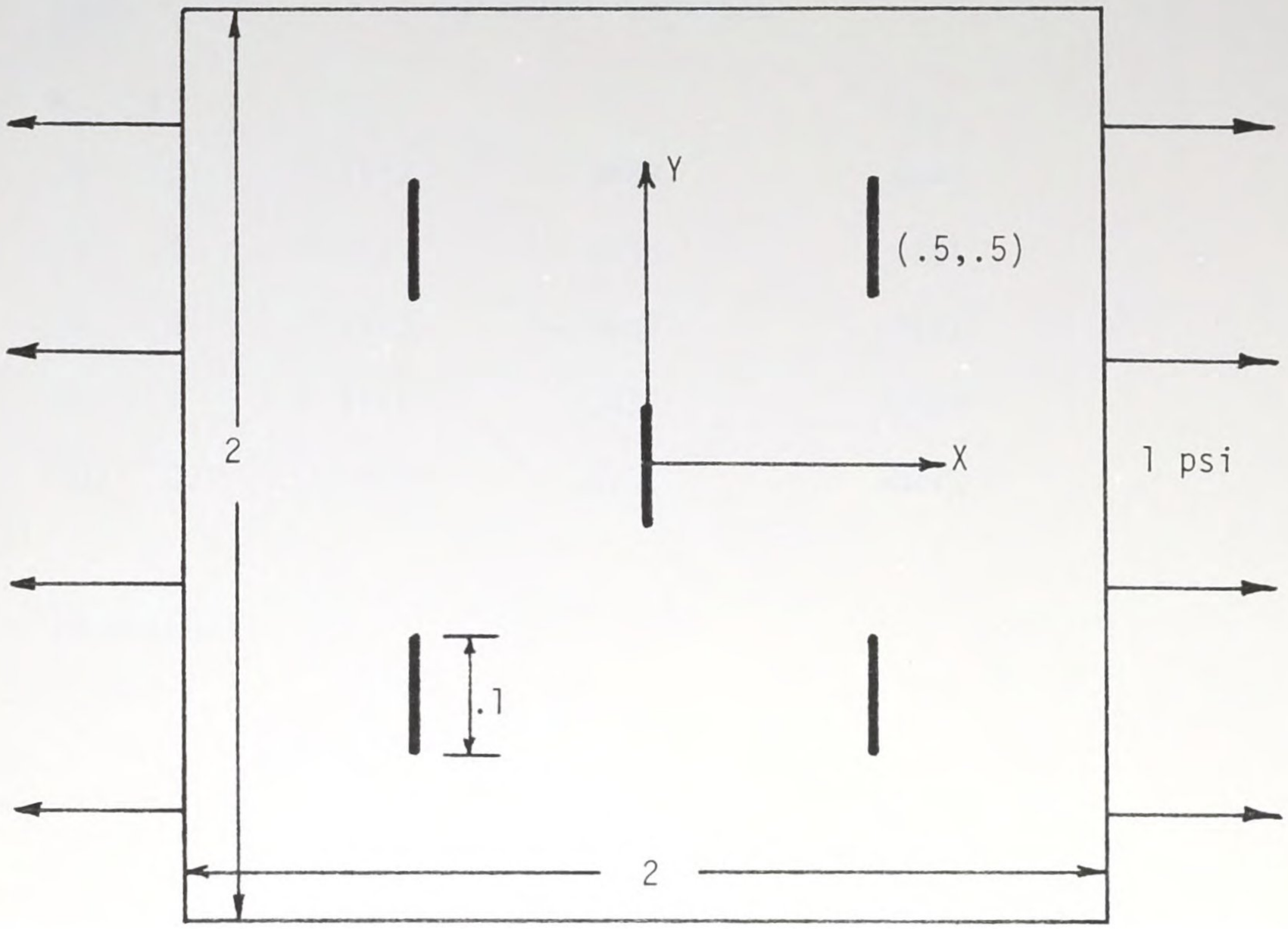

Figure 4.4. A square block containing five identical cracks at symmetrical locations in a state of uniform stress.

CRACK SITE		RESOLVED STRESSES		
x	y	σ_x	σ_y	τ_{xy}
.5	.5	1.1113	-.0483	.0444
-.5	.5	1.1111	.0436	.0164
-.5	-.5	1.1113	-.0483	.0444
.5	-.5	1.1111	.0436	.0164
0.	0.	1.1554	-.0432	.0213

CP = .4 seconds

Table 4.3. The results for the problem of Figure 4.4.

CHAPTER 5

CONCLUSIONS

A new point of view regarding the numerical treatment of distributed sources of internal stress has been presented in Chapter 2. The Fourier series approach to smearing point load type singularities over the infinite plane was emphasized because of its effectiveness in the numerical treatment of linear elasticity problems with body forces. Since a large class of nonlinear problems can be rearranged to look like linear problems with pseudo-body forces carrying the nonlinear effects, the numerical method is applicable to nonlinear problems as well. In addition, any source of stress whose influence on the surrounding medium is of the same functional form as that of a point load qualifies for a similar treatment. Dipoles of these sources are also admissable. Hence, the numerical procedure is also applicable to distributed crack problems which use dislocation dipoles in their treatment.

Although the dislocation model for a crack has been in use for quite some time [6], there appears to have been no attempts made to use it in fracture mechanics problems involving more than one crack. This is surprising since the model is easily incorporated into a numerical scheme (see Section 3.2 and Appendix G) which produces stress intensity factors for crack configurations which

are not easily treated by conventional methods [11, 12]. The dipole model is however not without limitations. There are two possible sources of error in the model. The first occurs in treating the crack as a point effect and the second in ignoring the variation in the resolved stresses over the length of the crack. The first source of error can easily be removed by using the results of Equations (3.7) and (3.8) in conjunction with Appendix C to refine the dipole stress fields of Equations (2.38a, b, c) taking into account the spatial extent of the crack. Similar to Equations (3.18), (3.19), and (3.20), the problem would be defined as

$$\underline{b} = \underline{C}\,\underline{w} + \underline{H}\,\underline{\sigma},$$

$$\underline{\sigma} = \underline{G}\,\underline{w} + \underline{Q}\,\underline{\sigma},$$

where the $\underline{H}$ and $\underline{Q}$ matrices are a bit more involved computationally but are nevertheless straightforward. The removal of the second source of error, however, presents an almost insurmountable problem since the distribution cited in Equation (3.3b) is valid only for a straight crack in uniform tension. If the stress field due to external sources (the resolved stress) varies appreciably over the length of the crack, as would be the case if the crack were near the boundary or another crack, this result is seriously in error. The true distribution is determined by satisfying Equation (3.3a) with σ replaced by $\sigma(x)$. The solution to this integral equation for a given $\sigma(x)$ is no simple matter and is further

complicated by the fact that for finite bodies, $\sigma(x)$ is not known until the end of the problem. Consequently, the removal of these errors involves as much work as would be required in solving the problem by conventional methods [11, 12].

An inherent source of error related to the practical aspects of crack modelling deserves attention. The treatment of cracks as straight slits is obviously an oversimplification. Naturally occuring cracks in, for example, metals and rock are expected to violate these conditions regularly. Fortunately, the straight line model is justifiable insofar as crack propagation is concerned since the Griffith criterion utilizes only gross properties of the crack, the crack surface area and the strain energy change in an infinite medium associated with the crack's presence, both of which are relatively insensitive to local variations in crack geometry. That is, it is reasonable to expect that there are a large number of crack configurations possible, all of which have the same surface area and produce the same strain energy change.

The modelling of a continuum of microcracks by a field of dipoles (latter part of Section 3.2) is an area which needs development. The dipole density concept was introduced in Chapter 2 primarily to facilitate the transition from a small collection of cracks, which would be handled by the method in Appendix G, to a dense array of microcracks, where the individual handling of these cracks would be prohibitively complicated. The utility of this approach remains to be seen and will undoubtedly find its application in the study of progressive damage due to crack growth.

APPENDICES

APPENDIX A

THE EVALUATION OF FOUR BASIC AREA INTEGRALS

The four basic integrals to be evaluated here are

$$I_k(a,b,m,n) = \int_{\infty} \frac{(a-x)^{3-k}(b-y)^k}{r^4} \cos mx \cdot \cos ny \, dA, \qquad (A.1)$$

where $k = 0, 1, 2, 3,$

$$r^2 = (a-x)^2 + (b-y)^2.$$

Figure A.1 will be used at all times in reference to these integrals. Each integral will be evaluated in four parts,

$$I = I_{PATCH} + I_{STRIP1} + I_{STRIP2} + I_{PLANE}. \qquad (A.2)$$

It is to be understood that $R \to \infty$, the limit being effected at the appropriate time. The integral below occurs frequently and can be found in any standard table of integrals,

$$\Phi(k,a) = \int_0^{\infty} \frac{\cos kx}{x^2+a^2} dx = \frac{\pi}{2|a|} e^{-|ka|}. \qquad (A.3)$$

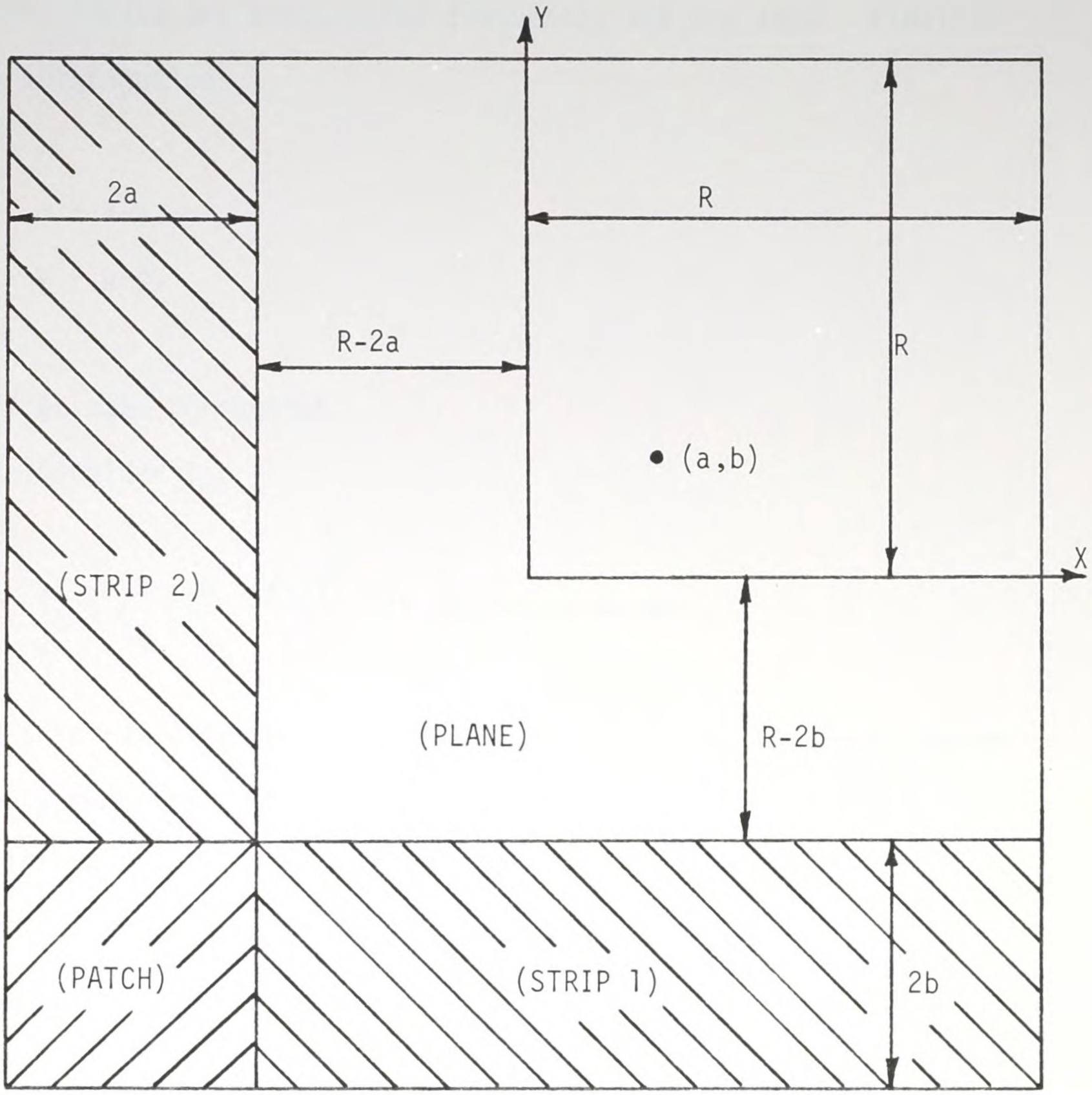

Figure A.1. The region of integration broken up into four parts.

Initially, the parameters m and n will be assumed to be greater than zero (unless otherwise specified). Odd integrands over symmetric limits are encountered frequently and are zero. Finally, the substitutions,

$$u = x-a,$$

$$v = y-b,$$

will be used throughout.

Consider I_o:

$$I_o = \int_{-R}^{R} \int_{-R}^{R} \frac{(a-x)^3}{r^4} \cos mx \cos ny \, dx \, dy.$$

The integral over the PATCH is zero because the integrand behaves like $\frac{1}{R}$ over the finite region of area, 4ab. The integral over STRIP1 is

$$I_{s1} = \int_{-R}^{-R+2b} dy \cos ny \int_{-R+2a}^{R} \frac{(a-x)^3}{r^4} \cos mx \, d\, x,$$

which can be written as

$$I_{s1} = \int_{-R-b}^{-R+b} dv \cdot \cos n\,(v+b) \int_{-R+a}^{R-a} du \cdot \frac{-u^3}{(u^2+v^2)^2}$$

$$(\cos mu \cdot \cos ma - \sin mu \cdot \sin ma),$$

or

$$I_{s1} = 2 \sin ma \int_{-R-b}^{-R+b} dv \cdot \cos n\,(v+b) \cdot J,$$

where

$$J = \int_{o}^{\infty} \frac{u^3 \sin mu}{(u^2+v^2)^2}\, du.$$

Now,

$$J = \frac{1}{2v} \cdot \frac{\partial}{\partial v} \cdot \frac{\partial^3}{\partial_m 3} \phi\,(m,v),$$

and since v is negative in I_{s1},

$$J = -\frac{1}{2v} \cdot \frac{\partial}{\partial v} \cdot \frac{\partial}{\partial m^3} \left[\frac{\pi}{2(-v)} e^{-m(-v)}\right] = \frac{\pi}{4}(2+mv)e^{mv}.$$

Consequently,

$$I_{s1} = \frac{\pi}{2} \sin ma \int_{-R-b}^{-R+b} (2+mv)e^{mv} \cos n(v+b)\, dv,$$

which vanishes in the limit since the integrand behaves like Re^{-mR} over a finite range of width 2b. The integral over STRIP2 is

$$I_{s2} = \int_{-R}^{-R+2a} dx(a-x)^3 \cos mx \int_{-R+2b}^{R} \frac{\cos ny}{r^4}\, dy,$$

which can be written as

$$I_{s2} = \int_{-R-a}^{-R+a} -du \cdot u^3 \cos m(u+a) \int_{-R+b}^{R-b} \frac{\cos nv \cdot \cos nb - \sin nv \cdot \sin nb}{(u^2+v^2)^2}\, dv,$$

or

$$I_{s2} = -2 \cos nb \int_{-R-a}^{-R+a} du \cdot u^3 \cos m\,(u+a) \cdot J,$$

where

$$J = \int_o^\infty \frac{\cos nv}{(u^2+v^2)^2}\, dv.$$

Now,

$$J = -\frac{1}{2u}\frac{\partial}{\partial u}\,\Phi\,(n,u),$$

and since u is negative in I_{s2},

$$J = -\frac{1}{2u}\frac{\partial}{\partial u}\left[\frac{\pi}{2(-u)}\, e^{-n(-u)}\right] = \frac{\pi}{4u^3}\,(nu-1)e^{nu}.$$

Consequently,

$$I_{s2} = -\frac{\pi}{2}\cos nb \int_{-R-a}^{-R+a} (nu-1)e^{nu}\cos m(u+a)\, du,$$

which vanishes in the limit since the integrand behaves like Re^{-nR} over a finite range of width 2a. It appears then that only the integral over the PLANE contributes to I_o:

$$I_o = I_P = \int_{-R+2a}^{R} \int_{-R+2b}^{R} \frac{(a-x)^3}{r^4} \cos mx \cos ny\, dy\, dx,$$

which can be written as

$$I_o = \int_{-R+a}^{R-a} \int_{-R+b}^{R-b} \frac{-u^3}{(u^2+v^2)^2} Q \, dvdu,$$

where $Q = \cos m(u+a) \cos n(v+b)$.

Now since the limits of integration are symmetric for both u and v, one need only extract from the expanded form of Q that part which is both odd in u and even in v. This results in

$$I_o = 4 \sin ma \cdot \cos nb \int_o^\infty du \cdot u^3 \cdot \sin mu \cdot J,$$

where

$$J = \int_o^\infty \frac{\cos nv \cdot dv}{(u^2+v^2)^2} .$$

As before,

$$J = -\frac{1}{2u} \frac{\partial}{\partial u} \Phi (n,v),$$

and since u is positive in I_o,

$$J = -\frac{1}{2u} \frac{\partial}{\partial u} \left[\frac{\pi}{2u} e^{-nu}\right] = \frac{\pi}{4u^3} (1+nu)e^{-nu}.$$

Now,

$$I_o = \pi \sin ma \cos nb \int_o^\infty (1+nu)e^{-nu} \sin nu \, du.$$

Introducing

$$K = \int_o^\infty e^{-nu} \sin mu \, du = \frac{m}{m^2+n^2},$$

I_o becomes

$$I_o = \pi \sin ma \cos nb \left(K - n \frac{\partial K}{\partial n}\right),$$

giving

$$I_o = \frac{\pi m(m^2+3n^2)}{(m^2+n^2)^2} \sin ma \cdot \cos nb. \qquad (A.4)$$

Consider next, I_1:

$$I_1 = \int_{-R}^{R} \int_{-R}^{R} \frac{(a-x)^2(b-y)}{r^4} \cos mx \cos ny \, dx \, dy.$$

The integrals over the PATCH, STRIP1, and STRIP2 are all zero for the same order of magnitude reasons used previously in the evaluation of I_o. The only contribution to I_1 then, is that due to the integral over the PLANE,

$$I_1 = I_P = \int_{-R+2a}^{R} \int_{-R+2b}^{R} \frac{(a-x)^2(b-y)}{r^4} \cos mx \cos ny \, dy \, dz,$$

which can be written as

$$I_1 = \int_{-R+a}^{R-a} \int_{-R+b}^{R-b} \frac{-u^2 v}{(u^2+v^2)^2} Q \, dv \, du,$$

where Q has been defined previously. As before, symmetric limits on both u and v call for that part of Q which is both even in u and odd in v, leaving

$$I_1 = 4 \cos ma \sin nb \int_0^\infty du \cdot u^2 \cdot \cos mu \cdot J,$$

where

$$J = \int_0^\infty \frac{v \sin nv}{(u^2+v^2)^2} dv.$$

By inspection,

$$J = \frac{1}{2u} \frac{\partial}{\partial u} \frac{\partial}{\partial n} \Phi(n,v),$$

giving

$$J = \frac{1}{2u} \frac{\partial}{\partial u} \frac{\partial}{\partial n} \left[\frac{\pi}{2u} e^{-nu}\right] = \frac{\pi n}{4u} e^{-nu}.$$

Finally,

$$I_1 = n\pi \cos ma \sin nb \int_0^\infty ue^{-nu} \cos mu \, du,$$

which, upon using the previously defined K, becomes

$$I_1 = n\pi \cos ma \cdot \sin nb \cdot \frac{\partial K}{\partial m},$$

giving

$$I_1 = \frac{\pi n(n^2-m^2)}{(m^2+n^2)^2} \cos ma \cdot \sin nb. \qquad (A.5)$$

The remaining integrals, I_2 and I_3, can be obtained from I_1 and I_o respectively by interchanging a with b and m with n. That this is true can be seen by making these exchanges in the original definitions of the integrals along with the dummy variable exchange of x with y. That is,

$$I_k(a,b,m,n) = I_{3-k}(b,a,n,m). \qquad (A.6)$$

It should not be <u>assumed</u> that these results are valid when either m or n are zero, the reason being that the order of magnitude arguments used in the STRIP integrals break down in this case. However, independent evaluation of these integrals reveals that the above results are applicable if either m or n is zero, but not both zero at the same time. That the validity of Equation (A.5), for example, is suspect for the case, m=n=0, is made apparent by the fact that different results are obtained for the limit depending on the order of the limiting process,

$$\lim_{n\to 0} \lim_{m\to 0} I_1 \neq \lim_{m\to 0} \lim_{n\to 0} I_1.$$

Consider $I_o(a,b,0,0)$. The PATCH integral is zero by the usual order of magnitude analysis. The STRIP1 and PLANE integrals are zero because their integrands are odd functions of u, integrated over symmetric limits. Therefore,

$$I_o = I_{s2} = \int_{-R}^{-R+2a} \int_{-R+2b}^{R} \frac{(a-x)^3}{r^4}\, dy\, dx$$

or,

$$I_o = -2 \int_{-R-a}^{-R+a} du\, u^3\, J,$$

where

$$J = \int_{o}^{R-b} \frac{dv}{(u^2+v^2)^2}.$$

The upper limit on this last integral can be replaced by R without affecting I_o since the net result is to add to J an amount not exceeding b/R^4, which when coupled with the integral over u produces a result of order 4ab/R which vanishes in the limit. Hence,

$$J = \int_{o}^{R} \frac{dv}{(u^2+v^2)^2} = \frac{1}{2u^3}\left(\tan^{-1}\frac{R}{u} + \frac{Ru}{R^2+u^2}\right).$$

Note that $\tan^{-1}\frac{R}{u}$ cannot be replaced by $\frac{\pi}{2}$ at this point because u assumes unbounded values. Now,

$$I_o = -\int_{-R-a}^{-R+a} \left(\tan^{-1}\frac{R}{u} + \frac{Ru}{R^2+u^2}\right) du,$$

which, in the limit as R becomes large approaches

$$I_o = -2a\left[\tan^{-1}\frac{R}{u} + \frac{Ru}{R^2+u^2}\right]_{u=-R} = a\left(\frac{\pi}{2}+1\right).$$

Finally, consider $I_1(a,b,0,0)$. As before, the PATCH integral is zero as are the STRIP2 and PLANE integrals due to integrands which are odd in v integrated over symmetric limits. Consequently,

$$I_1 = I_{s1} = \int_{-R}^{-R+2b}\int_{-R+2a}^{R} \frac{(a-x)^2(b-y)}{r^2}\, dx\, dy,$$

or,

$$I_1 = -2\int_{-R-b}^{-R+b} dv \cdot v \cdot J,$$

where

$$J = \int_o^{R-a} \frac{u^2 du}{(u^2+v^2)^2}.$$

Replacing the upper limit on the last integral by R adds to J an amount, $a/4R^2$ at most, which couples with the integral over v to produce a term of order ab/R which vanishes in the limit. Hence,

$$J = \int_o^R \frac{u^2 du}{(u^2+v^2)^2} = \frac{1}{2v}\left[\tan^{-1}\frac{R}{v} - \frac{Rv}{R^2+v^2}\right],$$

making

$$I_1 = - \int_{-R-b}^{-R+b} \left(\tan^{-1} \frac{R}{v} - \frac{Rv}{R^2+v^2}\right) dv,$$

and in the limit,

$$I_1 = -2b\left[\tan^{-1} \frac{R}{v} - \frac{Rv}{R^2+v^2}\right]_{v=-R} = b\left(\frac{\pi}{2} - 1\right).$$

The remaining integrals follow directly from Equation (A.6), which applies for all values of m and n.

APPENDIX B

DIPOLE TRANSFORMATIONS

In the generalized normal-shear dipole of Figure B.1a, let σ be the stress field generated by the edge dislocation located at the origin and let σ^* be the state of stress generated by the dipole shown. Then

$$\sigma^*(x,y) = \sigma(x,y) - \quad (x-h,\ y-k), \tag{B.1}$$

which for small h and k becomes

$$\sigma^* = \frac{\partial \sigma}{\partial x} \cdot h + \frac{\partial}{\partial y} \cdot k, \tag{B.2}$$

or, reverting back to the difference form,

$$\sigma^* = [\sigma(x,y) - \sigma(x-h,y)] + [\sigma(x,y) - \sigma(x,y-k),]. \tag{B.3}$$

Figure B.1b interprets this result symbolically.

Now examine the rotated normal dipole of Figure B.2a. Using the vector nature of b and adopting the notation,

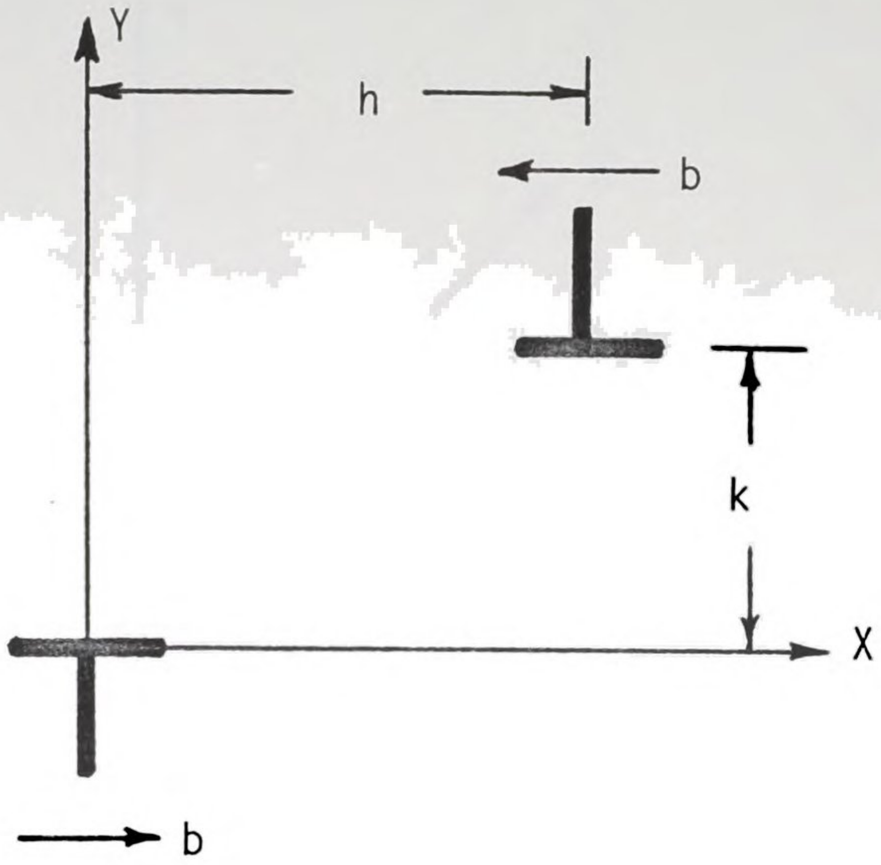

a. A generalized normal-shear dipole.

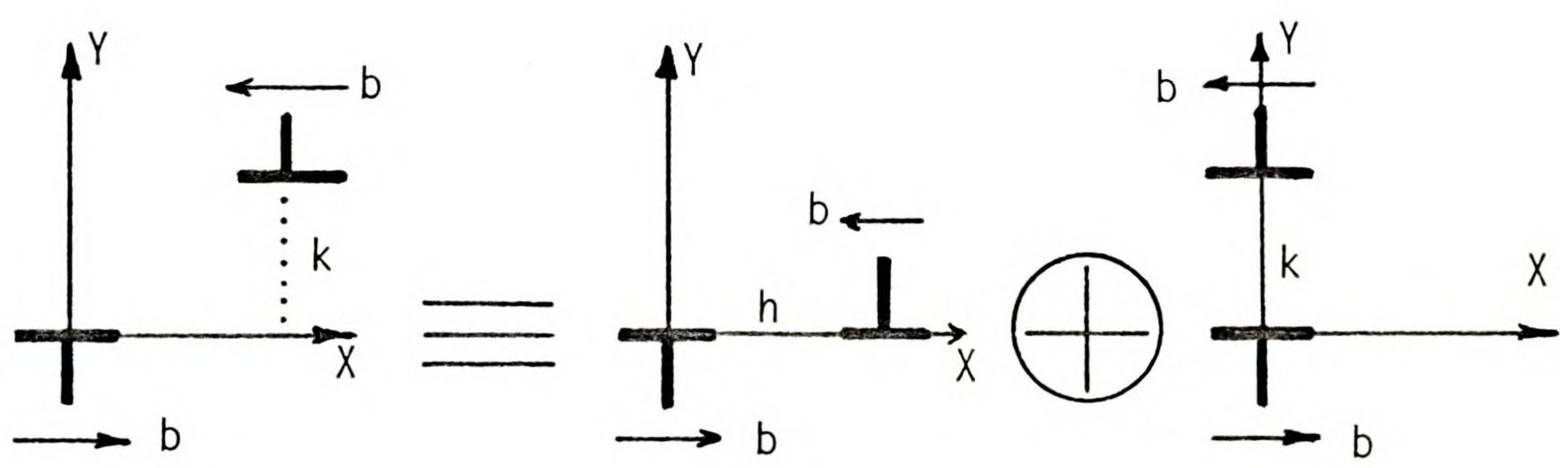

b. A normal-shear dipole decomposed into a normal and a shear dipole.

Figure B.1. The normal-shear dipole and its equivalent.

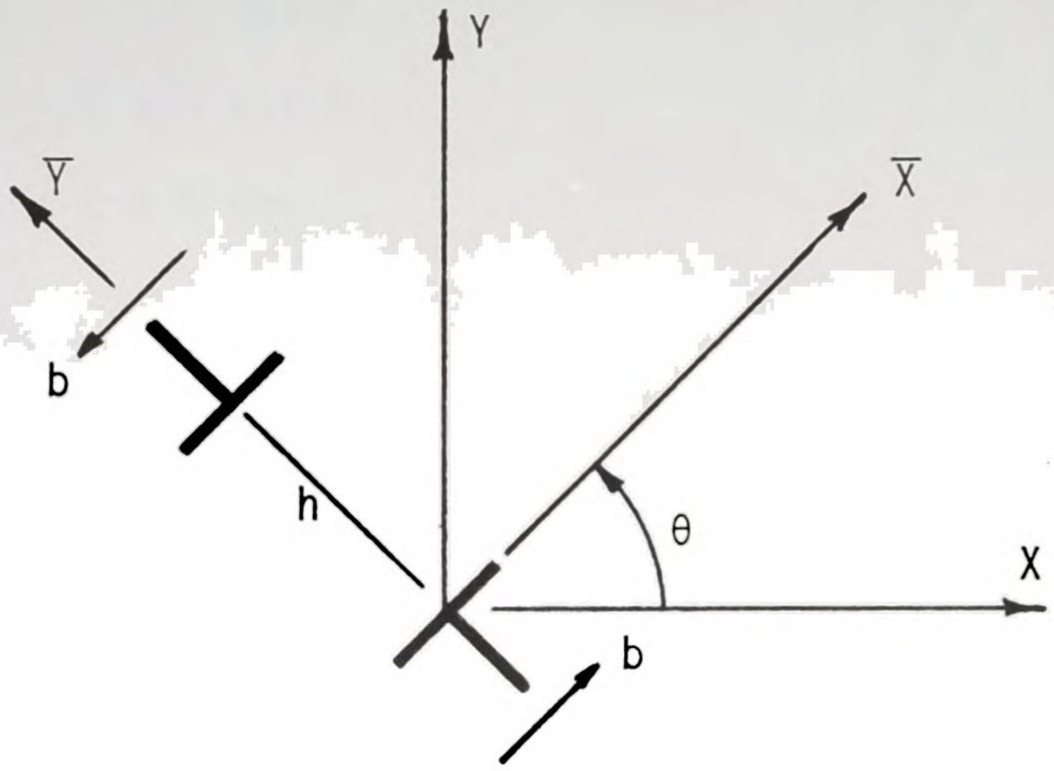

a. A rotated normal dipole of strength bh.

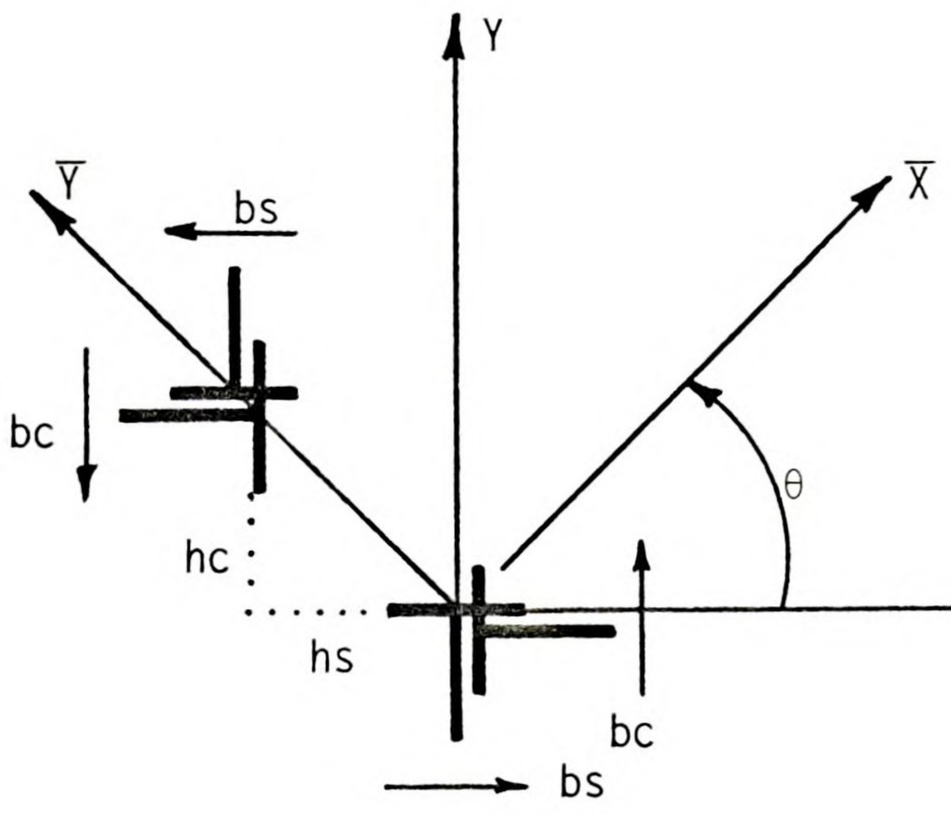

b. A normal and a shear dipole superposed.

Figure B.2. The rotated normal dipole and its equivalent normal-shear dipole pair.

$$b \cdot s = b \sin \theta$$
$$b \cdot c = b \cos \theta$$
$$h \cdot s = h \sin \theta \qquad (B.4)$$
$$h \cdot c = h \cos \theta,$$

the normal dipole can be reduced to the pair of normal-shear dipoles shown in Figure B.2b. Finally, with the aid of Figure B.1b, each of these normal-shear dipoles can be reduced to a normal and a shear dipole, yielding the four dipoles shown in Figure B.3a, which, when taken altogether, are equivalent to the rotated normal dipole of Figure B.2a. This quartet can be reduced to a trio by recalling that the first and fourth configurations generate the same stress field. Figure B.3b depicts this equivalence symbolically; the dipole strengths are written in parenthesis below each symbol.

The rotated shear dipole of Figure B.4a is treated in the same manner resulting in the equivalence depicted in Figure B.4b. That these transformation properties of dipoles bear a resemblance to the transformation properties of second order tensors is not surprising since the dipole strength is itself like a tensor in that it is the outer product of two vectors, the Burger's vector and the spacing. These properties can now be used to transform a general dipole state, (d_x, d_y, d_{xy}), to a rotated coordinate system. That is,

$$(d_{\bar{x}}, d_{\bar{y}}, d_{\bar{\bar{xy}}}) \equiv (d_x, d_y, d_{xy}), \qquad (B.5)$$

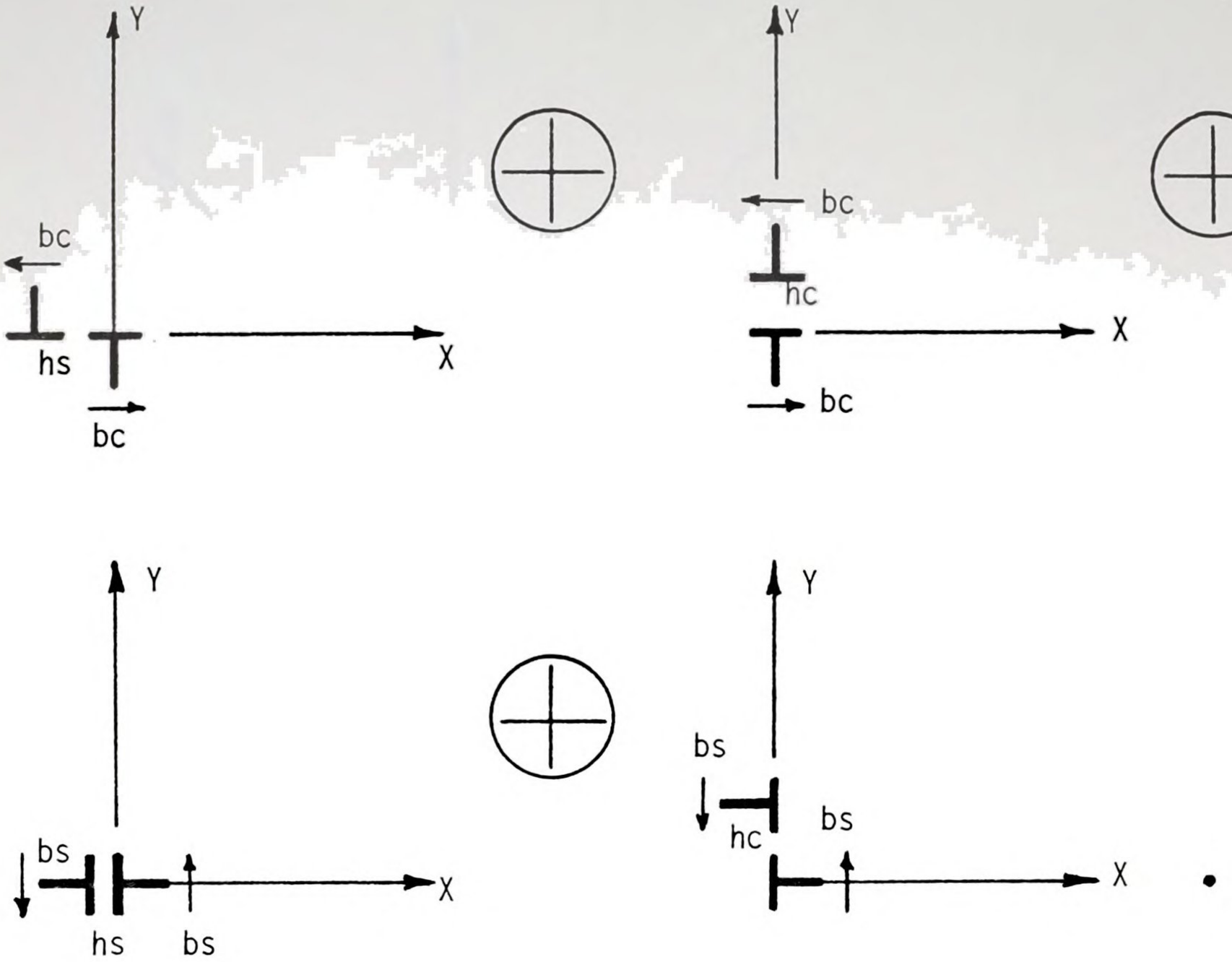

a. Two normal and two shear dipoles superposed.

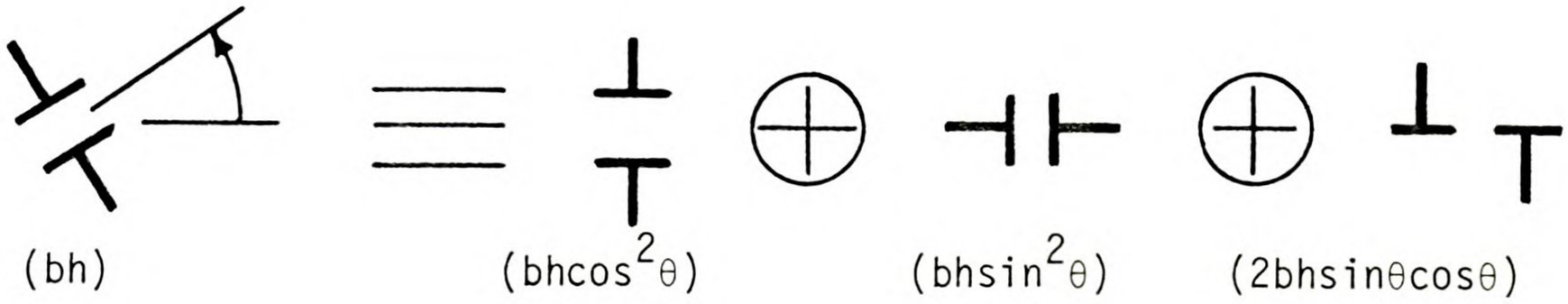

b. The transformation of a rotated dipole.

Figure B.3. Transformation properties of the normal dipole.

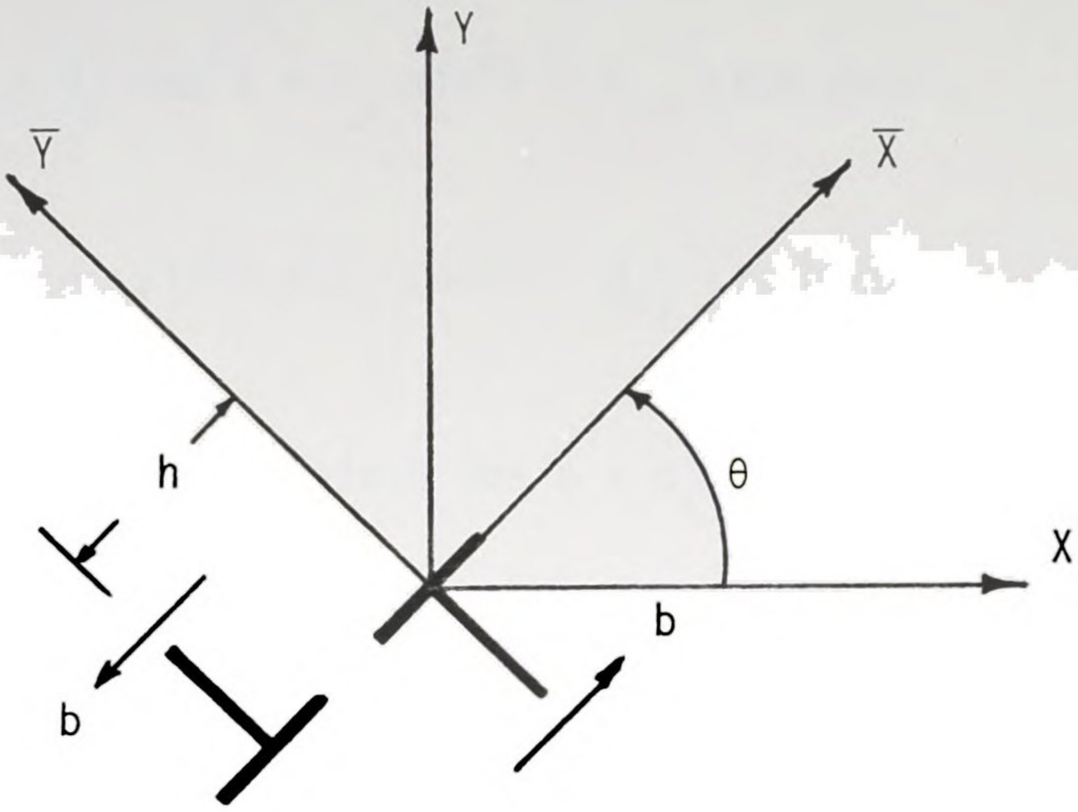

a. A rotated shear dipole of strength bh.

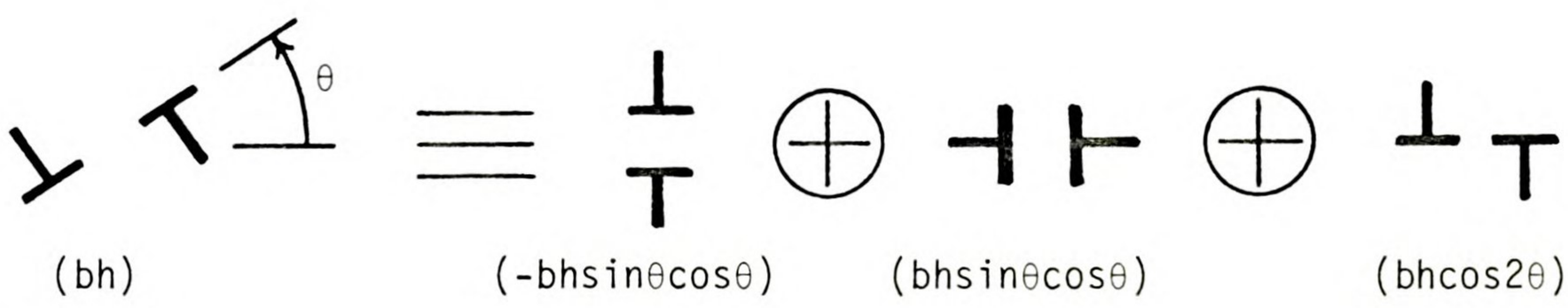

b. The transformation of a rotated shear dipole.

Figure B.4. Transformation properties of the shear dipole.

where the latter dipole state is given, provided that

$$d_{\overline{x}} = d_x \cos^2\theta + d_y \sin^2\theta + d_{xy} \sin\theta \cos\theta ,$$

$$d_{\overline{y}} = d_x \sin^2\theta + d_y \cos^2\theta - d_{xy} \sin\theta \cos\theta, \qquad \text{(B.6)}$$

$$d_{\overline{xy}} = 2(d_y - d_x) \sin\theta \cos\theta + d_{xy} (\cos^2\theta - \sin^2\theta).$$

It is worthwhile to note that the above transformations may be cast into a form which is consistent with second-order tensor transformations by redefining d_{xy} in Figure 2.6c to be

$$d_{xy} = \frac{1}{2} b_x h_x. \qquad \text{(B.7)}$$

This amounts to replacing d_{xy} in Equations (B.6) by $2d_{xy}$. The same type of situation is encountered in the transformation of strain; there are two definitions of shear strain in use, ε_{xy} and γ_{xy}. The choice of

$$\varepsilon_{xy} = \frac{1}{2} \gamma_{xy}$$

results in tensor transformation rules for strain.

APPENDIX C

THE EVALUATION OF FOUR BASIC LINE INTEGRALS

Under the substitution,

$$x = -c \cdot \cos\phi,$$

the four basic integrals quoted in Equation (3.6) assume the form

$$I_n = -\int_o^\pi \frac{b^{3-n}(a+\cos\phi)^n \cos\phi \, d\phi}{[(a+\cos\phi)^2+b^2]^2}, \qquad (C.1)$$

where

$$n = 0, 1, 2, 3.$$

The workload can be reduced to the evaluation of two simpler integrals,

$$J_o = \int_o^\pi \frac{\cos\phi \cdot d\phi}{(a+\cos\phi)^2+b^2},$$

$$J_1 = \int_o^\pi \frac{(a+\cos\phi)\cos\phi \, d\phi}{(a+\cos\phi)^2 + b^2}, \qquad (C.2)$$

from which,

$$I_o = \frac{b^2}{2} \frac{\partial J_o}{\partial b}$$

$$I_2 = -I_o - bJ_o, \tag{C.3}$$

$$I_1 = \frac{b}{2} \frac{\partial J_1}{\partial b},$$

$$I_3 = -I_1 - J_1.$$

It will be assumed hereafter, that $a>0$ and $b>0$.

Now,

$$(a+\cos\phi)^2 + b^2 = (\cos\phi - \alpha)(\cos\phi - \alpha^*),$$

where

$$\alpha = -a + bi,$$

and α^* is the complex conjugate of α. It is easy to verify that

$$J_o = \frac{1}{b} \mathrm{Im}(K),$$

$$J_1 = \pi + \mathrm{Re}(K), \tag{C.4}$$

where

$$K = \alpha \int_0^{\pi} \frac{d\phi}{\cos\phi - \alpha},$$

and where 'Re' and 'Im' denote the real and imaginary parts of the complex quantity, K, respectively. Under the substitution,

$$z = \tan \frac{\phi}{2},$$

K becomes

$$K = - \frac{\alpha}{1+\alpha} \int_{-\infty}^{\infty} \frac{dz}{z^2 - \beta^2}, \qquad (C.5)$$

where

$$\beta = \left(\frac{1-\alpha}{1+\alpha}\right)^{1/2} = u + iv,$$

with

$$u = \left(\frac{H}{2G}\right)^{1/2},$$

and

$$v = - \frac{b}{Gu},$$

where

$$F = ((1-a^2-b^2)^2 + 4b^2)^{1/2},$$

$$G = ((1-a)^2+b^2),$$

and

$$H = 1-a^2-b^2 + F.$$

Now,

$$K = \frac{\alpha}{1+\alpha} \oint \frac{\frac{1}{(z+\beta)} \cdot dz}{z-\beta}$$

where the circuit integral is taken around the closed path shown in Figure C.1. The integral over the circular part of this path vanishes in the limit as $R \to \infty$. Also, since β lies in the region enclosed by the path and since the function, $1/(z+\beta)$, is analytic everywhere inside this region, by Cauchy's integral theorem,

$$K = \frac{\alpha}{1+\alpha} \cdot 2\pi i \frac{1}{2\beta} = \frac{\pi i \alpha}{\beta(1+\alpha)}.$$

Substituting this result into Equation (C.4) and simplifying yields

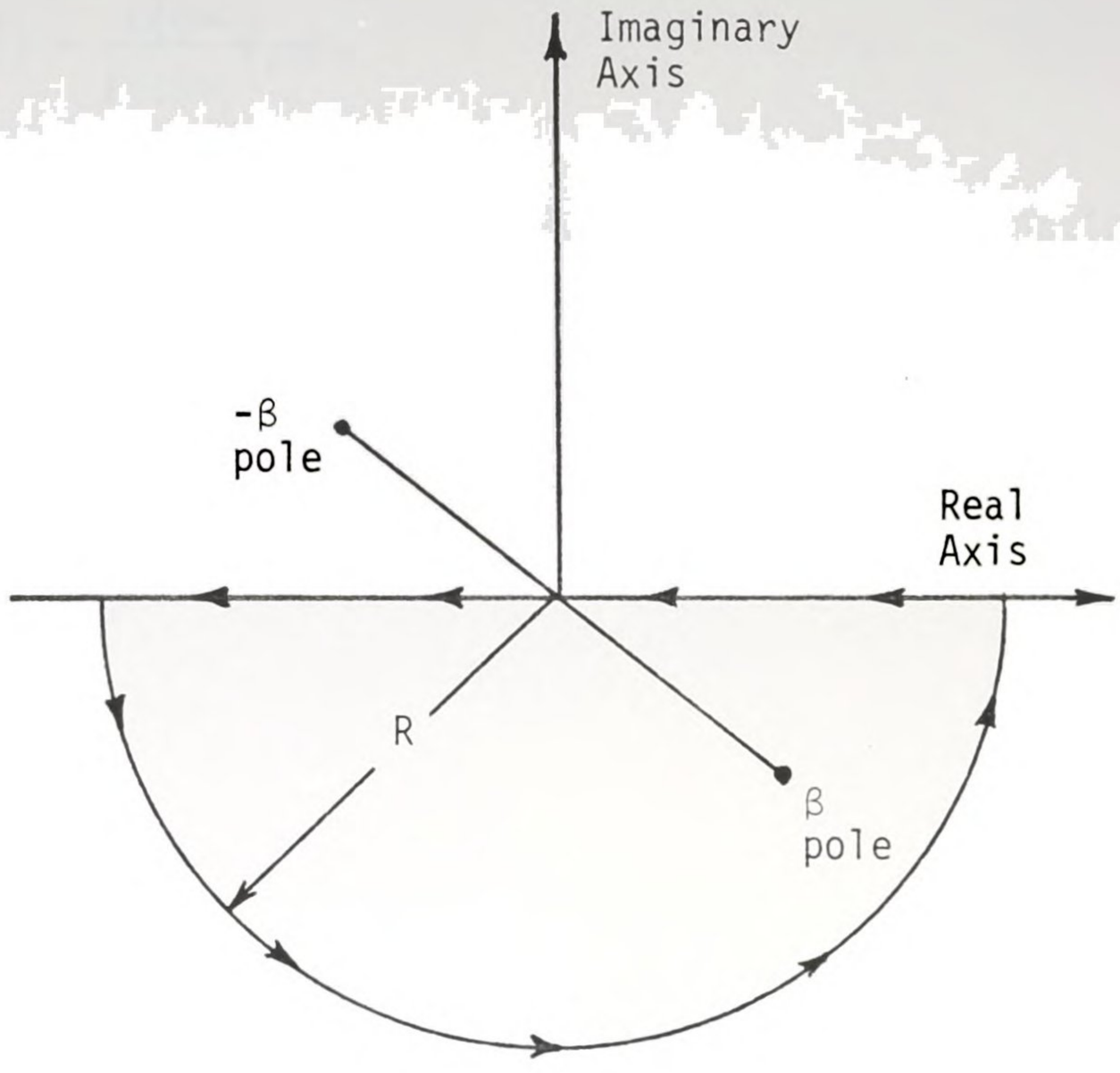

Figure C.1. Integration in the complex plane.

$$J_o = -\frac{\pi}{b}\ \frac{2b^2+(a-a^2-b^2)H}{F(2GH)^{1/2}}\ , \tag{C.6}$$

$$J_1 = \pi\left(1 - \frac{b(G+F)}{F(2GH)^{1/2}}\right),$$

which can now be used in Equations (C.3) to produce the desired integrals. An independent reevaluation of the four basic integrals for the special case, b=0, gives

$$I_o = I_1 = I_2 = 0, \tag{C.7}$$

whereas

$$I_3 = 0, \text{ for } a < 1 \tag{C.8a}$$

and

$$I_3 = \pi\left(\frac{a}{(a^2-1)^{1/2}} - 1\right), \text{ for } a > 1. \tag{C.8b}$$

In what follows, the crack tip coordinates, (r,θ), previously referred to in Figure 3.2 and defined by

$$a = 1 + r\cos\theta,$$

$$b = r\sin\theta, \tag{C.9}$$

will be used. Of particular importance is the limiting case, $r\to 0$. For small r, it is a simple matter to show that, asymptotically,

$$J_o = -\frac{\pi}{2(2r^3)^{1/2}} \sec\frac{\theta}{2},$$

$$J_1 = -\frac{\pi}{(2r)^{1/2}} \cos\frac{\theta}{2}. \qquad (C.10)$$

Now with

$$\frac{\partial}{\partial b} \equiv \sin\theta \frac{\partial}{\partial r} + \frac{\cos\theta}{r} \frac{\partial}{\partial\theta},$$

the first of the relations in Equation (C.3) becomes

$$I_o = \frac{r^2\sin^2\theta}{2} \left(\sin\theta \frac{\partial J_o}{\partial r} + \frac{\cos\theta}{r} \frac{\partial J_o}{\partial\theta}\right)$$

After tedious but straightforward manipulations, this and the remaining integrals are found to be, for $r\to 0$,

$$I_o = z \sin^3\frac{\theta}{2}\left(1 + 4\cos^2\frac{\theta}{2}\right),$$

$$I_1 = -z \sin^2\frac{\theta}{2}\cos\frac{\theta}{2}\left(1 - 4\cos^2\frac{\theta}{2}\right),$$

$$I_2 = z \sin\frac{\theta}{2}\left(1 + \cos^2\frac{\theta}{2}\left(1 - 4\sin^2\frac{\theta}{2}\right)\right), \qquad (C.11)$$

$$I_3 = z \cos\frac{\theta}{2}\left(2 + \sin^2\frac{\theta}{2}\left(1 - 4\cos^2\frac{\theta}{2}\right)\right),$$

where

$$z = \frac{\pi}{2(2r)^{1/2}}.$$

THE COMPUTER PROGRAM FOR
THE SUPERPOSITION METHOD

```
      PROGRAM TRACTN(INPUT,OUTPUT,TAPE1=INPUT,TAPE2=OUTPUT)
      DIMENSION XB(20,2),XS(20,2),XF(50,2),PHI(20),C(40,41)
      READ(1,*) NB,(XB(I,1),XB(I,2),I=1,NB),S
      READ(1,*) (PHI(I),I=1,NB)
      DO 1 I=1,NB $ PHI(I)=PHI(I)*ASIN(1.)/90.
      XS(I,1)=XB(I,1)+S*COS(PHI(I))
    1 XS(I,2)=XB(I,2)+S*SIN(PHI(I))
      READ(1,*) NF,(XF(I,1),XF(I,2),I=1,NF)
      READ(1,*) (C(I,2*NB+1),I=1,2*NB)
      DO 2 I=1,NB $ II=NB+I $ SA=SIN(PHI(I)) $ CA=COS(PHI(I))
      DO 2 J=1,NB $ JJ=NB+J $ X=XB(I,1)-XS(J,1) $ Y=XB(I,2)-XS(J,2)
      R=(X*CA+Y*SA)/(X*X+Y*Y)**2
      C(I,J)=X*X*R $ C(I,JJ)=X*Y*R $ C(II,J)=X*Y*R
    2 C(II,JJ)=Y*Y*R $ CALL MATRIX(2*NB,C)
      DO 4 I=1,NF $ P=Q=S=0.
      DO 3 J=1,NB $ X=XF(I,1)-XS(J,1) $ Y=XF(I,2)-XS(J,2)
      R=(X*C(J,2*NB+1)+Y*C(NB+J,2*NB+1))/(X*X+Y*Y)**2
      P=P+X*X*R $ Q=Q+Y*Y*R
    3 S=S+X*Y*R
    4 WRITE(2,*) XF(I,1),XF(I,2),P,Q,S
      END
      SUBROUTINE MATRIX(N,C) $ DIMENSION C(40,41)
      DO 1 K=1,N-1 $ DO 1 I=K+1,N $ S=C(I,K)/C(K,K) $ DO 1 J=K+1,N+1
    1 C(I,J)=C(I,J)-S*C(K,J) $ C(N,N+1)=C(N,N+1)/C(N,N) $ DET=C(N,N)
      DO 3 K=1,N-1 $ I=N-K $ DET=DET*C(I,I) $ S=0. $ DO 2 J=I+1,N
    2 S=S+C(I,J)*C(J,N+1)
    3 C(I,N+1)=(C(I,N+1)-S)/C(I,I) $ PRINT*,DET
      RETURN $ END

20 4. .2 4. .6 4. 1. 4. 1.4 4. 1.8 3.6 2. 2.8 2. 2. 2. 1.2 2. .4 2.
0. 1.8 0. 1.4 0. 1. 0. .6 0. .2 .4 0. 1.2 0. 2. 0. 2.8 0. 3.6 0. 4.
0. 0. 0. 0. 0. 90. 90. 90. 90. 90.
180. 180. 180. 180. 180. 270. 270. 270. 270. 270.
15 0. 0. 1. 0. 2. 0. 3. 0. 4. 0. 4. 1. 4. 2. 3. 2. 2. 2. 1. 2. 0. 2. 0. 1.
1. 1. 2. 1. 3. 1.
.02 .18 .5 .98 1.62 0. 0. 0. 0. 0. -5.62 -4.98 -4.5 -4.18 -4.02
.4 1.2 2. 2.8 3.6
-3.6 -2.8 -2. -1.2 -.4 1. 1. 1. 1. 1. 0. 0. 0. 0. 0. 0. 0. 0. 0. 0.
```

APPENDIX E

THE COMPUTER PROGRAM FOR BODY FORCES

```
      PROGRAM TRACTN(INPUT,OUTPUT,TAPE1=INPUT,TAPE2=OUTPUT)
      DIMENSION XB(20,2),XS(20,2),XF(20,2),PHI(20)
      COMMON/MATRIX/C(40,42)
      COMMON/RF/NX,NY,AA,BB,MX(20,2),MY(20,2),FX(20),FY(20),V
      PI=3.14159265358898
      READ(1,*) NB,(XB(I,1),XB(I,2),I=1,NB),S
      READ(1,*) (PHI(I),I=1,NB)
      DO 1 I=1,NB $ PHI(I)=PHI(I)*ASIN(1.)/90.
      XS(I,1)=XB(I,1)+S*COS(PHI(I))
    1 XS(I,2)=XB(I,2)+S*SIN(PHI(I))
      READ(1,*) NF,(XF(I,1),XF(I,2),I=1,NF)
      READ(1,*) (C(I,2*NB+1),I=1,2*NB)
      READ(1,*) NX,(MX(I,1),MX(I,2),FX(I),I=1,NX)
      READ(1,*) NY,(MY(I,1),MY(I,2),FY(I),I=1,NY)
      READ(1,*) AA,BB,V $ AA=PI/AA $ BB=PI/BB
      DO 1111 I=1,NB $ SA=SIN(PHI(I)) $ CA=COS(PHI(I))
      CALL BFORCE(XB(I,1),XB(I,2),TXX,TYY,TXY)
      C(I,2*NB+1)=C(I,2*NB+1)-TXX*CA-TXY*SA
 1111 C(NB+I,2*NB+1)=C(NB+I,2*NB+1)-TXY*CA-TYY*SA
      DO 2 I=1,NB $ II=NB+I $ SA=SIN(PHI(I)) $ CA=COS(PHI(I))
      DO 2 J=1,NB $ JJ=NB+J $ X=XB(I,1)-XS(J,1) $ Y=XB(I,2)-XS(J,2)
      R=(X*CA+Y*SA)/(X*X+Y*Y)**2
      C(I,J)=X*X*R $ C(I,JJ)=X*Y*R $ C(II,J)=X*Y*R
    2 C(II,JJ)=Y*Y*R $ CALL INVMTX(2*NB,1.,R)
      DO 4 I=1,NF $ CALL BFORCE(XF(I,1),XF(I,2),P,Q,S)
      DO 3 J=1,NB $ X=XF(I,1)-XS(J,1) $ Y=XF(I,2)-XS(J,2)
      R=(X*C(J,1)+Y*C(NB+J,1))/(X*X+Y*Y)**2
      P=P+X*X*R $ Q=Q+Y*Y*R
    3 S=S+X*Y*R
    4 WRITE(2,*) XF(I,1),XF(I,2),P,Q,S
      END
```

```
      SUBROUTINE BFORCE(X,Y,TXX,TYY,TXY)
      COMMON/BF/NX,NY,AA,BB,MX(20,2),MY(20,2),FX(20),FY(20),V
      Z=(1+V)/3.14159265358
      TXX=-.5*((1+Z)*X*FX(1)+(V-Z)*Y*FY(1))
      TYY=-.5*((V-Z)*X*FX(1)+(1+Z)*Y*FY(1))
      TXY=-.5*(1-Z)*(Y*FX(1)+X*FY(1))
      DO 1 I=2,NX $ A=AA*MX(I,1) $ B=BB*MX(I,2)
      P=SIN(A*X)*COS(B*Y) $ Q=COS(A*X)*SIN(B*Y)
      R=-1/(A*A+B*B)**2 $ V1=A*A+(2+V)*B*B
      V2=A*A-V*B*B $ V3=B*B-V*A*A $ V4=B*B+(2+V)*A*A
      TXX=TXX+R*A*V1*P*FX(I) $ TYY=TYY-R*A*V3*P*FX(I)
    1 TXY=TXY+R*B*V3*Q*FX(I)
      DO 2 I=2,NY $ A=AA*MY(I,1) $ B=BB*MY(I,2)
      P=SIN(A*X)*COS(B*Y) $ Q=COS(A*X)*SIN(B*Y)
      R=-1/(A*A+B*B)**2 $ V1=A*A+(2+V)*B*B
      V2=A*A-V*B*B $ V3=B*B-V*A*A $ V4=B*B+(2+V)*A*A
      TXX=TXX-R*B*V2*Q*FY(I) $ TYY=TYY+R*B*V4*Q*FY(I)
    2 TXY=TXY+R*A*V2*P*FY(I)
      RETURN $ END
```

APPENDIX F

THE EDGE DISLOCATION SUBROUTINE

```
      SUBROUTINE EDGE(X,Y,TXX,TYY,TXY)
      COMMON/DISL/NX,NY,AA,BB,MX(20,2),MY(20,2),FX(20),FY(20),E
      Z=.5/3.141592653589 $ TXX=E*((.5-Z)*Y*FX(1)-Z*X*FY(1))
      TYY=E*(Z*Y*FX(1)-(.5-Z)*X*FY(1))
      TXY=E*Z*(-X*FX(1)+Y*FY(1))
      DO 1 I=2,NX $ A=AA*MX(I,1) $ B=BB*MX(I,2)
      P=SIN(A*X)*COS(B*Y) $ Q=COS(A*X)*SIN(B*Y)
      R=E/(A*A+B*B)**2
      TXX=TXX+R*Q*FX(I)*B**3 $ TYY=TYY+R*Q*FX(I)*B*A*A
    1 TXY=TXY-R*P*FX(I)*A*B*B
      DO 2 I=2,NY $ A=AA*MY(I,1) $ B=BB*MY(I,2)
      P=SIN(A*X)*COS(B*Y) $ Q=COS(A*X)*SIN(B*Y)
      R=E/(A*A+B*B)**2
      TXX=TXX-R*P*FY(I)*A*B*B $ TYY=TYY-R*P*FY(I)*A**3
    2 TXY=TXY+R*Q*FY(I)*B*A*A
      RETURN $ END
```

```
C PROBLEM DEFINITION   B=C*W+H*D , S=G*W+Q*D , D=P*S.
      PROGRAM CRACK(INPUT,OUTPUT,TAPE1=INPUT,TAPE2=OUTPUT)
      DIMENSION XB(20,2),XS(20,2),XC(20,2),XF(20,2),PHI(20)
      DIMENSION B(60,40),D(20,2),P(60,3)
      COMMON/MATRIX/C(60,121)
      PI=3.1415926535898
C READ IN BOUNDARY GEOMETRY AND CALCULATE SOURCE LOCATIONS.
      READ(1,*) NB,(XB(I,1),XB(I,2),I=1,NB),S $ NBB=2*NB
      READ(1,*) (PHI(I),I=1,NB) $ DO 1 I=1,NB
      PHI(I)=PHI(I)*PI/180 $ XS(I,1)=XB(I,1)+S*COS(PHI(I))
    1 XS(I,2)=XB(I,2)+S*SIN(PHI(I))
C READ IN CRACK LOCATIONS, LENGTHS, AND ORIENTATIONS. CALCULATE P.
      READ(1,*) NC,(XC(I,1),XC(I,2),I=1,NC) $ NDD=3*NC
      READ(1,*) (D(I,1),D(I,2),I=1,NC)
      DO 10 I=1,NC $ I3=3*I $ I2=I3-1 $ I1=I3-2
      T=D(I,2)*PI/180 $ SA=SIN(T) $ CA=COS(T) $ Q=D(I,1)**2/2
      P(I1,1)=Q*SA*SA $ P(I2,2)=Q*CA*CA $ P(I3,3)=Q
      P(I1,3)=P(I2,3)=P(I3,1)=P(I3,2)=-Q*SA*CA
   10 P(I1,2)=P(I2,1)=0.
C CALCULATE Q AND STORE IN RH OF C, NDD+.
      DO 30 I=1,NC $ I3=3*I $ I2=I3-1 $ I1=I3-2
      DO 30 J=1,NC $ J3=3*J+NDD $ J2=J3-1 $ J1=J3-2
      IF(I.NE.J) GO TO 20 $ C(I1,J1)=C(I2,J2)=C(I3,J3)=1.
      C(I1,J2)=C(I1,J3)=C(I2,J1)=C(I2,J3)=C(I3,J1)=C(I3,J2)=0.
      GO TO 30
   20 X=XC(I,1)-XC(J,1) $ Y=XC(I,2)-XC(J,2)
      V1=X*X+Y*Y $ V2=Y*Y-X*X $ V3=2*X*Y $ V4=2*V2-V1 $ V5=-2*V2-V1
      V6=V1**3 $ V7=V1*V1-2*V3*V3 $ V8=-V7+2*V1*V2 $ V9=-V7-2*V1*V2
      C(I1,J1)=V8/V6 $ C(I1,J2)=C(I2,J1)=C(I3,J3)=V7/V6
      C(I2,J2)=V9/V6 $ C(I2,J3)=C(I3,J2)=V3*V5/V6
      C(I1,J3)=C(I3,J1)=V3*V4/V6
   30 CONTINUE
C FORM INVERSE OF (I-Q*P) AND STORE IN LH OF C.
      DO 40 I=1,NDD $ DO 40 J=1,NDD $ J1=3*((J-1)/3)
      J2=J1+NDD $ J3=J-J1 $ C(I,J)=(I/J)*(J/I) $ DO 40 K=1,3
   40 C(I,J)=C(I,J)-C(I,J2+K)*P(J1+K,J3) $ CALL INVMTX(NDD,0.,R)
      IF(R.NE.0.) GO TO 50 $ WRITE(2,49) $ GO TO 1000
   49 FORMAT(//,*SINGULAR B MATRIX*)
C CALCULATE G AND STORE IN RH OF C, NDD+.
   50 DO 60 I=1,NC $ I3=3*I $ I2=I3-1 $ I1=I3-2
      DO 60 J=1,NB $ J1=J+NDD
      X=XC(I,1)-XS(J,1) $ Y=XC(I,2)-XS(J,2) $ R=1/(X*X+Y*Y)**2
      C(I1,J1)=R*X**3 $ C(I2,J1)=C(I1,J1+NB)=R*Y*X*X
      C(I3,J1)=C(I2,J1+NB)=R*X*Y*Y
   60 C(I3,J1+NB)=R*Y**3
C FORM PRODUCT OF INVERSE OF (I-Q*P) AND G. CALL IT B.
      DO 70 I=1,NDD $ DO 70 J=1,NBB $ B(I,J)=0. $ DO 70 K=1,NDD
   70 B(I,J)=B(I,J)+C(I,K)*C(K,J+NDD)
```

```
C CALCULATE H AND STORE IN LH OF C.
      DO 80 I=1,NB $ SA=SIN(PHI(I)) $ CA=COS(PHI(I))
      DO 80 J=1,NC $ J3=3*J $ J2=J3-1 $ J1=J3-2
      X=XB(I,1)-XC(J,1) $ Y=XB(I,2)-XC(J,2)
      V1=X*X+Y*Y $ V2=Y*Y-X*X $ V3=2*X*Y $ V4=2*V2-V1 $ V5=-2*V2-V1
      V6=V1**3 $ V7=V1*V1-2*V3*V3 $ V8=-V7+2*V1*V2 $ V9=-V7-2*V1*V2
      C(I,J1)=(V8*CA+V3*V4*SA)/V6 $ C(NB+I,J2)=(V3*V5*CA+V9*SA)/V6
      C(I,J2)=C(NB+I,J3)=(V7*CA+V3*V5*SA)/V6
   80 C(I,J3)=C(NB+I,J1)=(V3*V4*CA+V7*SA)/V6
C FORM H*P AND STORE IN RH OF C, NDX+.
      NDX=NDD $ IF(NBB.GT.NDX) NDX=NBB
      DO 90 I=1,NBB $ DO 90 J=1,NDD $ J1=3*((J-1)/3)
      J2=J-J1 $ J3=J+NDX $ C(I,J3)=0. $ DO 90 K=1,3
   90 C(I,J3)=C(I,J3)+C(I,J1+K)*P(J1+K,J2)
C FORM (H*P)*B AND STORE IN LH OF C.
      DO 100 I=1,NBB $ DO 100 J=1,NBB $ C(I,J)=0. $ DO 100 K=1,NDD
  100 C(I,J)=C(I,J)+C(I,NDX+K)*B(K,J)
C ADD C TO H*P*B AND STORE IN LH OF C.
      DO 110 I=1,NB $ II=NB+I $ SA=SIN(PHI(I)) $ CA=COS(PHI(I))
      DO 110 J=1,NB $ JJ=NB+J $ X=XB(I,1)-XS(J,1) $ Y=XB(I,2)-XS(J,2)
      R=(X*CA+Y*SA)/(X*X+Y*Y)**2
      C(I,J)=C(I,J)+X*X*R $ C(I,JJ)=C(I,JJ)+X*Y*R
  110 C(II,J)=C(II,J)+X*Y*R
      C(II,JJ)=C(II,JJ)+Y*Y*R
C READ BOUNDARY CONDITIONS INTO (NBB+1)ST COLUMN OF C.
C CALCULATE W AND STORE IN FIRST COLUMN OF C.
      READ(1,*) (C(I,NBB+1),I=1,NBB) $ CALL INVMTX(NBB,1.,R)
      IF(R.NE.0.) GO TO 120 $ WRITE(2,119) $ GO TO 1000
  119 FORMAT(//,*SINGULAR C MATRIX*)
C CALCULATE RESOLVED STRESSES, S=B*W, AND STORE IN 2ND COLUMN OF C.
  120 DO 130 I=1,NDD $ C(I,2)=0. $ DO 130 J=1,NBB
  130 C(I,2)=C(I,2)+B(I,J)*C(J,1)
      DO 150 I=1,NC $ I3=3*I $ I2=I3-1 $ I1=I3-2
  150 PRINT*,I,XC(I,1),XC(I,2),C(I1,2),C(I2,2),C(I3,2)
 1000 CONTINUE
      END

20 1. -.8 1. -.4 1. 0. 1. .4 1. .8 .8 1. .4 1. 0. 1. -.4 1. -.8 1.
-1. .8 -1. .4 -1. 0. -1. -.4 -1. -.8 -.8 -1. -.4 -1. 0. -1. .4 -1. .8 -1.  4.
0. 0. 0. 0. 0. 90. 90. 90. 90. 90. 180. 180. 180. 180. 180.
270. 270. 270. 270. 270.
5 .5 -.5 .5 .5 -.5 .5 -.5 -.5 0. 0.
.1 90. .1 90. .1 90. .1 90. .1 90.
1. 1. 1. 1. 1. 0. 0. 0. 0. 0. -1. -1. -1. -1. -1. 0. 0. 0. 0. 0.
0. 0. 0. 0. 0. 0. 0. 0. 0. 0. 0. 0. 0. 0. 0. 0. 0. 0. 0. 0.
```

LIST OF REFERENCES

REFERENCES

[1] Banerjee, P.K. and Mustoe, G.G., 'The Boundary Element Method for Two Dimensional Problems of Elastoplasticity, in Recent Advances in Boundary Element Methods, Brebbia, C.A. editor, 1978, pp. 283-300.

[2] Telles, J.C.F. and Brebbia, C.A., 'On the Application of the Boundary Element Method to Plasticity', Appl. Math. Modelling, 1979, Vol. 3, pp. 466-470.

[3] Green, A.E. and Adkins, J.E., 'Large Elastic Deformations', 2nd ed., Clarendon Press, 1970.

[4] Little, R.W., Elasticity, Prentice Hall, 1973.

[5] Zienkiewicz, The Finite Element Method in Structural and Continuum Mechanics, McGraw-Hill, 1967.

[6] Hirth, J.P. and Lothe, J., Theory of Dislocations, McGraw Hill, 1968.

[7] Nye, J.F., 'Some Geometrical Relations in Dislocated Crystals', Acta Metallurgica, Vol. 1, 1953, pp. 153-162.

[8] Eshelby, J.D., 'The Continuum Theory of Lattice Defects', Solid State Phys., Vol. 3, 1956, pp. 79-144.

[9] Barenblatt, G.I., 'The Mathematical Theory of Equilibrium Cracks in Brittle Fracture', Adv. Appl. Mech., Vol. 7, 1962, pp.55-129.

[10] Cardew, G.E. and Howard Doss, 'An Edge Crack in an Elastic Strip and Related Problems in Fracture Mechanics and Viscous Flow', Int. J. Engng. Sci., 1976, Vol. 14, pp. 403-414.

[11] Sih, G.C., Fracture Mechanics, Noordhoff Int. Pub., 1973.

[12] Theocaris, P.S., and Ioakimidis, N.I., 'Stress Intensity Factors at Crack Tips near Boundaries or other Geometrical Discontinuities', Int. J. Fracture, Vol. 15, 1979, pp. 419-428.

[13] Crouch, S.L., 'A Note on Post-Failure Stress-Strain Path Dependence in Norite', Int. J. Rock Mech. Min. Sci., Vol. 9, 1972, pp. 197-204.

[14] Dragon, A. and Mroż, Z., 'A Continuum Model for Plastic-Brittle Behavior of Rock and Concrete', Int. J. Engng. Sci., Vol. 17, pp. 121-137.

[15] Hoek, E. and Bienawski, Z.T., 'Brittle Fracture Propagation in Rock under Compression', Int. J. Fracture Mech., Vol. 1, 1965, pp. 137-155.

[16] Leckie, F.A., 'The Constitutive Equations of Continuum Creep Damage Mechanics', Phil. Trans. R. Sco. Lond. A, Vol. 288, 1978, pp. 27-47.

[17] St. Pietruszczak and Mroż, Z., 'Numerical Analysis of Elastic-Plastic Compression Pillars with Account for Material Hardening and Softening', Report, Inst. of Fund. Research, Poland, 1980.

[18] Tanaka, K. and Mura, T., 'A Dislocation Model for Fatigue Crack Initiation', J. Appl. Mech., Vol. 48, 1981, pp. 97-103.

[19] Brady, B.T., 'A Mechanical Equation of State for Brittle Rock', Int. J. Rock Mech. Min. Sci., Vol. 7, 1970, pp. 385-421.

[20] Walsh, J.B. and Brace, W.F., 'Elasticity of Rock in Uniaxial Strain', Int. J. Rock Mech. Min. Sci., Vol. 9, 1972, pp. 7-15.

[21] Vakulenko, A.A. and Kachanov, M.L., Mekh. Tv. Tela., Vol. 4, 1970, pp. 159-180.

[22] Irwin, G.R., 'Fracture', Handbuch der Physik, Springer-Verlag Berlin, Vol. 6, 1958, p. 551.

[23] Westlake, J.R., A Handbook of Numerical Matrix Inversion and Solution of Linear Equations, Wiley and Sons, 1968.